A THREE-DIMENSIONAL COUPLED MICROELECTRODE AND MICROFLUIDIC ARRAY FOR NEURONAL INTERFACING

A Dissertation
Presented to
The Academic Faculty

By

Yoonsu Choi

In Partial Fulfillment
of the Requirements for the Degree
Doctor of Philosophy in the
School of Electrical and Computer Engineering

Georgia Institute of Technology
August 2005

A THREE-DIMENSIONAL COUPLED MICROELECTRODE AND MICROFLUIDIC ARRAY FOR NEURONAL INTERFACING

Approved by:

Dr. Mark G. Allen, Advisor
School of Electrical & Computer Engineering
Georgia Institute of Technology

Dr. A. Bruno Frazier
School of Electrical & Computer Engineering
Georgia Institute of Technology

Dr. Stephen P. DeWeerth
School of Electrical & Computer Engineering
Georgia Institute of Technology

Dr. Thomas E. Michaels
School of Electrical & Computer Engineering
Georgia Institute of Technology

Dr. Robert K. Feeney
Department of Biomedical Engineering
Georgia Institute of Technology

Date Approved: April 27, 2005

ACKNOWLEDGEMENTS

I would like to first thank Prof. Allen for his advice, mentoring, and research support throughout my doctoral studies. I also thank to my doctoral committee members, Prof. Frazier, Prof. DeWeerth, Prof. Michaels, and Prof. LaPlaca, for their evaluations of my research and their valuable comments that led to its improvement.

I want to acknowledge all the members of the Microsensor and Microactuator Group. I also thank to Richard Shafer for his technical assistance. I thank Gary Spinner and the Microelectronics Research Center (MiRC) cleanroom staff for their technical assistance and support of the cleanroom facilities.

I thank all faculty members and colleagues on this BRP project. In particular, I owe Jim Ross special thanks for his electrical measurement and dedicated collaboration on this project. I thank Jelena Vukasinovic for the design and measurement of the fluidic systems. I also thank Varad Vernekar, Maxine McClain, Ashley Marr, Nick Fogleman, Kacy Cullen, Yoonkey Nam, and Komal Rambani for their biological experiments with my structures. This research work has been supported by the National Institutes of Health [NIH-BRP (EB00786-01)].

My family has made my academic pursuits possible. I am forever indebted to my parents for their love, incredible understanding, and unconditional sacrifices.

Finally, I thank my best friend and lovely wife, Sunyoung, for her love, understanding, and sacrifices. Her presence, encouragement, and support over the years made this dissertation possible.

TABLE OF CONTENTS

ACKNOWLEDGEMENTS iii

LIST OF TABLES vii

LIST OF FIGURES viii

SUMMARY xiii

CHAPTER 1 INTRODUCTION 1

1.1 Objectives of 3-D Neuronal Interface System 1

1.2 Cell Culture Systems 9

1.3 3-D Cell Culture 11

1.4 3-D MEAs 14

CHAPTER 2 3-D SCAFFOLDS FOR 3-D CELL CULTURING 17

2.1 SU-8 Tower Arrays on Glass Substrates 17

2.1.1 High Aspect Ratio SU-8 Tower 17
2.1.2 Fabrication 19
2.1.3 Cell Culture 20

2.2 SU-8 Towers on SU-8 substrates 22

2.2.1 Adhesion of SU-8 Towers on Substrates 22
2.2.2 Fabrication 23
2.2.3 Cell Culturing on SU-8 Tower Arrays 27

2.3 Cross-Connects with Towers 29

2.3.1 Micro-Assembly 29
2.3.2 Fabrication 30
2.3.3 Cell Culturing 33

2.4 Cytotoxicity Test of SU-8 36

2.4.1 SU-8 Bits 36
2.4.2 Detoxification Treatments 38
2.4.3 Results and Discussion 40

CHAPTER 3 3-D FLUIDIC SYSTEM FOR 3-D CELL CULTURE 44

3.1 Objectives of 3-D MEMS Fluidic Systems 44

3.2 Eximer Laser Ablation 47

3.2.1 Laser Systems 47
3.2.2 Excimer Laser Ablation of SU-8 50

3.3 Hollow Towers with Laser Ablated Side Ports 53

3.3.1 Fluidic Design 53
3.3.2 Fabrication Process 57
3.3.3 Modified Fabrication Process 62
3.3.4 Fluidic Measurement 66

3.4 Solid Towers with Laser Ablated Channels 75

3.4.1 Fluidic Design 75
3.4.2 Fabrication Processes 76
3.4.3 Microfluidic Measurement 79

CHAPTER 4 A 3-D MULTI-ELECTRODE ARRAY 82

4.1 3-D MEA on Solid Tower Arrays 82

4.1.1 Introduction to 3-D Electrodes Electroplated on Parylene Molds 82
4.1.2 Characteristics of Parylene 85
4.1.3 Fabrication Process 88

4.2 Stimulation and Recording of 3-D MEA 96

4.2.1 Design of the Electronic Interface System 96
4.2.2 Electrical Measurement of 3-D MEA 101

CHAPTER 5 MICRONEEDLE ARRAYS 107

5.1 Introduction 107

5.2 Requirements of Microneedle Arrays 109

5.3 Microneedle Arrays for Brain Slice Cultures 112

5.4 Brain Slice Culture 121

5.5 Microneedle Arrays for Transdermal Drug Delivery 125

CHAPTER 6 CONCLUISIONS 129

6.1 Summary 129

6.2 Suggestions for Future Work 131

REFERENCES 133

LIST OF TABLES

Table 2.1 Detoxification treatments 38

Table 3.1 Common lasers used in industry. 47

Table 3.2 Excimer laser gas mixtures 48

Table 3.3 Harmonic generation frequencies of solid state lasers 49

Table 5.1 Cell Growth Media 122

LIST OF FIGURES

Figure 1.1 Conceptual view of the 3-D MEA including microfluidic channels for 3-D cell culturing. 2

Figure 1.2 Conceptual view of the microneedle array including microfluidic channels and microelectrode arrays. 5

Figure 1.3 Fabrication Sequence 7

Figure 1.4 (a) Micropipette (b) 2-D MEA (c) 2-D MEA combined with fluidic channels (d) Parylene cages 10

Figure 1.5 (a) Impedance measurement system (b) Impedance model of a planar MEA 11

Figure 1.6 (a) Aggregation (b) Nanofiber (c) P(PF-co-EG) macroporous hydrogel (d) Matrigel 13

Figure 1.7 (a) 100 MEA (b) Assembled MEA (c) Fork MEA (d) MEA including 3-D electrodes for brain slices 15

Figure 2.1 Perspective views of SU-8 towers on glass and silicon substrates 18

Figure 2.2 Fabrication sequence 19

Figure 2.3 Cell bridging in 3-D networks of cultured cells 21

Figure 2.4 Fabrication sequence 24

Figure 2.5 Top view of the SU-8 tower 25

Figure 2.6 SEM views of a variety of fabricated geometries 26

Figure 2.7 Phase contrast microscopy (200X magnification) of neural culture (a) on a polystyrene control and (b) around a tower on a SU-8 substrate 28

Figure 2.8 Fluorescent images of neural culture on a polystyrene control (left) at 200X magnification and around a set of tower on a SU-8 substrate (right) at 100X magnification. 29

Figure 2.9 Fabrication sequence 30

Figure 2.10 Individual structures with cross-connects 31

Figure 2.11 Assembly sequence 32

Figure 2.12 SEM picture of completed cross-connect scaffolds 33

Figure 2.13 SEM pictures of cultured neural networks on cross-connects 34

Figure 2.14 Phase contrast microscopy pictures of cultured neural networks on cross-connects 35

Figure 2.15 Fabrication procedures for SU-8 bits 37

Figure 2.16 Top view of the culturing dish and imaged areas 39

Figure 2.17 Cell viability at day 21 *in vitro* of cortical neuronal cultures adjacent to the SU-8 bits treated by the different detoxification schemes. 41

Figure 2.18 Cell viability at day 21 *in vitro* of E17 primary cortical neuronal cultures adjacent to SU-8 samples 43

Figure 3.1 Conceptual view of a 3-D microfluidic system 46

Figure 3.2 Excimer laser ablation on a 154 μm thick glass 51

Figure 3.3 Excimer laser ablation on an SU-8 block 52

Figure 3.4 Single tower of the 3-D perfusion system 54

Figure 3.5 Fabrication sequence 58

Figure 3.6 An inclined hollow tower array. (a) perspective view, (b) top view. 58

Figure 3.7 Cross-linked SU-8 and mask patterns which block the inside of hollow towers during patterning the square SU-8 substrate 59

Figure 3.8 Towers with laser created side holes 60

Figure 3.9 (a) Warped SU-8 substrates after releasing from glass substrates (b) Flattened SU-8 substrates with post baking with metal sheets 61

Figure 3.10 Fabrication sequence 63

Figure 3.11 (a) Top view of vertical towers, (b) Bottom view of the towers (Through holes can be seen from this bottom view) 65

Figure 3.12 Laser-bored side holes on the hollow towers 65

Figure 3.13 (a) a manifold for supplying fluid through the system (b) integration of 3-D perfusion devices and the chamber 66

Figure 3.14 Conceptual views of the PIV view planes 68

Figure 3.15 Hollow towers without side ports, (a) 480 μm, (b) 620 μm 69

Figure 3.16 Hollow towers with side ports, (a) 480 μm, (b) 620 μm 71

Figure 3.17 Single hollow tower for fluidic analysis 73

Figure 3.18 Fluidic measurement using PIV method 74

Figure 3.19 (a) Concept of laser patterned center channels and side holes, (b) Towers with laser created center channels 77

Figure 3.20 Different lengths of the center channels controlled by the power of the laser beam 78

Figure 3.21 The side ports on the solid towers 79

Figure 3.22 Single tower and its manifold pump connection shown next to a US penny 80

Figure 3.23 Evenly perfusing flow from six side ports 81

Figure 4.1 Conceptual view of a 3-D multi-electrode array 83

Figure 4.2 Merged lines using conventional photolithography 84

Figure 4.3 Straight lines using laser ablation 84

Figure 4.4 Parylene deposition process. 86

Figure 4.5 Molecular structures of parylenes 87

Figure 4.6 Fabrication sequence for electrodes on inclined surface 89

Figure 4.7 Electrodes on vertical towers (a) before removing a copper seed layer (b) after removing the seed layer 91

Figure 4.8 Electrodes on inclined tower structures (a) top view (b) perspective view on a close-up corner 91

Figure 4.9 SEM picture of 3-D Electrodes on a circular SU-8 substrate 92

Figure 4.10 3-D Electrodes on a circular SU-8 substrate after removing a copper seed layer and parylene molds 93

Figure 4.11 3-D Electrodes on a circular SU-8 substrate after removing a copper seed layer and parylene molds 93

Figure 4.12 3-D Electrodes on a circular SU-8 substrate after removing a copper seed layer and parylene molds 94

Figure 4.13 3-D Electrodes on a circular SU-8 substrate after removing a copper seed layer and parylene molds 95

Figure 4.14 3-D Electrodes on a circular SU-8 substrate after removing a copper seed layer and parylene molds 95

Figure 4.15 Results of artifact suppression experiments 98

Figure 4.16 The nonlinear model of the electrode and stimulation voltage. The electrode model consists of a nonlinear interface capacitance, $C_I(V)$, a nonlinear charge transger, $I_t(V)$, and a linear spreading resistance, R_S. The model of the stimulation switch is a time dependent resister, R(t). 100

Figure 4.17 (a) Artifact generated by the physical system. (b) Predicted artifact from the nonlinear model 101

Figure 4.18 Control panel for stimulation and recording on multi electrodes. 102

Figure 4.19 Results of stimulation and recording on MEA60. 103

Figure 4.20 Results of stimulation and recording of 3-D MEA 103

Figure 4.21 A) Circuit model for the microelectrode. The transfer resistance, R_T, is assumed to be infinite. R_S represents the spreading resistance. C_I is the interfacial capacitance, and R_M is the resistance of the media. B) Biphasic waveform applied at V_S 105

Figure 4.22 Impedance measurement of (a) electrodes of 3-D MEA (b) MEA60 106

Figure 5.1 Sharp SU-8 microneedles 110

Figure 5.2 Side opening of fluidic channels 111

Figure 5.3 Conceptual view of microneedle arrays for brain slice culture 113

Figure 5.4 Fabrication sequence 114

Figure 5.5 RIE etching procedure 116

Figure 5.6 Two steps of inlet of fluidic channels 118

Figure 5.7 (a) Microneedle arrays on circular SU-8 substrates (b) Fluidic channels inside microneedles 119

Figure 5.8 Insertion test of microneedle array (a) gold coated needle (b) parylene coated needle (c) bare SU-8 needle (d) perspective view of (c) 120

Figure 5.9 Fluidic perfusing system for brain slice culturing 121

Figure 5.10 (a) Conceptual side view of a culturing dish with imaging planes (b) Confocal microscope images from non-perfused tissue (c) perfused tissue 124

Figure 5.11 Metal coated microneedle array with different size of diameter of side openings: (a) 50 μm (b) 20 μm (c) 10 μm 127

Figure 5.12 metal coated microneedle array 127

Figure 5.13 Surface of porcine skin after insertion and removal of microneedles *in vitro* 128

Figure 5.14 (a) A microneedle array and its manifold pump connection shown next to a US penny. (b) Schematic design of the microneedle array with manifold pump connection. 128

SUMMARY

The objective of this research is to develop a three-dimensional (3-D) microfluidic/ electronic interface system for sustaining and monitoring 3-D neuronal networks. This research work is divided into two parts. One is the development of a 3-D multi-electrode array (MEA) with integrated microfluidic channels. The other is a microneedle array with embedded microelectrodes and microfluidic channels.

The 3-D MEA is composed of three elements that are essential for the development and monitoring of 3-D cultures of neurons. These components consist of scaffolds for cellular growth and structural stability, microfluidic channels for cell maintenance and chemical stimulation, and electrodes for electrical stimulation and recording. The scaffolds facilitate the development of focal contacts by which the cells can adhere to the substrate and provide structural pathways by which the cells can make synaptic connections to each other. Two kinds of scaffold structures have been fabricated. The first scaffolding scheme employs a double exposure technique that embeds SU-8 towers into an SU-8 substrate. The second scaffolding mechanism introduces interconnects between towers for the purpose of mechanically supporting 3-D cell cultures and facilitating 3-D synaptic connections. Microfluidic channels are combined for fine control of the cellular microenvironment by means of diffusive and convective fluidic processes. Hollow towers with three-layer side ports were developed by using double exposure techniques and excimer laser ablation. Because no micro-assembly is required, these simplified fabrication methods save several steps in the fabrication of microfluidic channels compared to conventional micro-machining technologies. The electrodes are combined into an integrated system that is capable of monitoring electrical activities and

the cellular impedances of neurons which are attached to the electrodes. The integration of fluidic channels and electrodes makes it possible to investigate cellular adhesion, motility and proliferation.

The second part of this research is to fabricate a microneedle array for monitoring brain slices, which will directly detect electrical signals from living brain slices. Although the microneedle array is targeting different 3-D neuronal networks, it also has three components and the fabrication steps are the same as those for the 3-D MEA. The only structural difference is the sharp, needle-like shapes of the scaffold for penetrating the brain slices. To generate the sharp tip, isotropic reactive ion etching (RIE) is performed on tapered SU-8 towers. High aspect ratio tower structures can be effectively generated with SU-8 and tapered shapes are created by backside exposure.

The resulting systems will enable a new field of neurobiological research, in which the collective properties of 3-D neuronal circuits can be observed and manipulated with unprecedented detail and precision, and at a level of control not possible in living animals.

CHAPTER 1

INTRODUCTION

1.1 Objectives of 3-D Neuronal Interface System

The biomedical and neurological research fields have requested new and advanced diagnostic tools, which allow for the monitoring of electrical activity and chemical responses of neuronal networks. As microelectromechanical system (MEMS) technology has advanced to satisfy neurological requirements, several different kinds of MEAs and fluid delivery devices have been reported for either *in vivo* (within the body) or *in vitro* (outside of the body) investigation of neuronal networks. Wire microelectrodes and glass micropipettes were the first instruments used to monitor electrical responses of single cells. Thereafter, various two-dimensional (2-D) MEAs were generated to extracellularly investigate populations of cells. Finally, microfluidic channels were integrated into MEAs, allowing cell culture systems to monitor responses from fluidic environment changes and chemical reactions by drug delivery [1-3].

2-D neuronal cultures on planar MEAs have become routine for neurological research that investigates everything from learning and memory to cell adhesion and proliferation. However, it is critical to develop cellular systems for *in vitro* measurement that mimic the 3-D *in vivo* environment. Several different cell types have been cultured in 3-D, and significant differences in cellular behavior (e.g. drug resistance, cell signaling, gene expression, and DNA repair capability) have been observed between these 3-D cultures and their 2-D counterparts, indicating that 3-D cultures may accurately mimic *in vivo* responses. In the nervous system, 3-D cultures have been shown to result in longer

neurite outgrowth, higher levels of survival, and different patterns of differentiation as compared to 2-D layers [4-6].

In this research, a 3-D microfluidic/electronic interface system for sustaining and monitoring 3-D neuronal networks is introduced. This research work is divided into two major parts, each part corresponding to a different application. One is the development of a 3-D MEA with integrated microfluidic channels for cultured neuronal networks. The other is a microneedle array with embedded microelectrodes and microfluidic channels for brain slices. Figure 1.1 shows the conceptual view of the 3-D MEA system. It is composed of scaffolds to aid in 3-D cell growth, microfluidic channels to control the fluidic functions, and an electrode array to monitor electrical activities.

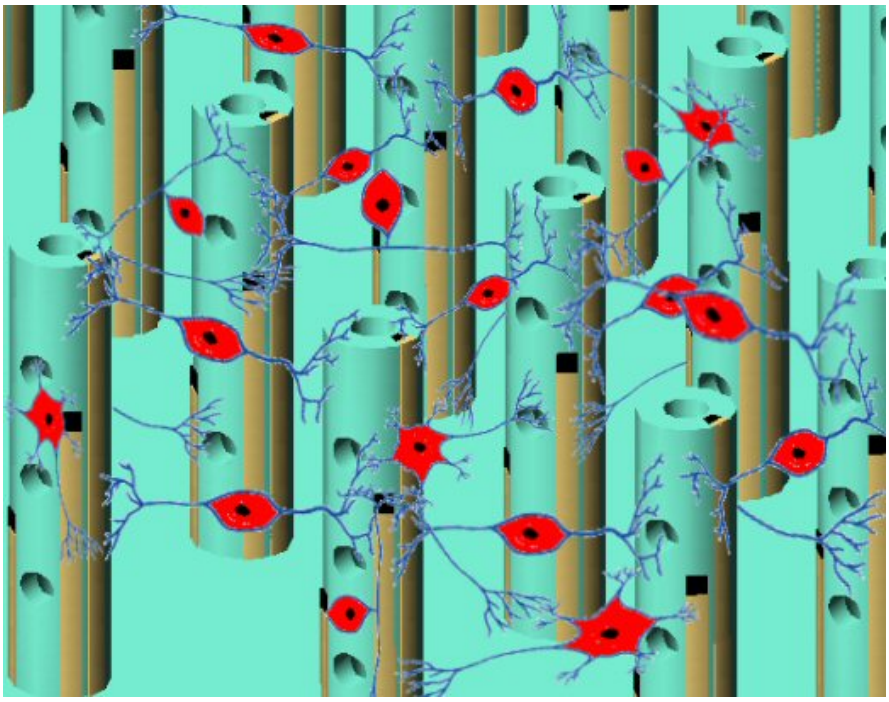

Figure 1.1 Conceptual view of the 3-D MEA including microfluidic channels for 3-D cell culturing.

The scaffolds facilitate the development of focal contacts (or adhesion plaques) by which the cells can adhere to the substrate. The scaffold also provides structural pathways by which the cells can make synaptic connections to each other. For these functionalities, two kinds of tower structures have been fabricated. The first scaffolding scheme employs a double exposure technique that embeds SU-8 towers into an SU-8 substrate. This method allows for aspect ratios to approach up to 35:1, and it successfully addresses typical adhesion and stability problems that occur between SU-8 and the substrate (SU-8 towers on a glass substrate will collapse with the slightest perturbation). In order to optimize the cellular scaffolds, high aspect ratio SU-8 tower structures on SU-8 substrates were made with a variety of substrate thicknesses, tower diameters, and center-to-center distances. The second scaffolding mechanism introduces interconnects between towers for the purpose of mechanically supporting 3-D cell cultures and facilitating 3-D synaptic connections. This method requires an ICP-etched silicon mold, and the proposed assembling method makes it possible to generate complicated scaffold structures.

Microfluidic channels are combined with inclined and vertical towers for fine control of the cellular microenvironment by means of diffusive and convective fluidic processes. Hollow towers with fluidic, three-layer side ports were developed by using double exposure techniques and excimer laser ablation. Because no micro-assembly is required, these simplified fabrication methods save several steps in the fabrication of microfluidic channels compared to conventional micro-machining technologies. Furthermore, this technology potentially allows for batch processing and mass production.

Finally, the 3-D electrodes and fluidic hollow towers are combined into an integrated system that is capable of monitoring electrical activities and the cellular

impedances of neurons which are attached to the electrodes. The 3-D electrodes have been generated on 3-D scaffolds and 3-D fluidic systems. Electroplated metal lines can be placed anywhere on the 3-D structures by conformal parylene coating and excimer laser ablation. After making the 3-D scaffolds or fluidic towers, a copper seed layer and parylene are conformally coated on the whole surface, followed by electroplating molds that were patterned by an excimer laser. 700 μm elevated 3-D electrodes could be patterned due to the good directionality of the excimer laser. The integration of fluidic channels and electrodes makes it possible to investigate cellular adhesion, motility and proliferation as well as analyze some electrical signals from neurons.

The second part of this research is to fabricate a microneedle array for monitoring neural networks in living brain slices. There are two structural requirements (fluidic channel, sharp needle) to keep brain slices living and detect some electrical signals from them. The fluidic channels are useful for specific drug delivery applications but those are not necessary in cultured cell networks, since nutrients can be directly applied on the culturing dish with pipettes. It is, however, hard to supply nutrients to the neurons deep inside brain slices because the living tissue of the brain slices is a strong barrier for any chemical to penetrate inside them. The other requirement for this application is the needle shaped structures to insert into brain slices. Without sharp tips, the MEA can be broken or the brain slice tissues can be damaged. To satisfy these requirements, a microneedle array including 3-D electrodes and fluidic channels is developed in this research. Figure 1.2 shows the conceptual view of the microneedle array.

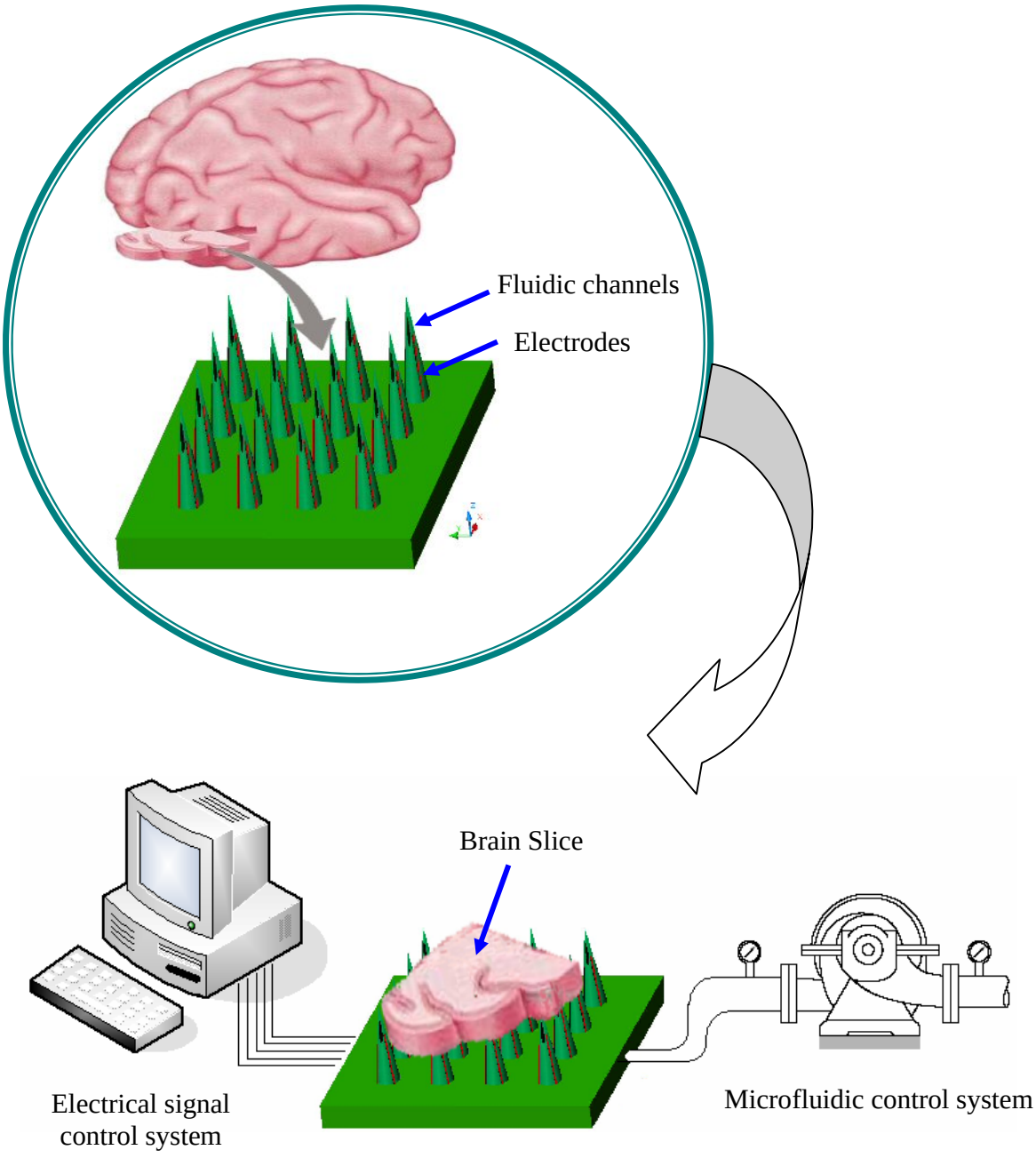

Figure 1.2 Conceptual view of the microneedle array including microfluidic channels and microelectrode arrays.

Although the microneedle array is targeting different 3-D neuronal networks, it also has three components and the fabrication steps are the same as those for the 3-D MEA. The only structural difference is the sharp needle shapes of the scaffold for penetrating the brain slices, instead of scaffolds for 3-D cell culturing. To generate the sharp tip, isotropic reactive ion etching (RIE) is used with tapered SU-8 towers. High aspect ratio tower structures can be effectively generated with SU-8 and the tapered-towers can be made by backside exposure. Although isotropic RIE etching of SU-8 towers are similar to silicon microneedle processing, the process time is just 5 to 10 minutes which is one or two orders of magnitude less than silicon processing. Since these microneedles are made of epoxy, it is easy to control the etching rate as well as benefiting from the relatively faster processing time compared to silicon processes.

In this research, several 3-D fabrication techniques have been introduced to generate 3-D scaffolds, sharp needles, 3-D fluidic channels and 3-D electrodes. These fabrication methods are not particular techniques for a singular application but general techniques that can be applied to various 3-D structures. Even in this research, there are two different systems that have almost the same fabrication steps.

Figure 1.3 shows the fabrication sequence of both systems comparing two different structures built using the same fabrication steps. The first step is photolithography for generating high aspect ratio tower structures. Hollow and solid towers can be created just by utilizing different mask patterns. Tapered-solid towers are also generated by controlling the exposure energy of the UV light. To make the sharp tips of the microneedles, RIE etching is used on the tapered towers. For fabricating cell culturing systems, this RIE etching step is skipped.

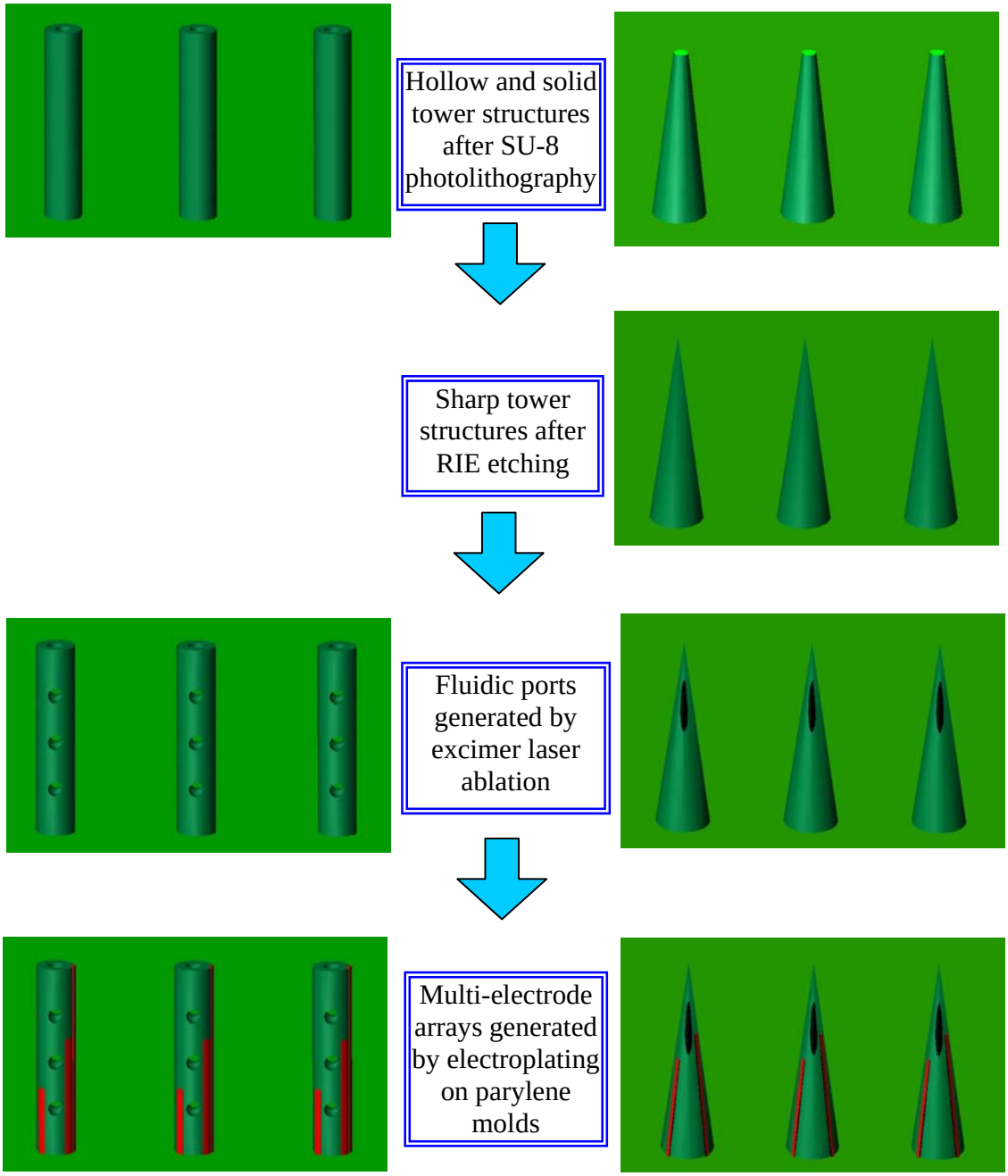

Figure 1.3 Fabrication Sequence

An excimer laser has been used to make the side ports for hollow towers and vertical channels for microneedles. At the last step in the fabrication sequence, the 3-D electrodes are generated by electroplating on laser-patterned parylene molds. The detail of this process will be explained in the following chapters.

The following section describes the cell culturing systems with emphasis placed on action potential measurements and impedance measurements. This will give fundamental biological background for this research. Some 3-D cell culturing methods will be explored with respect to several biological materials, which can be combined with these proposed 3-D monitoring systems. 3-D MEAs, which have been used for implantable *in vivo* applications, will be discussed as well as their limitations as an *in vitro* culturing device. Chapter 2 presents 3-D scaffolds for 3-D cell culturing. High aspect ratio SU-8 tower arrays and 3-D cross-connect scaffold structures are explained. The 3-D fluidic systems are presented in chapter 3. Three different fabrication methods have been used for generating different fluidic applications. 3-D electrodes are outlined in chapter 4. The integrated 3-D MEA with fluidic functionality will be explained in detail, after demonstration of 3-D electrodes on solid tower arrays. In chapter 5, the microneedle arrays are presented. Since all the other processes are the same as those for 3-D MEAs, this chapter details the fabrication of the needle shape and laser-ablated fluidic channels. Finally, conclusions and future works are presented in Chapter 6.

1.2 Cell Culture Systems

The nervous systems of all living things consist of neurons. Nerve tissues, comprised of many associated neurons, are the principal components of the brain and spinal cord. Neurons communicate with each other through electrical pulses, or action potentials, so the ability to read these signals and record them in a computer system holds the promise of new insights into neurological processes. Several research groups have made electrodes that can record action potentials from attached cells to investigate the functionality of neurons.

Wire microelectrodes and glass micropipettes were the first devices used to monitor electrical responses from neurons. Figure 1.4(a) shows a micropipette measuring electrical signals from a neuron [7, 8]. Planar MEAs were developed to extracellularly record these measurements from populations of neurons; these devices improved the possibility for long-term recordings and prevented cell damages that occurred with micropipettes. Figure 1.4(b) shows cultured neurons on a planar MEA [2]. When microfluidic channels were integrated into MEA systems, the ability of the cell culturing system was expanded to allow for monitoring responses from fluidic environmental changes and chemical reactions by drug delivery. Microfluidic channels combined with electrodes are shown in Figure 1.4(c) [9]. Parylene cages used to generate specific cell networks as shown in Figure 1.4(d) [10]. Since the parylene structures were used as barriers, the neurons were fixed in place and only neurites could spread to connect neuronal networks.

Another important electrical property that can be monitored in cultured cell systems is impedance, which makes it possible to observe the effects of cell proliferation

(impedance increase) as well as micromotion of the cells (fluctuations in observed impedance). The impedance can be measured by applying an AC voltage between a small measurement electrode and a relatively big reference electrode in a cultured cell system.

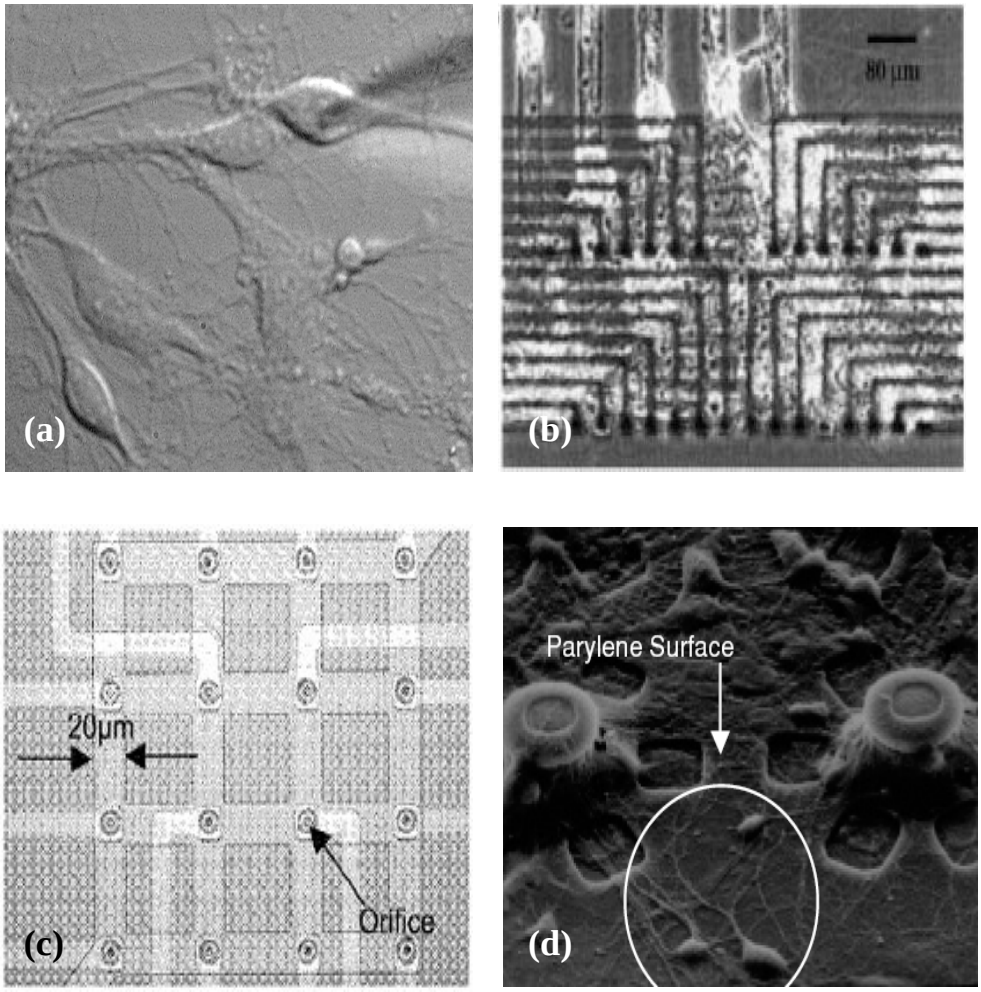

Figure 1.4 (a) Micropipette (b) 2-D MEA (c) 2-D MEA combined with fluidic channels (d) Parylene cages

This method was shown to be extremely useful for examining the attachment, spreading and motion of cultured cell populations. Separation between cell and substrate

and membrane capacitance values could also be monitored using impedance measurements.

Figure 1.5(a) shows an impedance measurement system. Changes in impedance were observed as cells moved over, around and through the pores through the two electrodes, one on the substrate and the other under the substrate [11]. Planar electrodes have also been used for the impedance measurement and the electrical modeling of the electrode as illustrated in the Figure 1.5(b) [12].

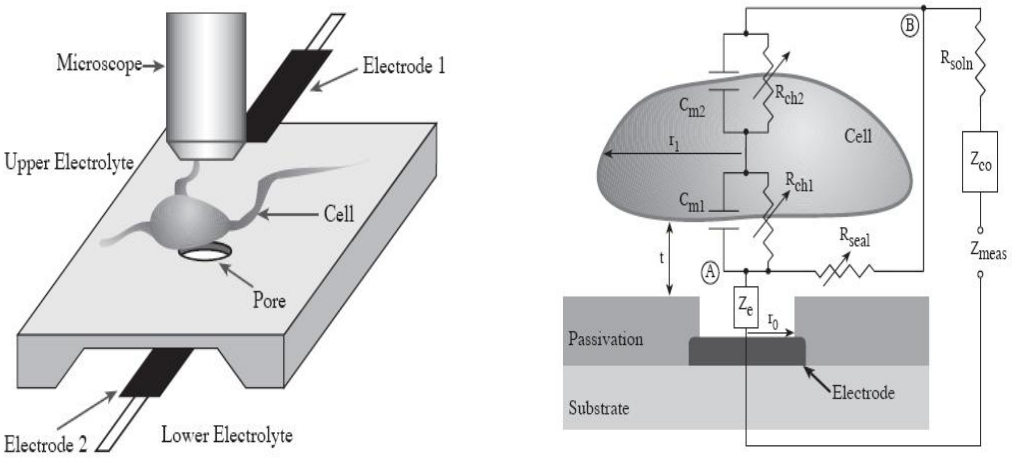

(a) (b)

Figure 1.5 (a) Impedance measurement system (b) Impedance model of a planar MEA

1.3 3-D Cell Culture

3-D cell culturing has been investigated in tissue engineering for generating implantable tissues that can replace the damaged organs in a human body. It is important to develop *in vitro* cellular systems that mimic the 3-D *in vivo* environment as closely as possible. Several methods that employed aggregation, nanofiber, P(PF-co-EG) macroporous hydrogel, and matrigel have been used for 3-D cell culturing. These cell

culture techniques can be incorporated into 3-D MEA devices for monitoring 3-D, *in vitro* neuronal networks. Each of these methods will be explored briefly.

When dissociated cells are suspended in a rotatory culture, the cells collide with the vortex of the culture medium, formed by the rotatory motion of the fluid, and they form clusters (or aggregates). The size of the aggregates formed is a function of a variety of factors, including the speed of rotation of the incubator. Within hours after the formation of the aggregates, the cells sort out by migration, resulting in the construction of histologically identifiable structures, which closely reproduce the essential architectural features of their tissues of origin. Figure 1.6(a) shows rat brain cells in aggregates after 7 days of culture [6, 13-15].

Electrospun 3-D nanofibrous structures are characterized by a wide range of pore diameter distributions, high porosity, high surface area to volume ratio, and morphological similarities to natural collagen fibrils. These physical characteristics promote favorable biological responses of seeded cells including enhanced cell attachment and proliferation *in vitro*. A 3-D nanofibrous poly(ε-caprolactone)(PCL) scaffold was used for 3-D cell culturing as shown in Figure 1.6(b) [4].

For 3-D scaffolds, P(PF-co-EG) macroporous hydrogels were fabricated using a simultaneous gas foaming and free-radical crosslinking approach to entrap the resulting macropores within the hydrogel. Pores were formed by the reaction between L-ascorbic acid and sodium bicarbonate that evolved carbon dioxide. Cross-linking was initiated by a pair of redox initiators, ammonium persulfate and L-ascorbic acid. Figure 1.6(c) shows a cell culturing using P(PF-co-EG) macroporous hydrogels [5, 16-18].

Matrigel, an artificial basement membrane, has been used to induce three-dimensional cell culturing. Cells were mixed with matrigel and reorganized into three-dimensional structures. Several different kinds of cells can be grown in matrigel, and they demonstrate both functional and morphological differentiation and reorganization similar to that of their *in vivo* counterparts. Figure 1.6(d) shows a matrigel structure combined with cultured cells [19, 20].

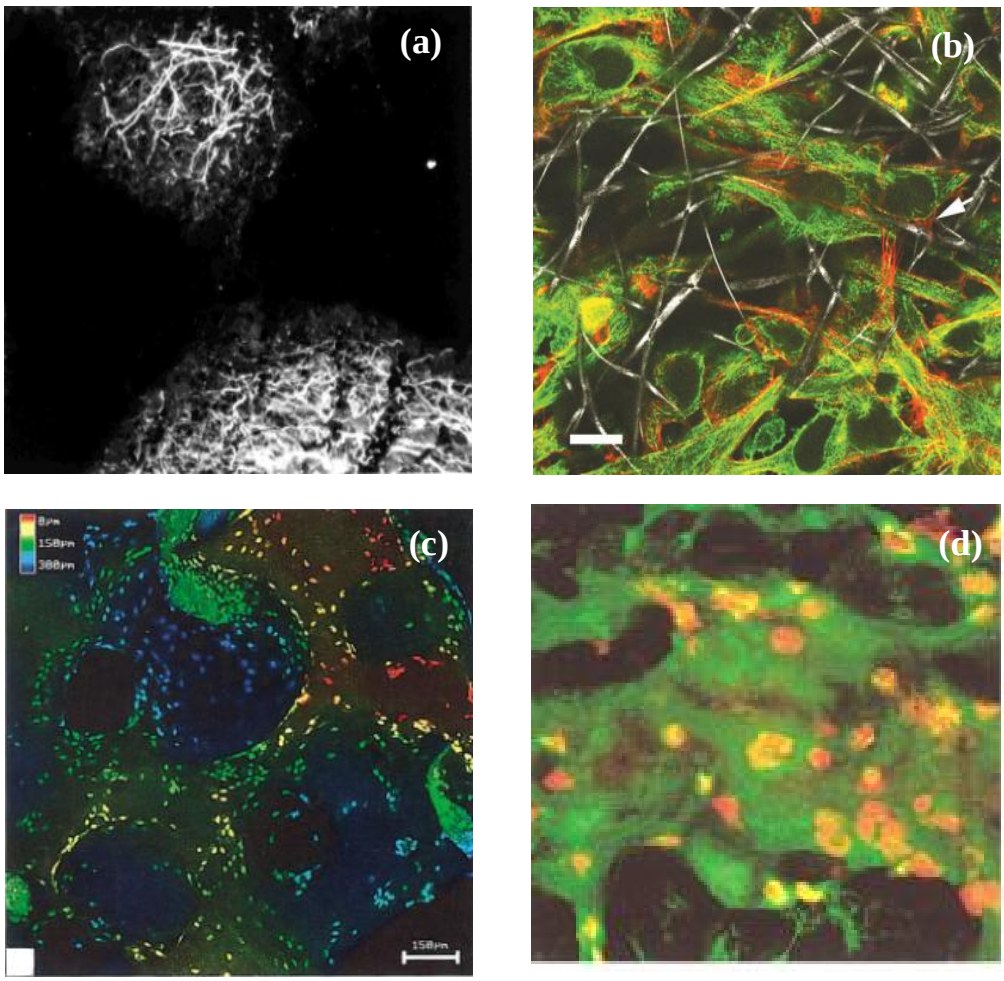

Figure 1.6 (a) Aggregation (b) Nanofiber (c) P(PF-co-EG) macroporous hydrogel (d) Matrigel

1.4 3-D MEAs

Four major types of 3-D MEA have been developed for *in vivo* implantable applications. Although these devices are not suitable for the goal of this research – 3-D microfluidic/electronic interface neuronal culture system – the 3-D concept and various approaches are useful to investigate the 3-D cell culturing systems.

The first commercialized 3-D MEA was introduced by the University of Utah. There are 100 electrodes protruding from a very thin (0.2 mm) substrate. Each needle is electrically isolated from the other, and is about 0.09 mm thick at the base and 1.5 mm long. The main steps in the fabricating process are thermomigration, combination of mechanical and chemical micromachining, metal deposition, and array encapsulation with polyimide. Figure 1.7(a) shows the picture of the electrode array. These needles are remarkably strong and can easily withstand the forces introduced by insertion. However, because the electrodes are generated using thermomigration, each needle can have only one electrode. Furthermore, incorporating with fluidic channels is not possible with this fabrication scheme [21].

A method to machine 2-D probes and assemble a 3-D MEA is provided by the University of Michigan. Figure 1.7(b) shows the overall structure of a microassembled 3-D array. It consists of a micromachined silicon platform with an integrated ribbon cable, a number of 2-D planar probes, and two spacer bars. The probes are inserted into the slots on the platform and are held orthogonally to the platform by the spacers. The most distinguished advantage of this device is that there are several electrodes on each needle so that the array can sample neural signals simultaneously at various locations along the direction of penetration. However the assembling process is tedious and requires a large

time investment. Since the height of the central part of the probe above the platform is 1 mm, the projected part is too thick and displaces a lot of tissue when the whole array is implanted into the tissue. The space bar also makes it difficult to integrate fluidic channels into this device [22].

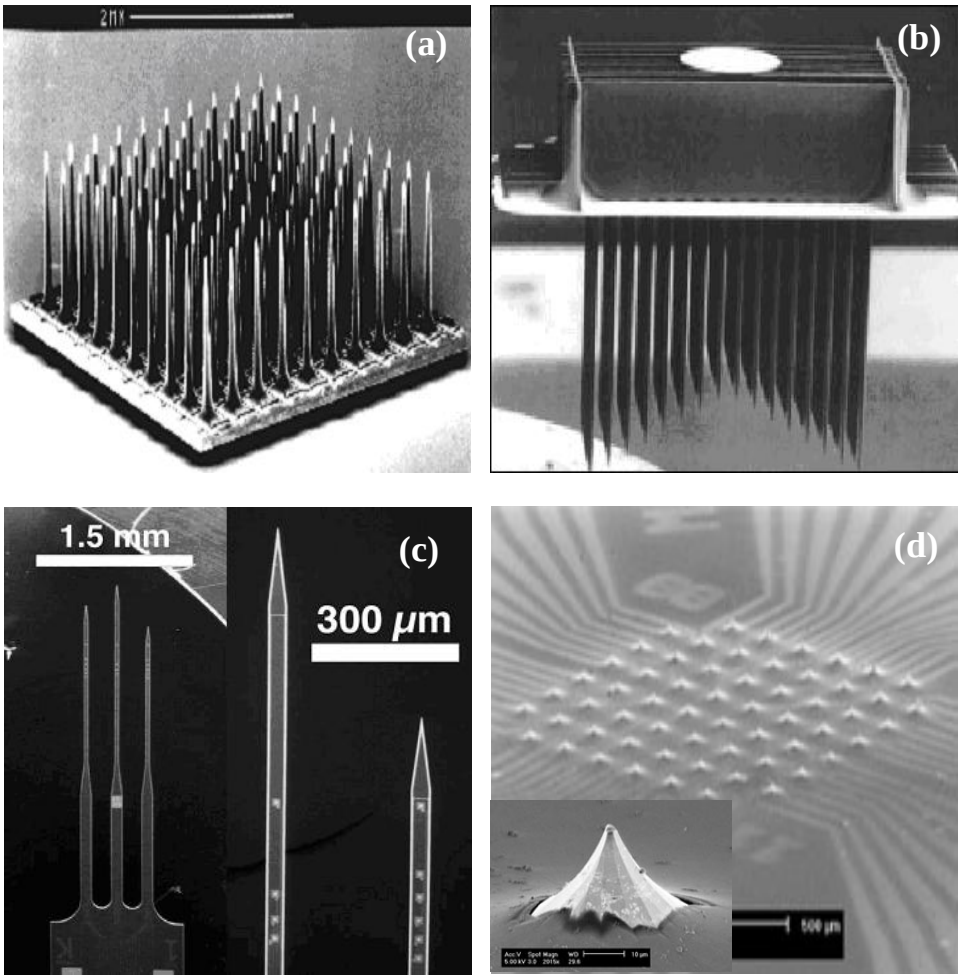

Figure 1.7 (a) 100 MEA (b) Assembled MEA (c) Fork MEA (d) MEA including 3-D electrodes for brain slices

Another type of 3-D MEA is the probe proposed by Stanford University. It consists of one column of needles as a fork shape (Figure 1.7(c)) [23]. There are 16 iridium electrodes near the tips of the shafts. Key features in the fabrication process include a plasma etch to shape the probes, low-stress PECVD silicon nitride film as the insulation layer, and two metal levels for the electrodes and for the interconnect traces. This one column structure can be integrated with microfluidic channels but the limited number of electrodes restricts its range of application.

Recently a 3-D MEA for recording acute brain slice preparations was reported as shown in Figure 1.7(d). However the height of the protruding 3D electrodes is not high enough to generate 3-D cultured neuronal networks [24].

CHAPTER 2

3-D SCAFFOLDS FOR 3-D CELL CULTURING

2.1 SU-8 Tower Arrays on Glass Substrates

2.1.1 High Aspect Ratio SU-8 Tower

The first target of this research was to generate 3-D scaffolds for culturing 3-D networks of neurons. High aspect ratio micromachined SU-8 towers were chosen for these fundamental structures. The photosensitive epoxy SU-8 was particularly suitable because of its mechanical stability, biocompatibility, and potential for high aspect ratio fabrication [25-27].

The *in vitro* culturing of living cells has been used as a valuable technique for examining the properties of different cell types without the limitations of, or reliance on, a living host organism. Moreover, three dimensional neuronal cultures are required to ensure enhanced cellular survival and functionality in networks more representative of tissue-engineered structures and systems [28-31].

A simple example of a scaffold for growth of 3-D cellular networks is an array of high aspect ratio polymeric towers extending normally from an integral polymeric substrate. This configuration facilitates neuronal cell growth on and between the towers in addition to enabling future perfusion through microfluidic channels, as well as electrical stimulation and monitoring via microelectrodes. 3-D cultures may be expected to be more active in modeling the brain because of greater opportunities for connections in the additional dimension. The high aspect ratio structures allow study of thick brain slices (>150 μm), thereby more closely resembling the *in vivo* environment.

A straightforward approach to the 3-D structures would be to form polymeric towers adhered to a glass, polymeric or otherwise suitable substrate. A number of techniques exist to fabricate these structures. For example, a thick photoresist could be cast on a substrate, the towers photolithographically defined, and the photoresist developed to leave polymeric towers adhered to the substrate. Therefore, the photosensitive epoxy SU-8 is a reasonable choice based on its proper characteristics. The first approach of 3-D scaffolds is composed of high aspect ratio SU-8 towers as shown Figure 2.1.

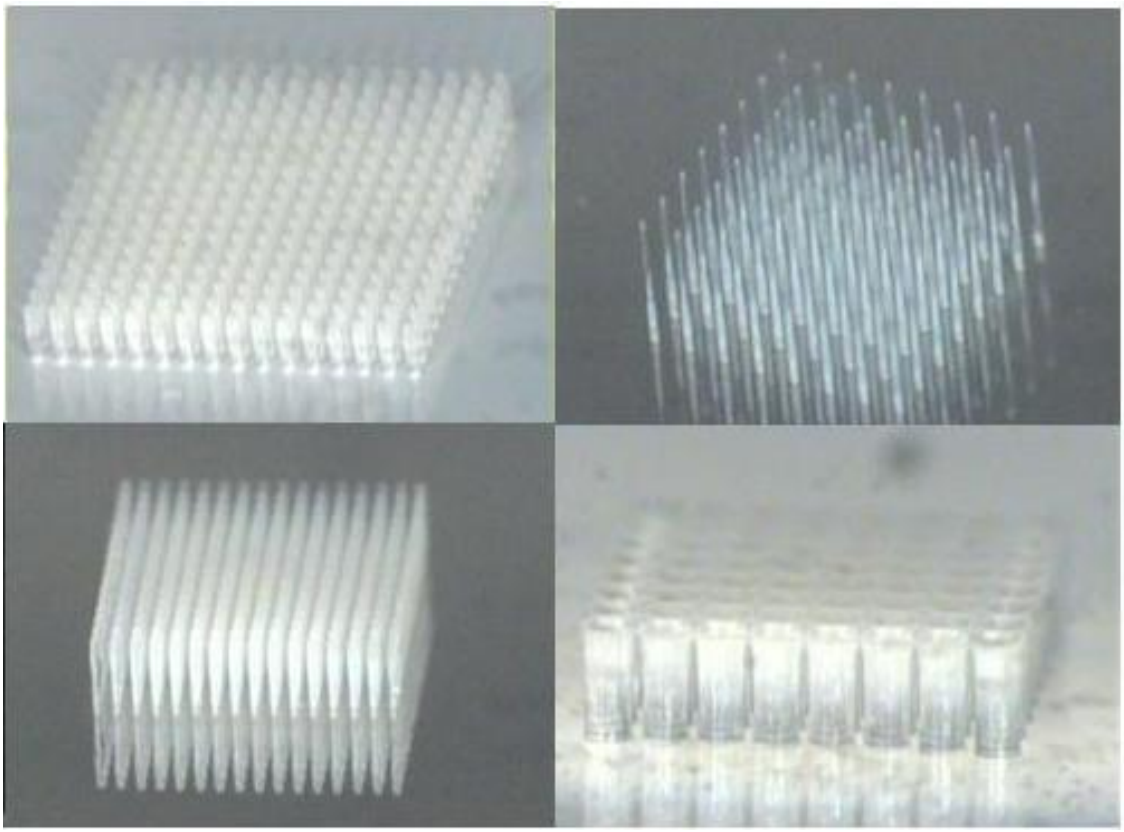

Figure 2.1 Perspective views of SU-8 towers on glass and silicon substrates

2.1.2 Fabrication

Glass and silicon wafers are used for the substrates. To promote adhesion, RIE treatment is used to roughen the substrate surface followed by deposition of a titanium adhesion layer. A 700μm thick layer of SU-8 2025 is applied on a glass substrate by measuring weight. After soft baking (40 hours at 95°C on a hotplate), the sample is exposed with 5000mJ/cm^2 exposure dose. Before developing, post-exposure baking is required for 1 hour at 95°C on a hotplate to crosslink 700μm tall SU-8 towers. The sample is then developed, removing the uncrosslinked regions and resulting in tower arrays on glass substrates. The tower diameters and spacing ranged from 50μm to 250μm. Figure 2.2 shows the fabrication steps. Structural tower arrays of 8 x 8 and 16 x 16 were fabricated and tested as a foundation for cellular culturing of neurons.

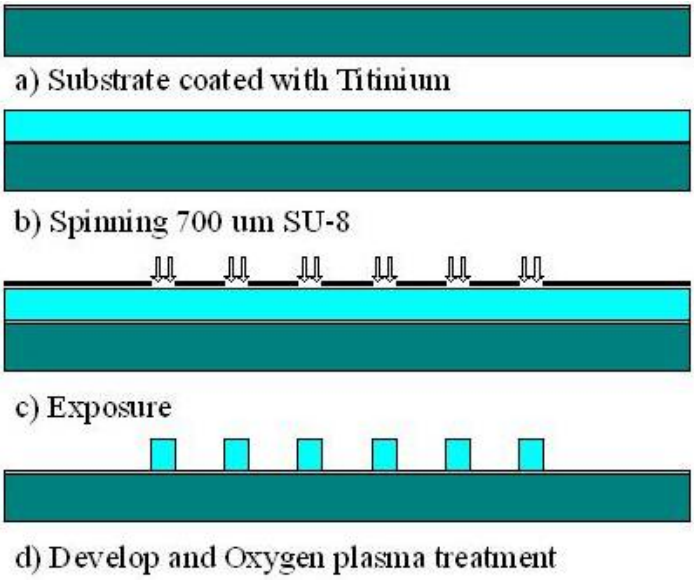

Figure 2.2 Fabrication sequence

2.1.3 Cell Culture

Before delving into detailed explanations of the biological experiments, it should be noted that most of the biological experiment were performed by Dr. Bruce Wheeler's lab at the University of Illinois at Urbana-Champaign, Dr. Gregory Brewer's lab at the Southern Illinois University School of Medicine, and Dr. Michelle LaPlaca's lab at Georgia Tech. The fabrications and material characterizations were performed at the MSMA lab at Georgia Tech. Prior to application of cells onto the tower structures, a sequence of sterilization steps is required to ensure the viability of the neural culture. First, substrates are soaked in ethanol overnight to leach out any potential organic contaminants that can be toxic to cell growth. And samples were dried under vacuum at 90°C for at least 2 hours to remove any solvents that could be remained during the soaking process. The samples are then soaked in a 500 μL of PDL (poly-D-lysine, 0.1 mg/mL in deionized (DI) water, Sigma) for 1 ~ 2 hours. PDL is the most common protein that promotes the cell adhesion. After PDL adsorption, samples are rinsed thoroughly in DI water to remove any unbounded PDL and gently dried with nitrogen gas. Extra care is taken in blow-dry process not to damage the 3-D structures. As a final step, these samples are soaked briefly (20 s) in 70 % ethanol to prevent microbial contaminations and after blow-drying the sample, it is quickly transferred to sterile Petri-dish.

Hippocampal neurons are taken from embryonic day 18 rats, mechanically dissociated and delivered in Hibernate E from BrainBits^{TM} (Brainbits, Springfield, IL). Hippocampus tissues are triturated and plated at a density of 200 cells/mm^2 under serum-free and glia free condition. The cell plating medium is Neurobasal/B27 (Invitrogen,

Carlsbad, CA) containing 25 M glutamate and 0.5 mM glutamine. Plated cells are incubated at 37 C in 9% O_2, 5% CO_2 through the culture. After 4 days, one-half of the medium is changed with Neurobasal/B27 medium containing 0.5 mM glutamine [32].

Several preparing steps are required to take pictures of neurons using SEM. First, half of the media is removed and the culture is rinsed in 1x PBS (phosphate buffer solution, pH 7.4) twice very gentle. Fixative, 4% paraformaldeyde in PBS, is added at room temperature for 20 min. After the primary fixation, the culture is rinsed in a buffer (1x PBS) and dehydrated through a series of ethanol in ascending percentages (25 %, 50 %, 75 %, 100 %).

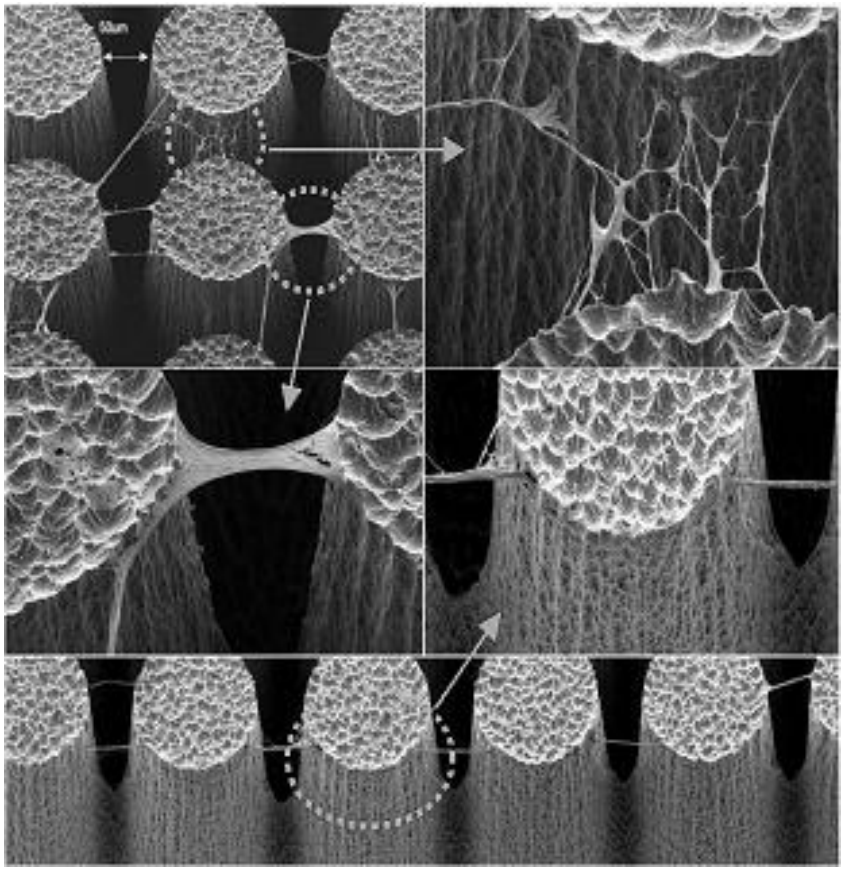

Figure 2.3 Cell bridging in 3-D networks of cultured cells

After ethanol dehydration, the culture is dried by soaking in hexamethyldisilizane (HMDS) for 3 min twice and put in a desiccator under house vacuum for at least 1 hr. Then, it is mounted on an SEM stub with carbon sticky stub adhesive and sputter-coated with gold/palladium for 60 sec. After conductive coating, silver paint is applied to make a ground connection with coated film. Figure 2.3 shows the SEM pictures of 3-D neural cell culture on SU-8 towers.

2.2 SU-8 Towers on SU-8 Substrates

2.2.1 Adhesion of SU-8 Towers on Substrates

Although the SU-8 towers on glass substrates were successfully created and used for cell culturing, the yield rate was less than 50%. The major reason for this failure was due to poor adhesion between the SU-8 and the glass substrates. Since the coefficient of thermal expansion (CTE) of SU-8 is around 30 and the CTE of glass is 10, the poor adhesion cannot be avoided using normal lithography, such as the use of heating and UV exposure. RIE treatments and titanium adhesion promotion layers are helpful, but the yield rate still remains about 30 % for structures that have aspect ratios over 15:1.

The towers structures will be used in a saline solution, and chronic biological studies will be performed on these scaffolds. Therefore the adhesion problem could be a critical barrier for further research that will include various functions on the tower structures. Reliable structures must be created from the onset, and it has been considered that the adhesion between the tower and substrate may not be durable in aggressive (e.g. aqueous and saline) environments. The SU-8 towers are generated on SU-8 substrates for this reason. In this section, a fabrication method is introduced in which towers and

substrate are formed from a unitary polymeric piece, thus eliminating the adhesion problem and providing a 3-D micromachined scaffold particularly appropriate for cell culturing.

2.2.2 Fabrication

Fabrication is effectively simplified by a double exposure technique [25], allowing tower structures and an integral SU-8 substrate to be formed from the same epoxy deposition, thereby addressing column-to-substrate adhesion issues that have traditionally limited the aspect ratios achieved with conventional fabrication techniques. Aspect ratios up to 35:1 have been achieved, and successful cell culturing has been demonstrated.

The fabrication sequence is summarized in Figure 2.4 and begins with patterned chromium on a glass mask as a temporary substrate. A one-millimeter-thick layer of SU-8 2100 is spun on the patterned chromium side of the mask enabling good contact between the SU-8 and the pattern. The pattern used is a checkerboard later utilized in dividing the completed devices into individual arrays. After soft baking (44 hours at 95°C on a hotplate), the sample is exposed to a relatively (5000mJ/cm2 for a 700μm thick film) low exposure dose (200mJ/cm2) from the bottom through the glass plate to cross-link a 300μm thick SU-8 plateau (still embedded in unexposed SU-8 film) immediately adjacent to the transparent portions of the underlying chromium mask. Prior to developing, the sample is exposed from the top using a large exposure dose (5000mJ/cm2) through a tower mask to crosslink 700μm tall SU-8 towers. Then, post-exposure baking is required for 1 hour at 95°C on a hotplate to crosslink exposed SU-8 towers and substrates.

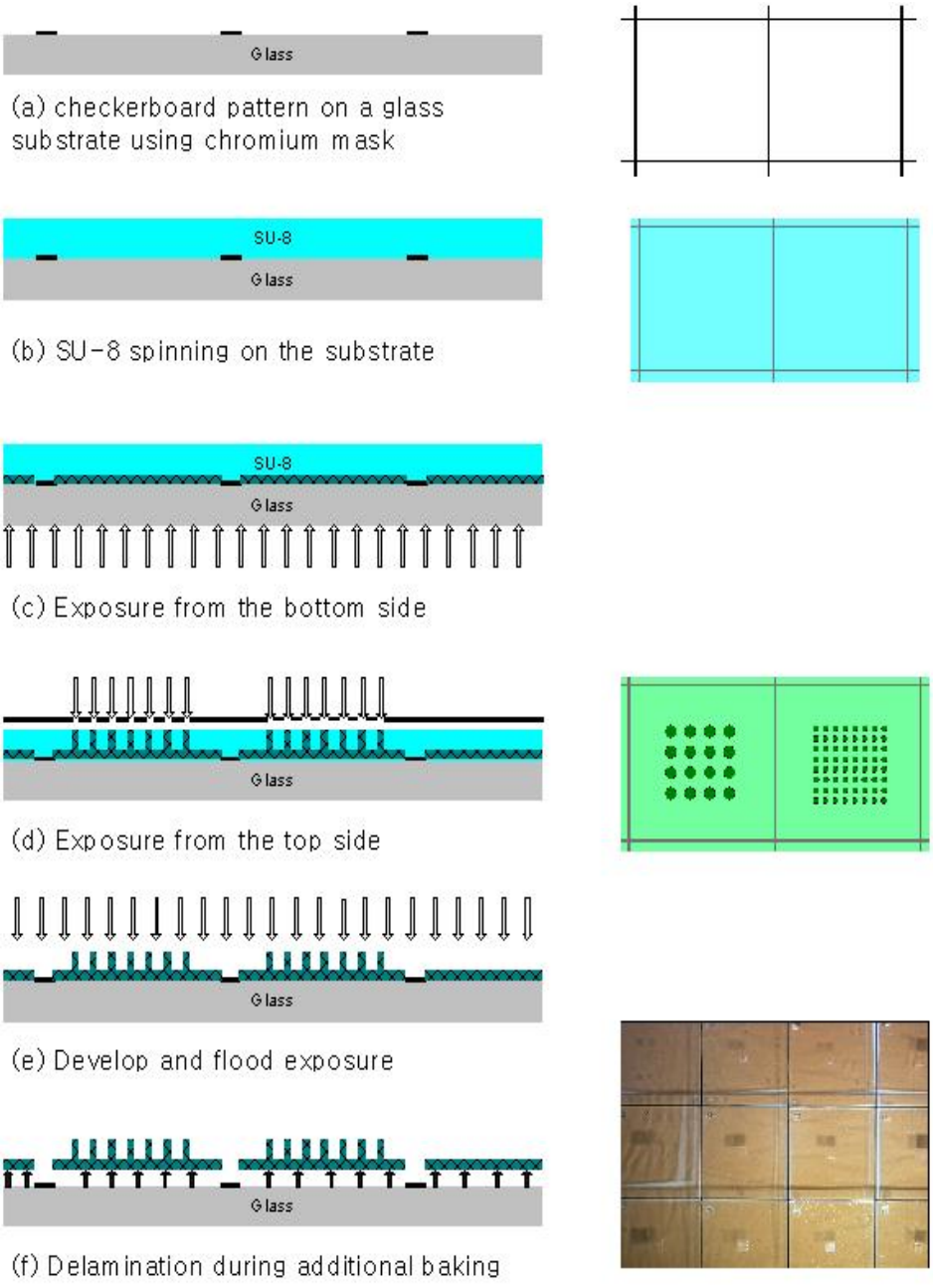

Figure 2.4 Fabrication sequence

After development, a topside flood exposure is performed to further solidify the structure. Individual arrays suitable for culturing are then formed by separation of the individual tower-bearing polymeric substrates from the glass mask via an additional bake at 95°C for 40 minutes.

Structures over 700 μm tall with aspect ratios as high as 35:1 have been fabricated. Arrays of 8 x 8 and 16 x 16 towers with tower diameters ranging from 20 μm to 200 μm and edge-to-edge tower spacing ranging from 100 μm to 225 μm are fabricated using the technique outlined above. Figure 2.5 shows a top view of the completed SU-8 towers, while Figure 2.6 shows SEM views of a variety of fabricated geometries.

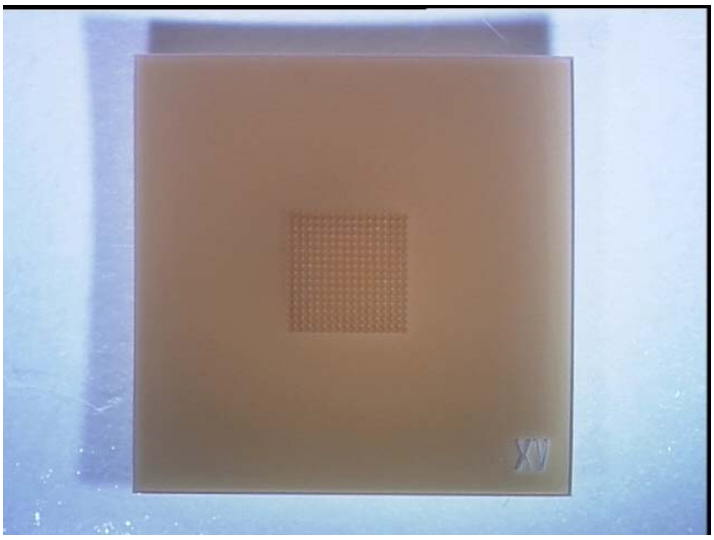

Figure 2.5 Top view of the SU-8 tower

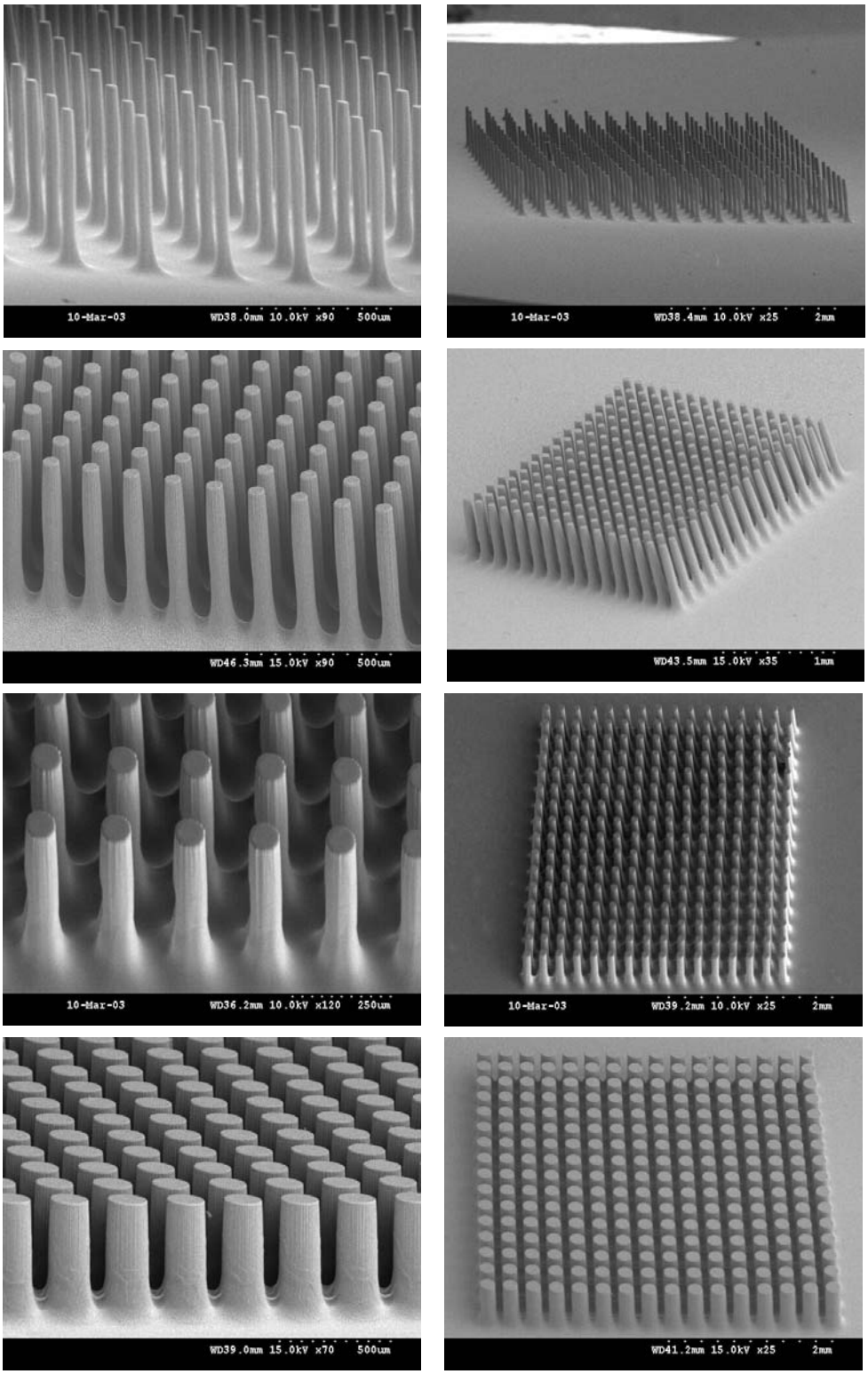

Figure 2.6 SEM views of a variety of fabricated geometries

2.2.3 Cell Culturing on SU-8 Tower Arrays

This section describes how the SU-8 tower based substrates were tested for cell culture. Sterilization, detoxification, and surface treatment schemes were investigated for optimal biocompatibility before the ones used in this cell culture study were selected for cell culture.

First, the substrates were detoxified by dry heating at 110°C for three days, then by wet heating in DI water at 45 °C for one day, followed by a one hour drying at 45°C in an oven. Once dry the surfaces were sterilized under UV light for 2 hours. After sterilization, the surfaces were incubated in a poly-L-lysine solution 0.005%, M.W. 70,000 ~ 150,000 Daltons (Sigma Chemical Co., St. Louis, MO), at 37°C in an incubator for 1 day, at the end of which the poly-L-lysine coating solutions were aspirated.

Surfaces prepared in the above manner were seeded with embryonic day seventeen primary cortical neurons at a seeding density of 900 cells/mm^2. All procedures involving animals were done in accordance with the Georgia Institute of technology Institute Animal Care and Usage Committee. The cells were plated in Neurobasal Medium supplemented with 2% B-27 (both from Invitrogen Corporation, Carlsbud, CA) and 500 μM L-Glutamine (Cellgro, VA). The first media change was done 1 day post plating by removing half the media and replacing it with 1.25 times fresh media. A similar media change was done approximately every 5 days until day 20 when a terminal live-dead assay (Live/Dead Viability/Cytotoxicity Kit, Molecular Probes, Eugene, OR) was performed.

Figure 2.7 , A and B show phase contrast microscopy images (Nikon Eclipse TE 300) after 1 day of culture on the polystyrene control (6-well cell culture plate, Corning

Incorporated, Corning, NY) and SU-8 substrates respectively. Both figures A and B show neurons having formed cell processes

Figure 2.8(a) and (b) show fluorescent microscopy pictures after twenty days of neural culture on the same two surfaces. In both A and B, the bright green colored (punctate) spots are the neuronal cell bodies and the green meshwork (diffuse) are the neural processes. Microscopic imaging on SU-8 substrates is challenging because of an apparent auto-fluorescent property of SU-8. As can be seen, the neurons were viable in a network around the towers even after 20 days in culture on the SU-8 surfaces, indicating the potential of these structures for use in MEMS based 3-D neural interfaces.

Using those techniques, we have developed a specialized process for fabricating micro-scaled SU-8 structures, and detoxifying, surface coating and sterilizing them for use in neural cell culture applications.

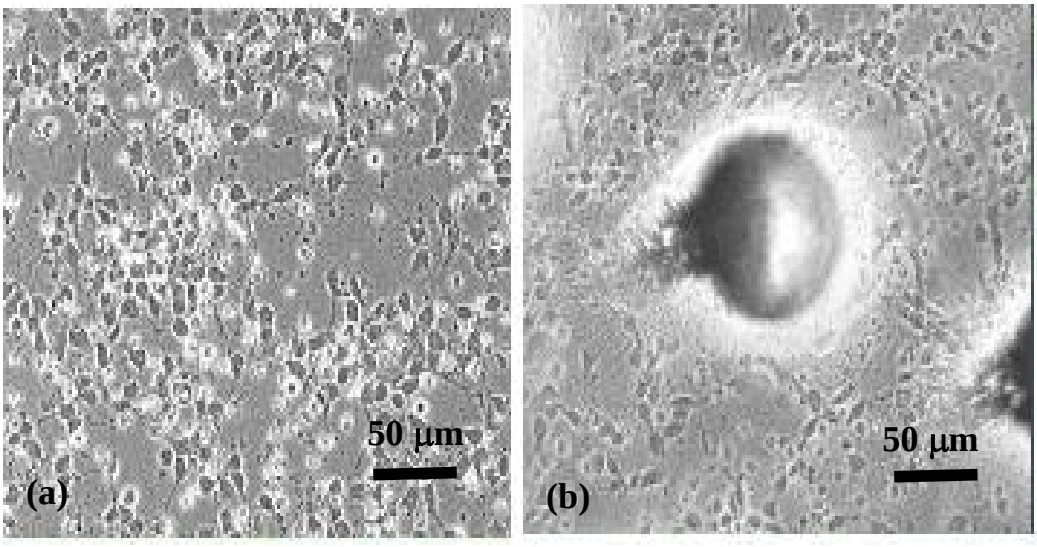

Figure 2.7 Phase contrast microscopy (200X magnification) of neural culture (a) on a polystyrene control and (b) around a tower on a SU-8 substrate

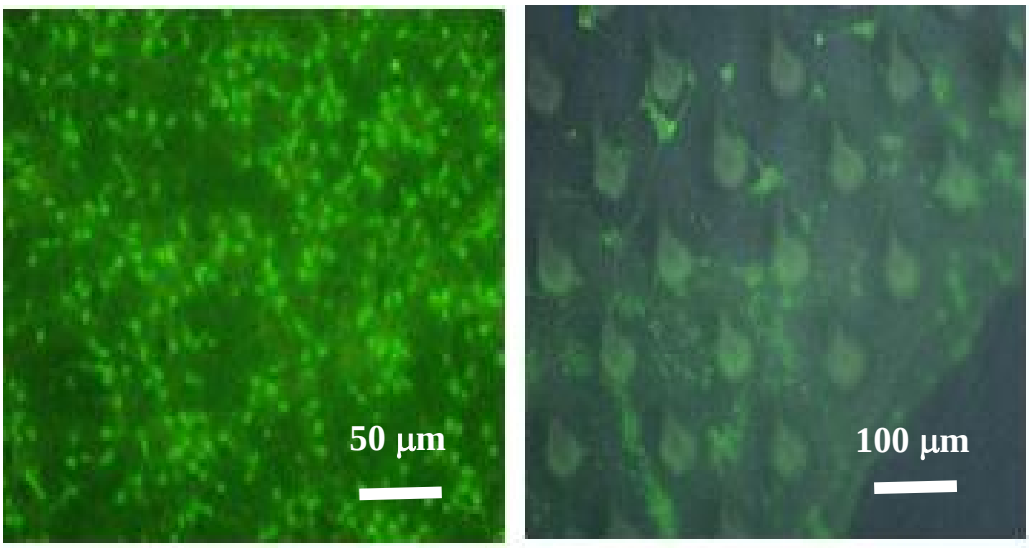

Figure 2.8 Fluorescent images of neural culture on a polystyrene control (left) at 200X magnification and around a set of tower on a SU-8 substrate (right) at 100X magnification.

2.3 Cross-Connects with Towers

2.3.1 Micro-Assembly

An advanced structure of scaffolds introduces cross-connects between towers for the purpose of mechanically supporting 3-D cell cultures [33-36]. These 3-D scaffolds consist of high aspect ratio SU-8 towers and cross-connects, which were combined by micro-assembly [37, 38]. Several dimensions of towers and cross-connects have been tested to find optimal structures of scaffolds for cell culturing. 500 ~ 700 μm height and 50 ~ 250 μm diameter towers were used for neuronal culturing first. Then, to promote 3-D culturing, 20 ~ 100 μm width cross-connects were combined with towers. A micro-assembly technique was proposed to make a complex set of scaffolds from a single tower

and cross-connect array. Hippocampal neurons of rat embryos have been cultured on the developed structures and showed the various neuronal connections between cultured neurons.

2.3.2 Fabrication

Figure 2.9 shows the fabrication sequence which has two layers of SU-8 structures. A 20μm thick layer of SU-8 2025 is spun on a glass substrate and the tower and associated SU-8 substrate patterns are subsequently exposed. After post-baking to cross-link the exposed area, an additional 300μm thick SU-8 layer is added without developing the first layer. This additional layer serves as a basis for the cross-connect pattern and extends the substrate. The cross-connect and extended substrate patterns are exposed and post-baked to cross-link the patterns. Finally, all layers of the sample are developed simultaneously.

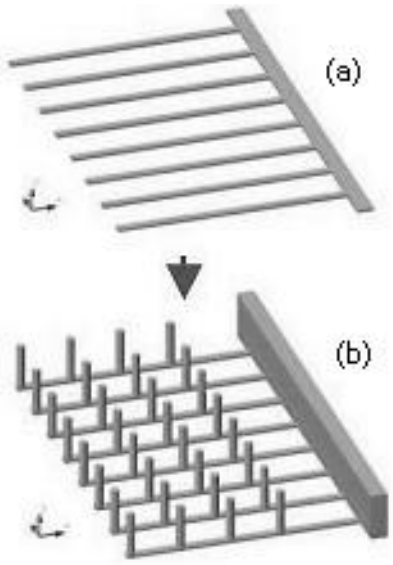

Figure 2.9 Fabrication sequence

Individual structures with cross-connects are separated from the substrates as shown in Figure 2.10. These individual structures are then consecutively placed in an ICP-etched silicon mold as seen in Figure 2.11. Although this assembly has been performed by hand, the size of the SU-8 bar which was generated with cross-connect structures during photolithography is big enough to integrate into an automated assembly system, if necessary. Figure 2.10(b) shows a 10 x 0.3 x 0.3 mm, SU-8 bar which has 10 μm diameter, 300 μm length cross-connect scaffolds. There is a big recess in the silicon mold as shown in Figure 2.11(a). The 10mm long SU-8 bars are aligned inside of the 10mm x 10mm recess and the tiny cross-connect structures fit in the 4mm x 4mm center holes.

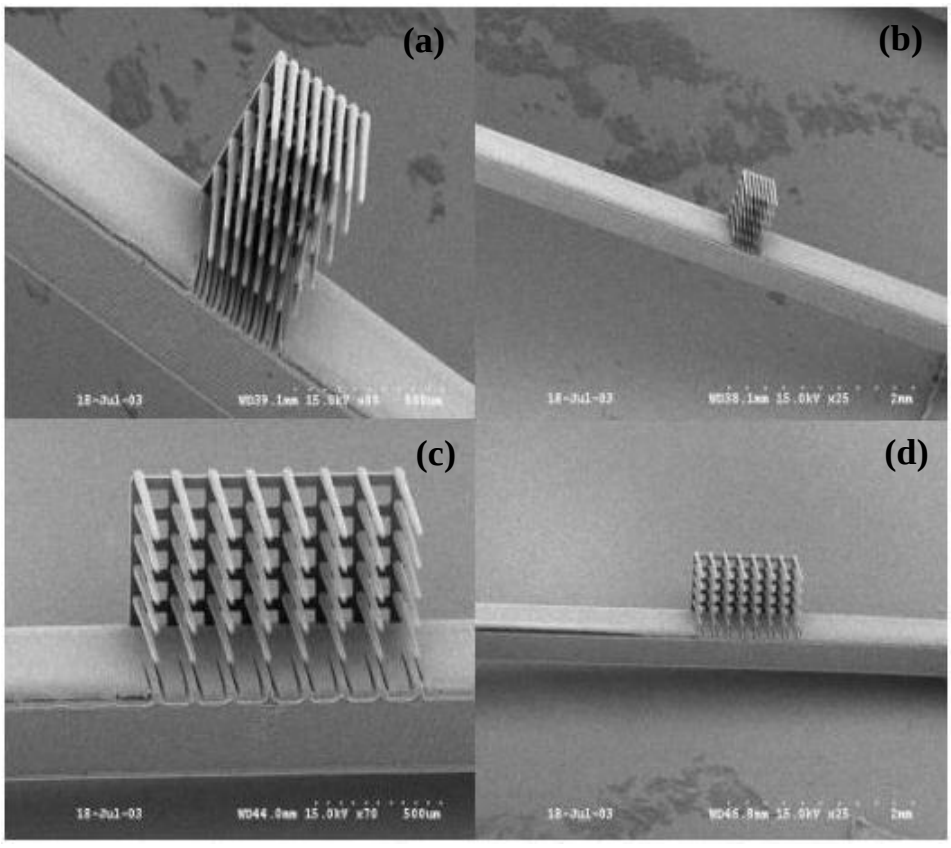

Figure 2.10 Individual structures with cross-connects

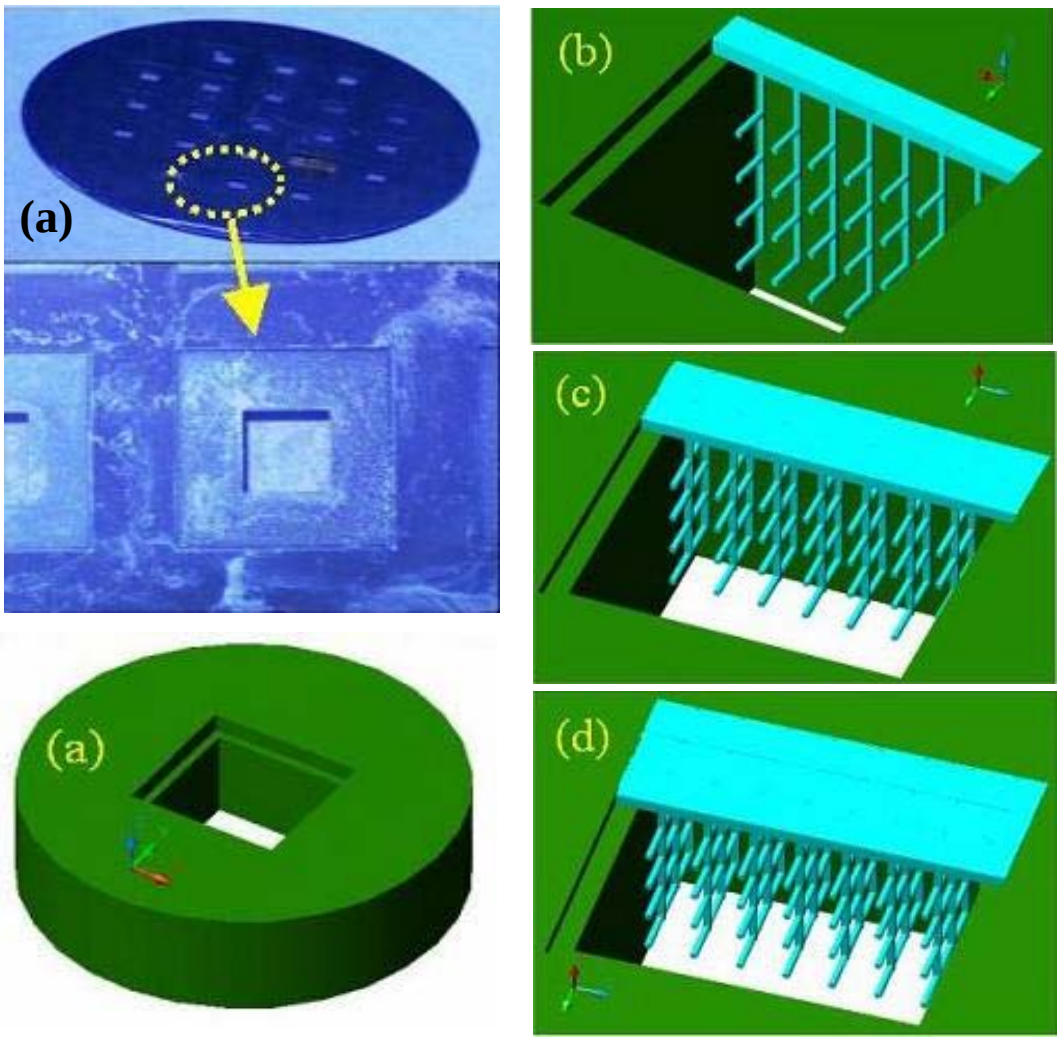

Figure 2.11 Assembly sequence

After filling the mold with individual structures, a thin bonding layer of SU-8 is spun on and patterned into squares. To augment biocompatibility, a thin layer of parylene is then coated over the entire surface. Figure 2.12 shows the completed tower structures which were combined with cross-connects. Different combinations of scaffolds are possible by placing various shapes and number of cross-connect and vertical towers

together. For examples, Figure 2.12(a) shows four columns of individual scaffolds that are combined and Figure 2.12(c) shows three columns of individual scaffolds that are bonded together. Different spacings of cross-connects can be realized as shown in Figure 2.12(c) and Figure 2.12(d)

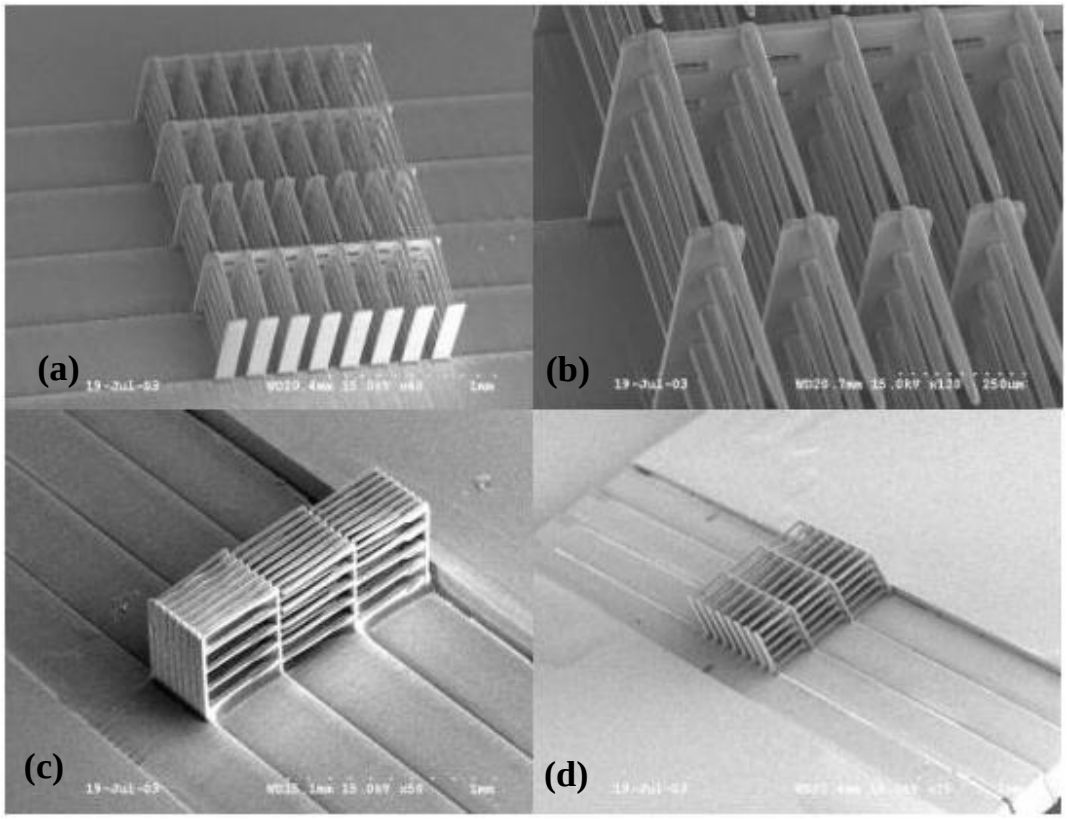

Figure 2.12 SEM picture of completed cross-connect scaffolds

2.3.3 Cell Culturing

Figure 2.13(a) shows the perspective overall view of 3-D structures with neurons growing on the surface. Two neurons that are well spread and attached to the round shaped surface can be seen in the inset. The outgrowth of neurites is very healthy and

presumably making connections between each other. Due to the low plating density, there are a few cells available for each bar. Some cell process bridging the edge and make web-like connections in Figure 2.13(c). At the left top corner, there is a healthy neuron attached to the vertical wall. One can see growth cones in this cell. Figure 2.14(d) shows neurons growing healthy on flat SU-8 surface beside the 3D structure. The status of the culture was judged by observing the cell growth in this region. Figure 2.13(a) ~ (d) were taken by SEM while Figure 2.14(a) ~ (d) were made by transmitted light microscopy (phase contrast).

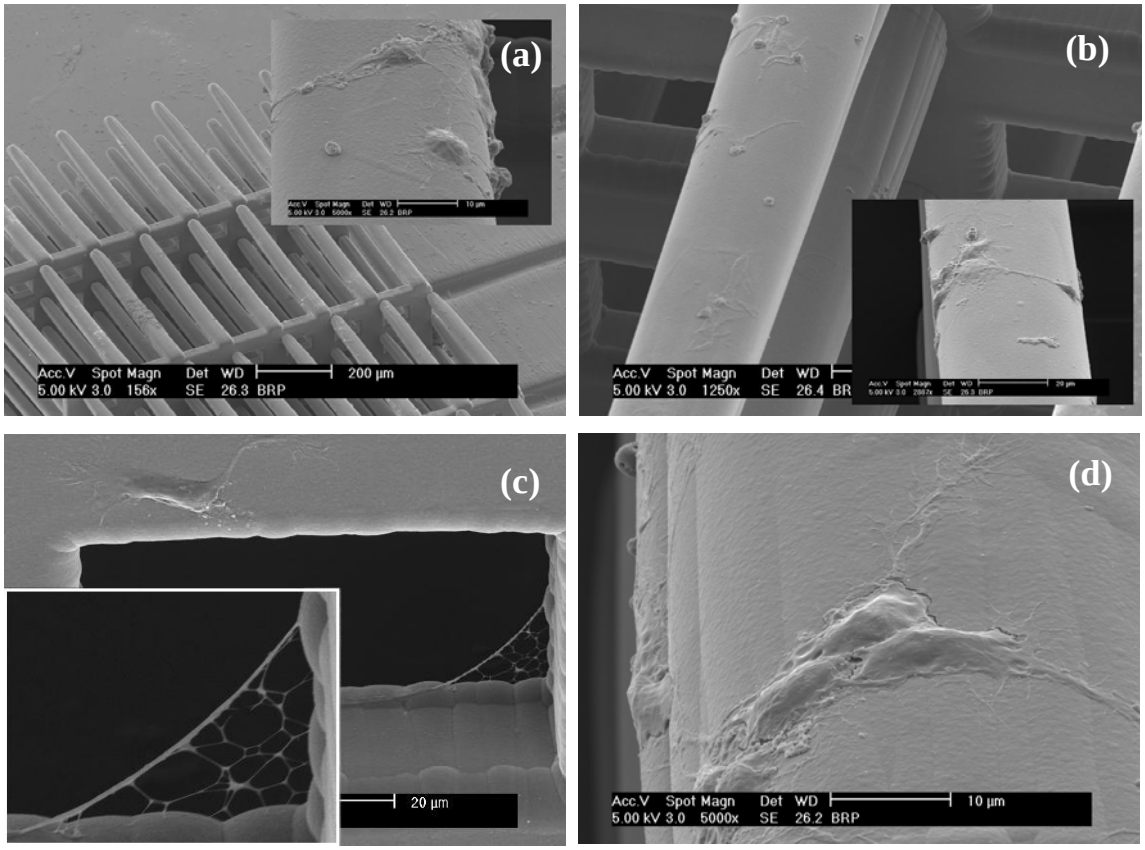

Figure 2.13 SEM pictures of cultured neural networks on cross-connects

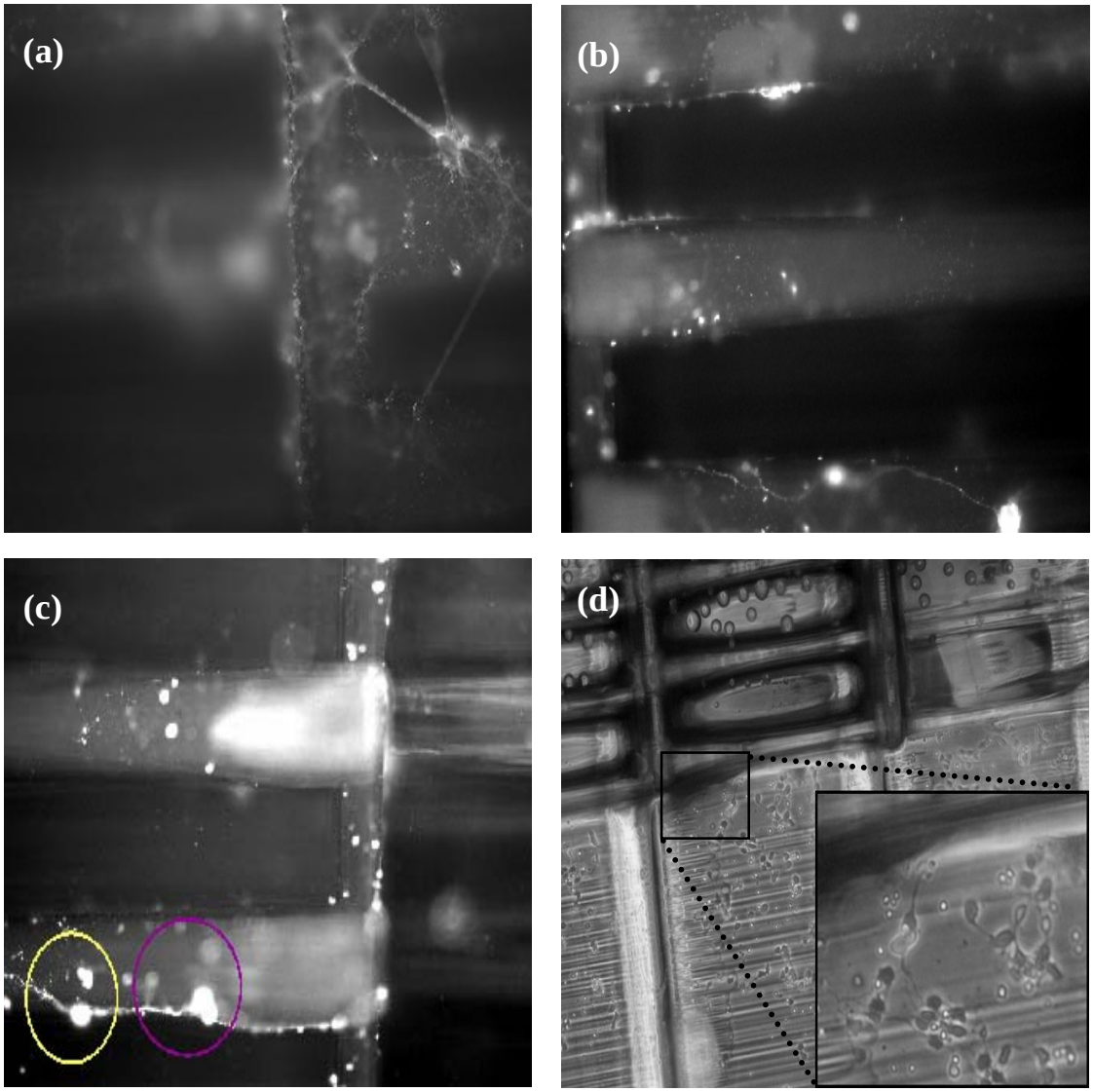

Figure 2.14 Phase contrast microscopy pictures of cultured neural networks on cross-connects

2.4 Cytotoxicity Test of SU-8

2.4.1 SU-8 Bits

As the fields of BioMEMS and microfluidics have expanded to include broader areas, SU-8 has become an attractive material to implement various structures for applications within these areas of research because of its powerful properties - mechanical stability, transparency, and potential for high aspect ratio fabrication. Although SU-8 has been used as a thick insulation layer for several MEAs, even for some commercial products, the cytotoxicity (the quality of being poisonous to cells) of SU-8 has not been widely published. Since SU-8 was used as the basic fabrication material in this research work, systematic investigation of SU-8 cytotoxicity was required. This is especially true given that the thicknesses of SU-8 devices developed in this thesis are large compared with previous devices. A simple SU-8 structure was chosen to concentrate on cytotoxicity. 1cm x 1cm square SU-8 pieces were made of various thicknesses. Eight different combinations of treatments were selected to find optimal protocols for reducing the cytotoxicity of SU-8. In this cytotoxicity research of SU-8, the cell culturing and analysis have been performed by Dr. Michelle LaPlaca's lab in Georgia Tech.

Figure 2.15 shows the fabrication sequence of the SU-8 pieces. A 1 μm thick sacrificial layer of copper was coated on a glass substrate by a DC sputterer. Then a 100 μm thick layer of SU-8 2025 was spin-coated at 500 rpm on the same substrate. After soft baking the spin coated SU-8 for 2 hours at 95°C on a hotplate, the SU-8 sample was exposed to a 500 mJ/cm^2 UV exposure dose through a mask to cross-link the exposed 100 μm thick SU-8 plateaus. The mask had a checkerboard pattern which helped in

dividing the large substrate into arrays of smaller individual substrates of 1cm x 1cm size. Following the UV exposure the SU-8 substrates were post-baked on a hotplate at 95°C for 30min. The sample was then developed using PGMEA, removing the uncross-linked regions and resulting in 100μm thick SU-8 plateaus separated by the checkerboard pattern. The individual structures were separated by immersing the SU-8-sample-carrying glass substrates in an etching mixture of 33% water, 33 % sulfuric acid and 33% hydrogen peroxide for 3 hrs with gentle agitation. The released samples were rinsed thoroughly in water and placed for soaking in water for 5 days after which they were rinsed again with water and dried. After de-lamination, the samples were ready for the various detoxification treatments.

(a) SU-8 spin coating on a copper covered glass substrate

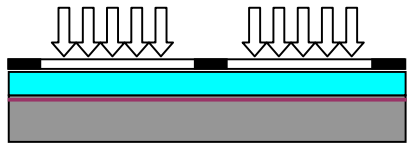

(b) After soft baking, exposure with a checkerboard pattern

(c) After post baking, developing with PGMEA

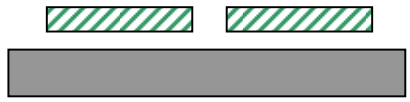

(d) Delamination after seed layer removal

Figure 2.15 Fabrication procedures for SU-8 bits

2.4.2 Detoxification Treatments

Detoxification treatments included UV exposure (90J/cm^2), 30 minute soaking in liquid CO_2, and 3 days heating at 150 °C performed either alone or in combination, with the objective of increasing the biocompatibility of the SU-8 structures. The nine detoxification experimental treatments tested in this study are listed in table 2.1. Four SU-8 pieces exposed to a treatment constituted one sample of that treatment. Four such samples were tested for each treatment in the leaching assay.

Table 2.1 Detoxification treatments

1) 150°C, 3 days, vacuum
2) UV, 90 J/cm^2, 365 nm
3) CO_2 , 2~10 °C, 900psi
4) 150°C + CO_2*
5) 150°C + UV
6) CO_2 + UV
7) 150°C + UV + CO_2
8) Untreated SU-8 control
9) Polystyrene control
10) Polystyrene + PDMS control
11) Polystyrene + PDMS + Glass control

* Treatment 1 followed by treatment 3; similar nomenclature for treatment 5, 6 and 7

A quantity of 184 Sylgard elastomer (Dow Corning Corporation, Midland, MI) was added to its hardening agent in a 9:1 ratio. Likewise, a quantity of 186 elastomer (Dow Corning Corporation, Midland, MI) was added to its hardening agent. These two mixtures were then mixed thoroughly 1:1 and filled in a 1ml B-D latex-free syringe.

Using the syringe, approximately 10 µl of the Sylgard paste was applied to fix the SU-8 pieces to the bottom of the six well plates. Two pairs of SU-8 pieces were fixed to each of the wells. The adhesive was cured at room temperature for 48 hours. The six well plates containing the fixed pieces were placed in a Bio-hazard hood, and sterilized with 70 % Ethanol under UV for 30 minutes. After 30 minutes the ethanol was replaced with sterile filtered de-ionized (DI) water and UV treatment was continued for another 30 minutes. Finally the DI water was aspirated off and the samples were dried under UV light for another 60 minutes.

Six well plates prepared in the above manner were seeded with embryonic day seventeen primary cortical neurons. Prior to plating, the chambers were pre-treated with 0.005% poly-L-lysine (PLL, Sigma) (>4 hours). The cells were plated at a culture density of 100,000 cell/cm^2. Cultures were kept at 37°C and 5% CO_2-95% humidified air and fed every 3-4 days by replacing the media with fresh media pre-warmed to 37°C.

Phase contrast imaging of the neurons on the polystyrene adjacent to the SU-8 pieces was done on days 3, 7, 11, 15, 19 in culture in order to observe the neural network formation. Three randomly selected regions from each well were photographed and counted for statistical analysis as shown in Figure 2.16.

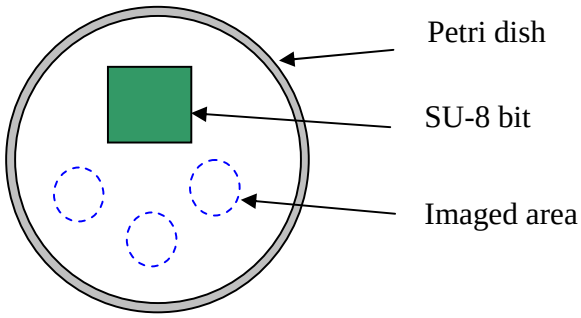

Figure 2.16 Top view of the culturing dish and imaged areas

Terminal live dead assay was performed on day 21 using fluorescent probes for distinguishing live and dead cells (LIVE/DEAD Viability/Cytotoxicity Kit; Molecular Probes, Eugene, OR). Cell cultures were incubated with 2 μM calcein AM and 4 μM ethidium homodimer-1 (EthD-1) at 37° C for 30 min and rinsed in 0.1M phosphate buffered saline (PBS, Invitrogen). The percent of viable cells was calculated by counting the number of live cells (fluorescing green by AM-cleavage) and the number of cells with compromised membranes (nuclei fluorescing red by EthD-1). After viability/cytotoxicity assay, cells were viewed using fluorescent microscopy techniques performed using a Nikon Eclipse Microscope. Fluorescent images viewed with the Nikon were captured using a Sony digital photo camera (DKC5T5/DMC) and analyzed using Image-Pro Plus. The number of live and dead cells was counted for a quantitative assessment of cytocompatibility. From this, the cell viability was calculated as percentage of live cells compared to total number of cells. Data are presented as mean ± the standard error of the mean (SEM). General linear model ANOVA was performed followed by Dunn's pairwise comparisons (p-value < 0.05 was considered significant).

2.4.3 Results and Discussion

Figure 2.17 summarizes the results of the study. Statistical analysis shows that vacuum heating for 3 days at 150C improves neuro-cytocompatibility of SU-8. In comparison to the untreated SU-8 negative controls the CO_2 and UV treatments appear to make SU-8 more toxic. Finally, CO_2 and UV along with heat, either individually or pairwise, were not found to be significantly different from untreated SU-8 for cell viability.

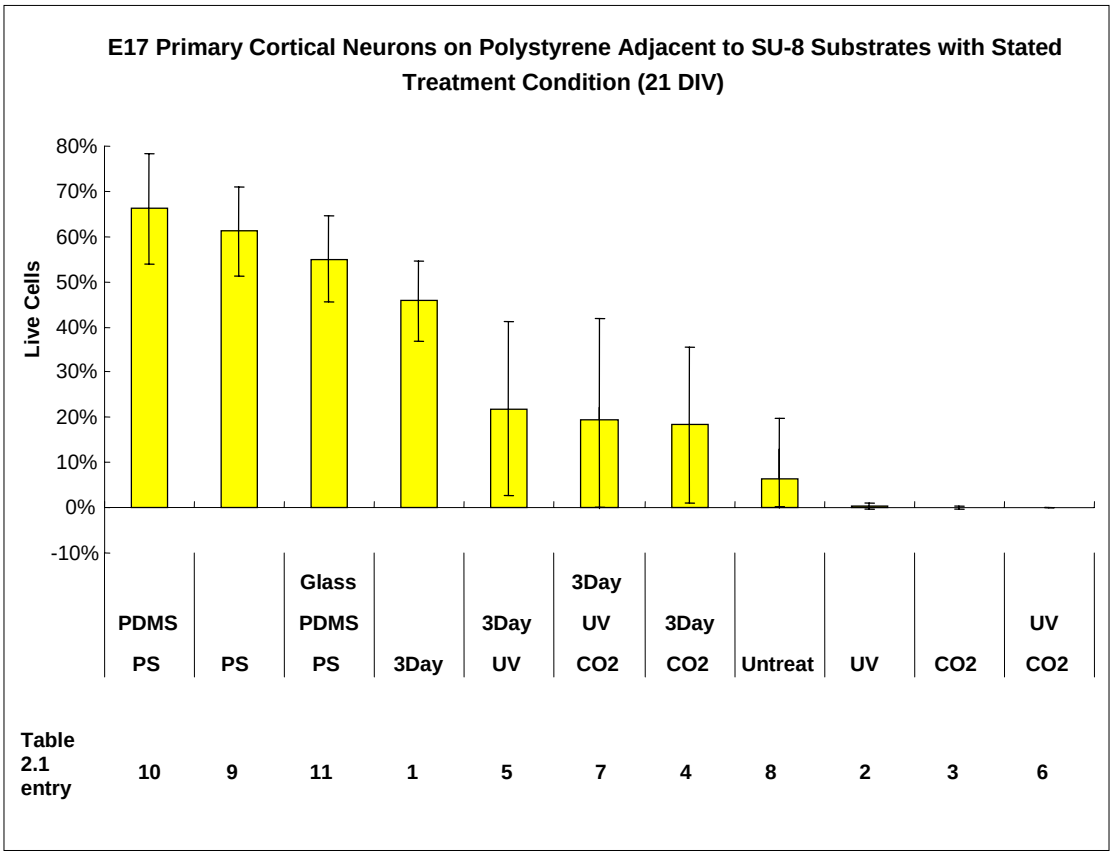

Figure 2.17 Cell viability at day 21 *in vitro* of cortical neuronal cultures adjacent to the SU-8 bits treated by the different detoxification schemes.

Results indicate that the toxic leachants may diffuse out of the SU-8 and kill the neurons in culture. Heat coupled with vacuum is most effective in reducing the cytotoxic effect of the leachants. With this study an effective treatment for detoxifying the SU-8 pieces was identified. Figure 2.17(a)~(k) show representative fluorescent live-dead images for the various treatments compared.

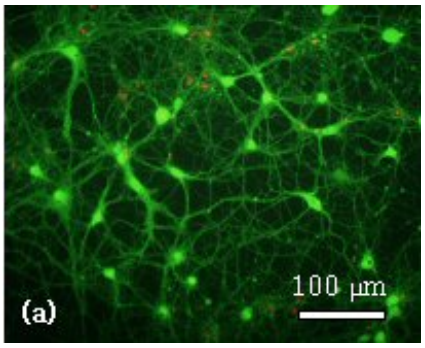

Polystyrene + PDMS control

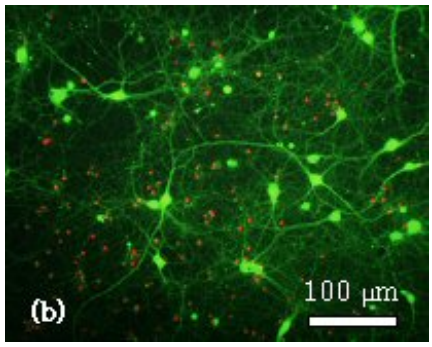

Polystyrene control

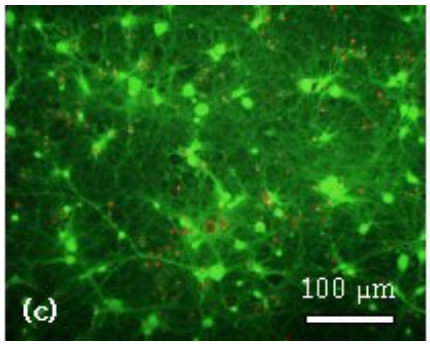

Polystyrene + PDMS + Glass control

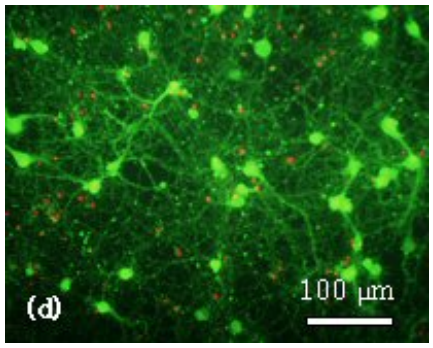

Heat treatment

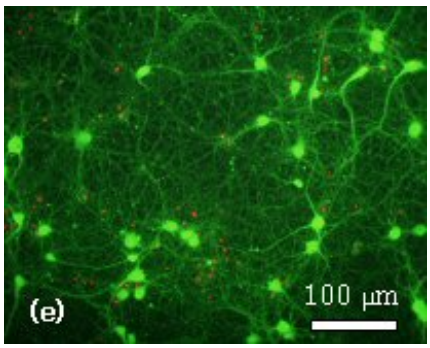

Heat + UV treatment

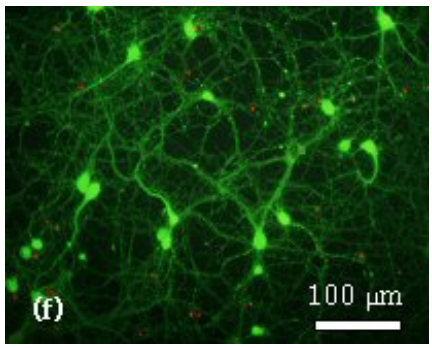

Heat + UV + CO_2 treatment

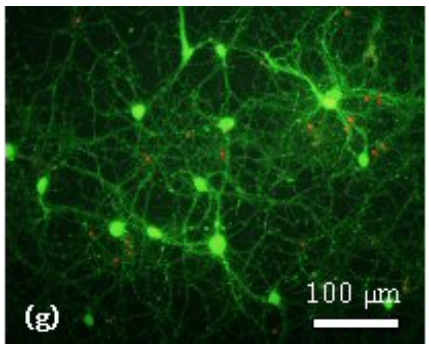

Heat + CO_2 treatment

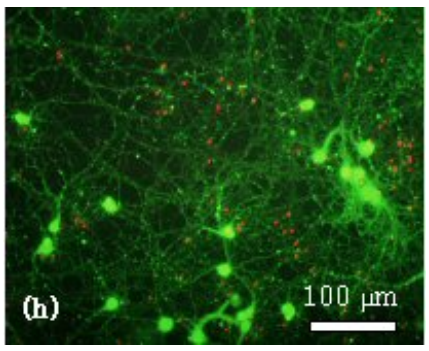

No treatment

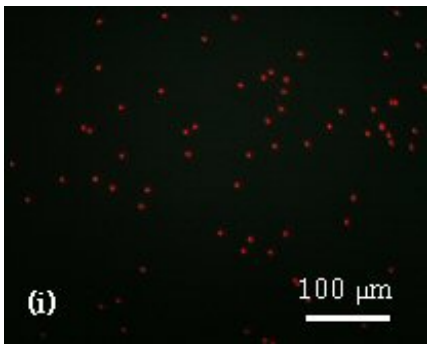

UV treatment

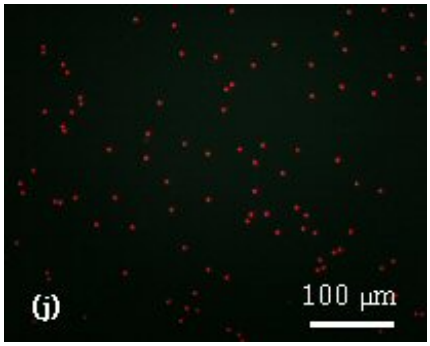

CO_2 treatment

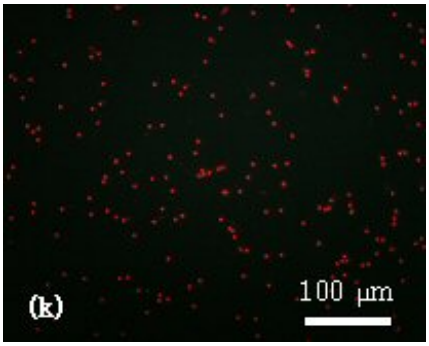

UV + CO_2 treatment

Figure 2.18 Cell viability at day 21 *in vitro* of E17 primary cortical neuronal cultures adjacent to SU-8 samples

CHAPTER 3

3-D FLUIDIC SYSTEM FOR 3-D CELL CULTURE

3.1 Objectives of 3-D MEMS Fluidic Systems

In recent years, the application of MEMS devices and processes have expanded to include numerous fields that lie outside the purview of straight forward electro-mechanical devices and structures, and have come to include such fields as microfluidics and bioMEMS. As research into such applications has expanded, structures of ever increasing complexity have emerged. These complex entities, however, are often difficult to produce because their fabrication schemes contain multiple layers that may require repeated photolithography steps, sometimes as many as ten or more, where each step can generate compounding patterning mistakes as well as introducing the potential for general processing errors [39, 40]. This fabrication challenge, in many cases, serves as a barrier to easy commercialization of these technologies. Simplifying the fabrication steps, therefore, should be of paramount importance when considering designs for new structures. This chapter presents an emerging technology possessing a uniquely efficient fabrication method that can be applied to neuroscience research and introduces complex 3D systems that could be created by this simplified MEMS technology.

With the complexity of bioengineered systems continuing to increase, there is a need for the creation of complex 3-D structures for cellular growth and culturing. It is critical to develop cellular systems for *in vitro* measurement that mimic the 3-D *in vivo* environment as closely as possible. This is necessary for enhanced cellular survival as well as functionality in networks more representative of natural structures and systems.

Fine control of the cellular microenvironment by means of diffusive and convective fluidic processes enables high-resolution spatial and temporal manipulation of critical cell functions [18, 41].

Previously, various microfluidic systems for biological and chemical research fields have been generated along with the emerging fabrication technology for fluidic devices [42-48]. To meet the requirements of creating complex 3-D structures, developments in stereolithography [49, 50], injection molding with PDMS [51, 52], and laser chemical vapor deposition have been reported [53]. Each technique, however, possesses limitations - low resolution, soft structures and high cost, respectively. A photosensitive SU-8 epoxy structure is an attractive candidate for these microfluidic systems because of its high aspect ratio fabrication capability and potential for efficient ablation using excimer laser. Because SU-8 is transparent, it is for 2-D microfluidic channels that give a clear view of fluidic functionality.

Figure 3.1 shows the conceptual view of the proposed system. Each tower has three side ports at various heights that are generated using an excimer laser. This configuration facilitates neuronal cell growth on and between the towers in addition to enabling fluidic perfusion through microfluidic channels. In order to address the requirements of this 3-D environment, a 3-D cellular perfusion system has been demonstrated with SU-8 hollow towers including laser-bored side holes [54]. Using double exposure on bulk SU-8, it was possible to eliminate one whole photolithographic cycle and create strong structures in a manner similar to bulk casting. Then, precisely controlled laser machining was used to make side holes in the hollow towers. Due to the inclination of the towers, a normal-

incidence laser produced vertically-staggered holes along the sidewalls of the towers, achieving 3-D perfusion capability [37, 55].

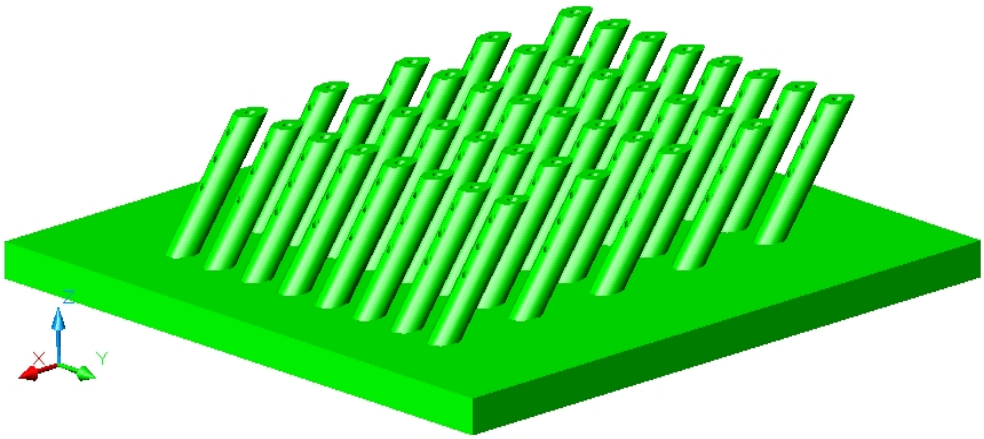

Figure 3.1 Conceptual view of a 3-D microfluidic system

Since the SU-8 substrates that were created by double exposure were only partially exposed, there was some warping of the polymer and a resultant geometric mismatch to other fluidic systems. To compensate for this problem, the fabrication steps were modified to make flat substrates with double photo-patterning and single development. In addition, laser ablation on vertical towers that were tilted was also used instead of inclined towers and vertical laser ablation. These hollow towers were composed of one long central channel from the bottom substrate to the top-center hole and laser ablated side holes. Because of the direction of fluidic flow toward the top hole, the flow rate and size of the side ports produced some limitations. Hollow towers that have only side holes were also generated to meet this additional requirement. After making solid towers, center holes were generated using laser ablation. By varying the intensity of the laser, the height of the laser holes can be controlled. Next, the side ports were generated using

excimer laser ablation again. These various 3-D fluidic systems were demonstrated to follow the design of fluidic systems that produced an even flow rate from the top hole to the side ports.

3.2 Eximer Laser Ablation

3.2.1 Laser Systems

To implement 3-D microfluidic systems, an excimer laser has been used in addition to the conventional MEMS fabrication facilities. A laser (Light Amplification by Stimulated Emission of Radiation) is a device which generates or amplifies light. The light generated by a laser source is nearly monochromatic and highly coherent. And its directionality and high intensity make it an attractive tool for micromachining [56]. The emission of light is caused by the excitation and relaxation of chemical species between metastable and stable energy levels. The four basic types of laser media are: gas, solid state, semiconductor and liquid dye. Only gas and solid state lasers are practical for most industrial machining applications. Table 3.1 shows four common lasers which are commercially available.

Table 3.1 Common lasers used in industry.

Type	Medium	Wavelength	Practical Resolution
Gas Lasers	Excimer	192~351 nm	5 μm
	CO2	10 μm	200 μm
Solid State Lasers	Nd:YAG	1.064 μm	50 μm
	Nd:YLF	1.047 μm	50 μm

Table 3.2 Excimer laser gas mixtures

Mixture	Wavelength	Gas Lifetime	Average Power
F_2	157 nm	10^5 pulses	5 Watts
ArF	193 nm	10^6 pulses	30 Watts
KrCl	222 nm	2 x 10^6 pulses	30 Watts
KrF	248 nm	10^7 pulses	50-100 Watts
XeCl	308 nm	2 x 10^7 pulses	50-150 Watts
XeF	351 nm	10^6 pulses	50 Watts

Because of the resolution and divergence of the light, the excimer laser has been used in this research. The excimer laser is a gas type laser system. There are several mixtures of gases for excimer lasers and each produces a different wavelength of light as shown in Table 3.2. Gas-charged chambers with excitation electrodes along the length of the chamber generate a beam with a relatively uniform energy distribution across the beam itself. Their operational frequency is determined by the ability to charge and discharge capacitors across the electrodes. For example, ArF excimer laser produces an intense coherent beam of ultraviolet light through the electrical stimulation of a gas mixture containing Argon and Fluorine. Pulses of high voltage electricity cause atoms of Argon and Fluorine to bind. When the newly formed molecules of argon fluoride break apart they release packets of light energy with a wavelength of 193 nanometers which go on to stimulate other argon fluoride molecules to break up and release more light energy. This light energy exits the system in a continuous beam and is delivered to the target in a series of pulses.

A CO_2 laser, which is the most common used laser system in industry, uses a gas mixture of CO_2:N_2:He. The CO_2 molecules constitute the active lasing medium, the N_2 gas serves as an energy transfer mechanism and the He atoms enhance the population inversion by depopulating the lower energy states. The population inversion and lasing transition in a CO_2 laser is established between vibrational and rotational energy states. Most CO_2 lasers are pumped by a gas discharge. Although it has good characteristics (low-cost, high efficiency, wide range of power output capabilities, long penetration depth), 200 μm minimum resolution makes it hard to use for micromachining applications.

Solid state lasers are constructed by doping a rare earth element or metallic element into a variety of host materials. The most common host materials are $Y_3Al_5O_{12}$ (YAG), $LiYF_4$ (YLF) and amorphous glass. The Nd:YAG and Nd:YLF lasers are the most common solid state lasers in industry. Typical solid state lasers are pumped optically by arc lamps or flashlamps. Arc lamps typically are used for continuous wave pumping; flashlamps are used with pulsed lasers. Usually in solid state laser systems, harmonic generation is used for creating different wavelengths as shown in Table 3.3. However, total output energy of the shorter wavelength component is typically reduced to one-half the energy of the incident radiation or less.

Table 3.3 Harmonic generation frequencies of solid state lasers

	Fundamental	Doubled	Tripled	Quadrupled
YAG	1064 nm	532 nm	355 nm	266 nm
YLF	1047 nm	523 nm	349 nm	262 nm

There are two kinds of major interactions between laser beams and materials when the laser is used for patterning some materials. One is photo-ablation which can be achieved with the excimer laser. When the intense beam of ultraviolet laser is directed upon a material, photo-ablation of material is produced at a rate which is less than a micron per pulse. The other is a thermal effect which is induced by high power of the laser as light is absorbed and converted into heat. Optical scattering is an interaction of light as it passes through matter, in which the direction of the incident rays is changed by molecules or small particles present in the medium. Scattering plays an important role in the spatial distribution of absorbed energy.

The excimer laser produces a cool beam of highly precise ultraviolet laser. Instead of burning tissue, the excimer actually breaks the chemical bonds between the individual molecules of materials, all with little or no damage to surrounding areas. The resolution of excimer laser can be a few micrometers by this photo-ablation as well as its low wavelength. Because of the coolness of photo-ablation and high resolution, the excimer has been used for various biomedical and bioMEMS applications.

3.2.2 Excimer Laser Ablation of SU-8

The high efficiency of the excimer laser ablation of SU-8 makes it possible to generate the complex 3-D SU-8 fluidic systems. Due to the practical smallest size of 5 μm and taper shape of the excimer laser ablation, there are some limitations for laser micromachining. Figure 3.2 shows taper shapes of excimer laser ablation on a Pyrex glass with various numbers of pulses of the laser beam [57]. Figure 3.2(a) shows the depth of ablation from 1 pulse, 5 pulses, 10 pulses and finally to 65 pulses by 5 pulse

increments. Figure 3.2(b) shows the ablation patterns from 35 pulses to 100 pulses with the same one of Figure 3.2(a). Although the ablation rate is 0.2 μm/pulse, it is hard to see any more ablation after 80 pulses with 5 pulse increments. After that, the increment of the number of pulses was set to 50 and 1000. Figure 3.2(c)(d) shows 50 to 600 by 50 pulses increments and 1000 to 10,000 by 1000 pulses increments. Because of the taper shape and poor ablation efficiency, the ablation depths are saturated at some points. Even with 10,000 pulses, the depth is 66 μm comparing 23 μm with 100 pulses.

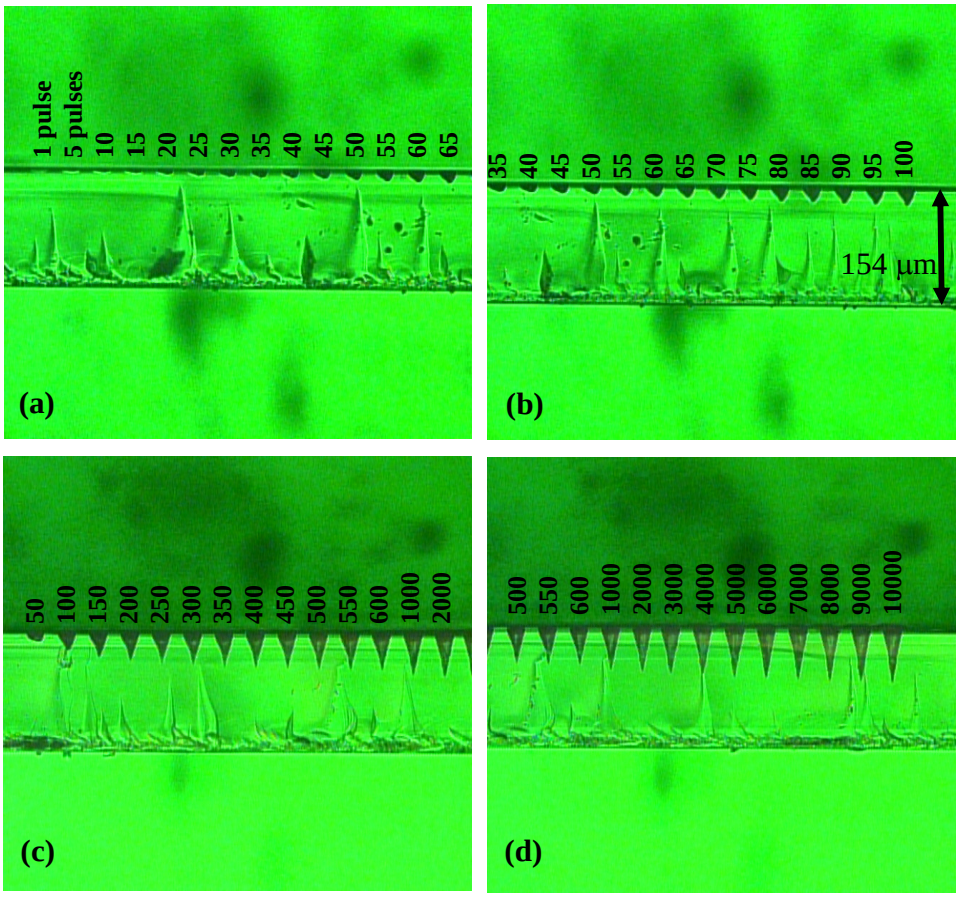

Figure 3.2 Excimer laser ablation on a 154 μm thick glass

Figure 3.3 shows the various depths which were generated on the SU-8 block. The ablation rate of SU-8 is 0.8 μm/pulse and this rate is kept up to 3000 pulses. Over 3000 pulses, it shows the saturated depth of SU-8. For equal comparison, the laser system was fixed for all cases with 200mJ Power, 90 Hz frequency, 10 demagnification, 300 μm shadow mask (30 μm diameter hole) and 97% attenuation.

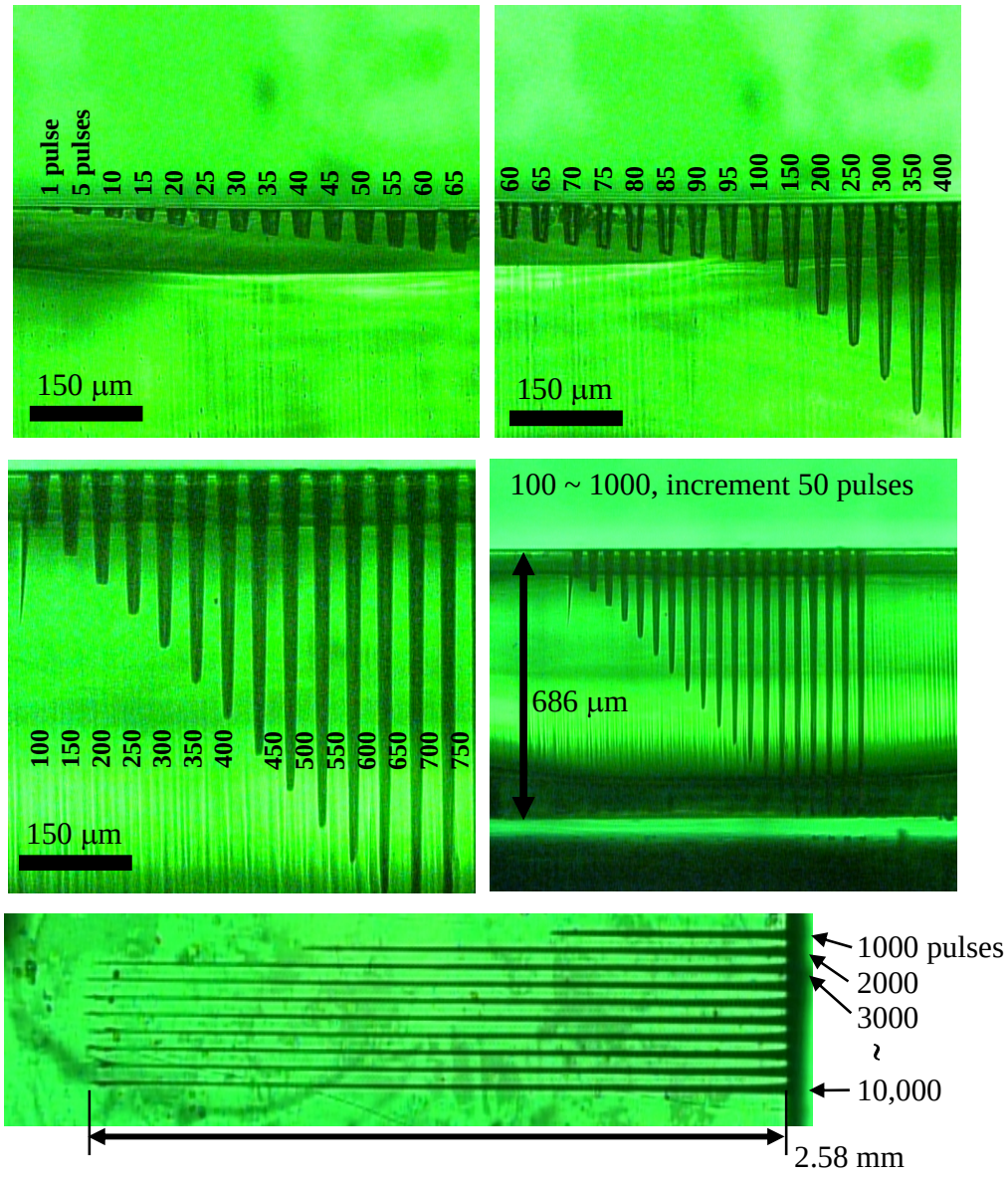

Figure 3.3 Excimer laser ablation on an SU-8 block

3.3 Hollow Towers with Laser Ablated Side Ports

3.3.1 Fluidic Design

The primary object of the 3-D fluidic perfusion systems is to supply nutrients to 3-D cultured cell networks for supporting *in vitro* cell biology research. Although the side ports have different heights as shown in the Figure 3.1, it is necessary to keep the same volume of flow rate from every port; otherwise different flow rates from different side ports might cause a severe deformation of the 3-D shapes of the cultured cell networks due to uncontrolled circulation and flow. Figure 3.4 shows a single tower that has seven output ports and one input port as a model structure for fluidics design. To get an analytical solution for an evenly perfusing system, some fixed parameters should be considered - the height of the hollow towers, the diameter of the center channels, and the volume flow rate from the side ports. With these fixed parameters, the optimal size of the diameters of the side ports is derived using 1-D quasi analysis to obtain the same flow rate from every port.

The liquid is assumed to be water for this design and accordingly density is considered constant throughout the whole flow field. From conservation of mass, the input flow rate should be same as the total output flow rate as:

$$Q_o = 6Q_h + Q_e \tag{1}$$

Where,

Q_o = Entrance flow rate

Q_e = Exit flow rate

Q_h = Flow rate through the each hole on the side

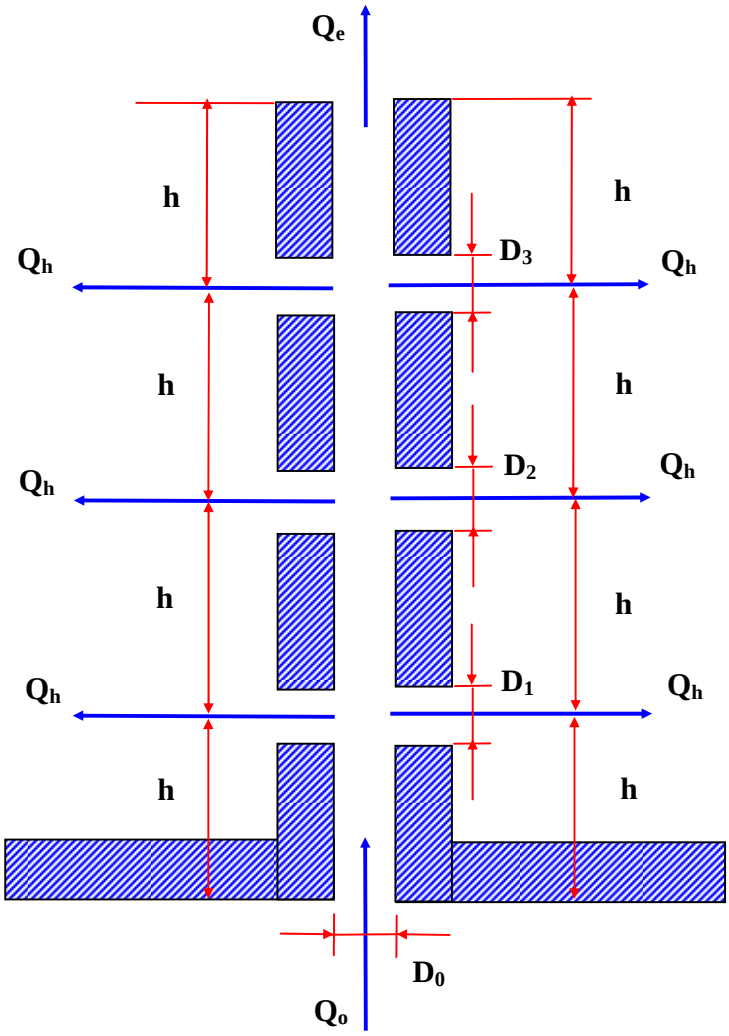

Figure 3.4 Single tower of the 3-D perfusion system

For convenience, the characteristic velocity into the inlet is assumed to be 100μm/sec. Reynolds number and the entrance length before a fully developed state are given as follows.

$$\mathrm{Re} = \frac{UD}{\nu} = \frac{10^{-4} m/s \cdot 10^{-4} m}{1.12 \times 10^{-6} m^2/s} = 8.93 \times 10^{-3} \ll 1$$
$$\frac{L_e}{D} = 0.06 \times \mathrm{Re} = 5.36 \times 10^{-4} \quad (2)$$

Therefore, the flow could be considered as laminar and fully developed. The momentum equation for a circular duct is given by the Hagen-Poiselle Law.

$$Q = \frac{\pi D^4 (\Delta p - \gamma L)}{128 \mu L} \quad \text{or,} \quad \Delta p = \gamma L + \frac{128 \mu L}{\pi D^4} Q \quad (3)$$

where Q is the volume flowrate, μ is the dynamic viscosity, γ (= $\rho \times g$) is the weight per unit volume fluid density, L is the length of the pipe, and D is the diameter of the pipe.

With the axial velocity chosen as 100μm/sec and the diameter of the channel, 100μm, the input volume flow rate is 7.85×10^{-13} m^3/s. Although an axial flow speed of 100 μm/sec was assumed, the design parameter can be modified easily if the speed needs to be changed for a different fluidic environment.

To get an evenly perfusing fluidic system, the volume flow rates from all six side-ports and one exit port should be the same. Since the height and pressure of each port is different, controlling the size of the side ports will make the volume flow rate the same for every output for the fluidic system. From equation (3), the pressure difference of each part of the hollow towers can be obtained as equation (4) and (5). $P_1 \sim P_3$ are the pressures of the center channels where each side ports are placed. P_4 is the pressure at the top exit hole of the center channel. H is the total length of the hollow channel.

$$
\begin{aligned}
p_o - p_1 &= \gamma h + \frac{128\mu h}{\pi D_o^4} Q_o \\
p_1 - p_2 &= \gamma h + \frac{128\mu h}{\pi D_o^4} (Q_o - 2Q_h) \\
p_2 - p_3 &= \gamma h + \frac{128\mu h}{\pi D_o^4} (Q_o - 4Q_h) \\
p_3 - p_4 &= \gamma h + \frac{128\mu h}{\pi D_o^4} Q_e
\end{aligned}
\tag{4}
$$

$$
\therefore p_o - p_4 = \gamma H + \frac{128\mu h}{\pi D_o^4} \left(3Q_o - 6Q_h + Q_e\right) \tag{5}
$$

The flow through the side ports is also assumed to be fully-developed. The volume flow rate through the side port can be determined from Poiselle flow again, where 't' is the thickness of the SU8 channels. There is no gravitational terms here, since this flow is horizontal compared to the vertical flow as in equation (4). The volume flow rates from the six side ports are:

$$
Q_h = \frac{\pi D^4}{128\mu t} \Delta p \tag{6}
$$

$$
Q_h = \frac{\pi D_1^4 \left(p_1 - p_4 - 3\gamma h\right)}{128\mu t} = \frac{\pi D_2^4 \left(p_2 - p_4 - 2\gamma h\right)}{128\mu t} = \frac{\pi D_3^4 \left(p_3 - p_4 - \gamma h\right)}{128\mu t} \tag{7}
$$

Therefore, the equation for the diameter of a side port, D_1, can be derived as :

$$
\therefore \left(\frac{D_2}{D_1}\right)^4 = \frac{p_1 - p_4 - 3\gamma h}{p_2 - p_4 - 2\gamma h} \quad , \quad \left(\frac{D_3}{D_2}\right)^4 = \frac{p_2 - p_4 - 2\gamma h}{p_3 - p_4 - \gamma h} \tag{8}
$$

$$D_1^4 = \left(\frac{128\mu t}{\pi}\right)\frac{Q_h}{p_1 - p_4 - 3\gamma h} \tag{9}$$

When the exit flow rate is the same as the other six side ports, the flow rate from each port is 1.12×10^{-13} m^3/s and the different sizes for the side port can be selected from these equations as D_1=39μm, D_2=48μm and D_3=78μm. Although an even flow rate is chosen for this fluidic application, it is also possible to design various flow rates for each port for different fluidic flow.

3.3.2 Fabrication Process

The first fabrication method presented for generating 3-D perfusion devices is a double exposure technique on a bulk SU-8 with an inclined direction, allowing tower structures and an integrated SU-8 substrate to be formed from the same epoxy deposition. Figure 3.5 shows the fabrication sequence and Figure 3.6 shows the inclined hollow towers generated by a double exposure technique. A one-millimeter-thick layer of SU-8 was spun on a glass substrate. After soft baking, the sample was exposed at an incline to a large exposure dose to cross-link the 700μm tall SU-8 hollow towers. The second mask alignment of the square substrates posed some challenges during implementation. Since the first layer of structures consisted of inclined hollow towers and was not developed by the end of the process, it was hard to align the second layer to the undeveloped and inclined first layer. However, post-baking-induced shrinkage of the cross-linked SU8 hollow towers which facilitated the visual alignment of the second mask to make an SU8 hollow tower substrate.

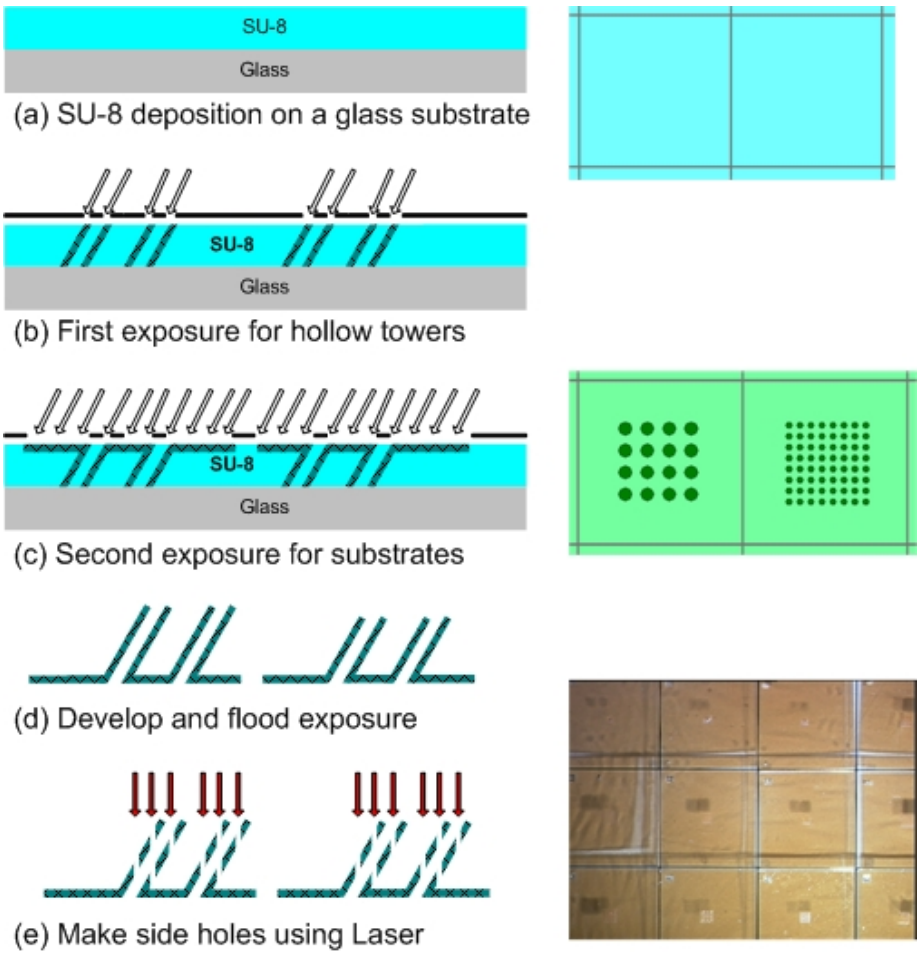

Figure 3.5 Fabrication sequence

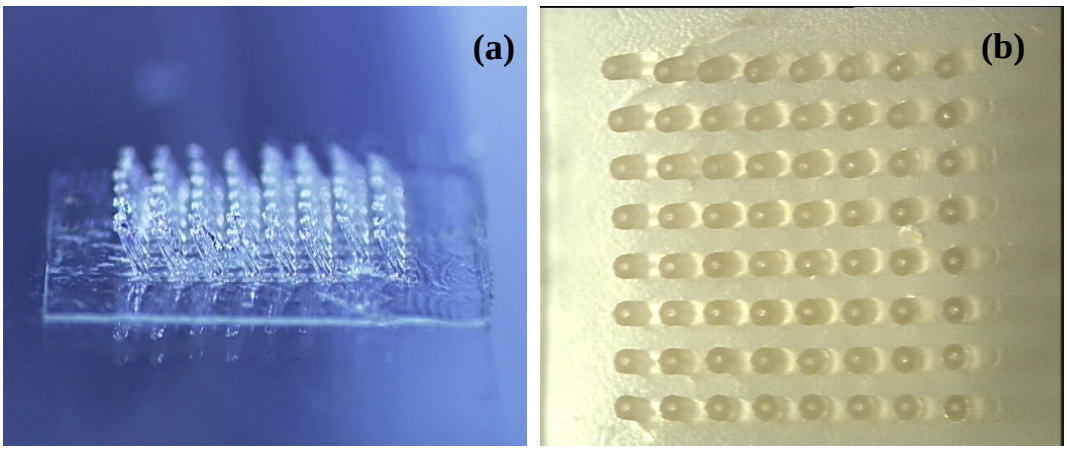

Figure 3.6 An inclined hollow tower array. (a) perspective view, (b) top view.

Figure 3.7 illustrates the difference between crosslinked and un-crosslinked sections of the SU-8 surface aligned to the second mask patterns which were shown on the top of the 1mm thick SU-8. With the second mask, which covered the center holes, the sample was exposed to a relatively low UV radiation dose in the same inclined direction to cross-link a 300μm thick SU-8 plateau (still embedded in the unexposed SU-8 film). Only a 300 μm depth of SU-8 was cross-linked due to the low exposure dose that was utilized. The sample was then developed, removing the un-crosslinked regions and resulting in individualized tower arrays on polymeric substrates, with fluidic communication between the backside of the substrate and each fluidic port.

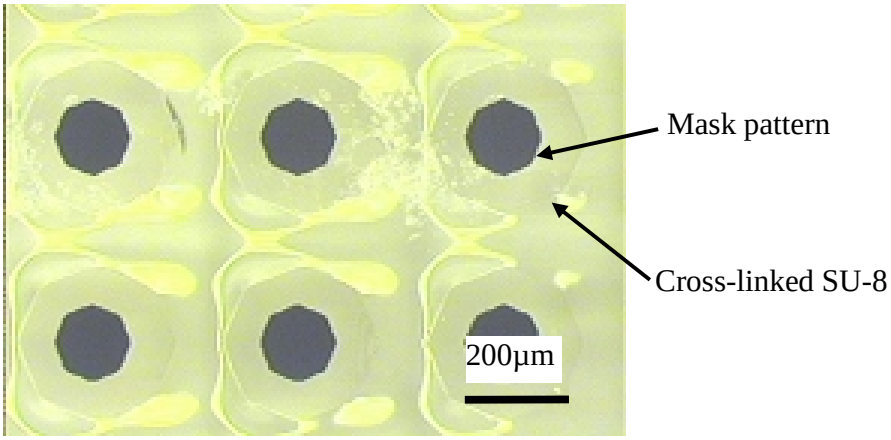

Figure 3.7 Cross-linked SU-8 and mask patterns which block the inside of hollow towers during patterning the square SU-8 substrate

After creating the inclined hollow towers, excimer laser ablation was used to bore the side holes into the sides of the hollow structures. Directionality of the laser beam made it possible to get practically straight patterns on the inclined sidewalls in addition to boring straight toward the bottom several hundred microns below the surface level. Excimer laser ablation involves using a shadow mask technique wherein the laser beam

passes through a metal plate prior to entering the focusing optics. This has the advantage of allowing photoreduction of the mask pattern onto the sample. After passing through focusing optics, the beam interacts with the sample that sits on a movable stage. The stage movement is controlled with a computer program containing the pattern information for the samples. An in-line attenuator in conjunction with laser pulse frequency and energy, along with stage speed, interact to determine the energy delivered to the sample. Using excimer laser ablation, side ports of three different heights were created on 700 μm tall inclined SU-8 structures. Laser ablation offers fabrication simplification advantages over traditional photolithographic techniques. Although excimer laser patterning is a serial technique, it has been proven commercially viable in applications such as trimming and pad ablation. Figure 3.8 shows the final hollow towers with side ports.

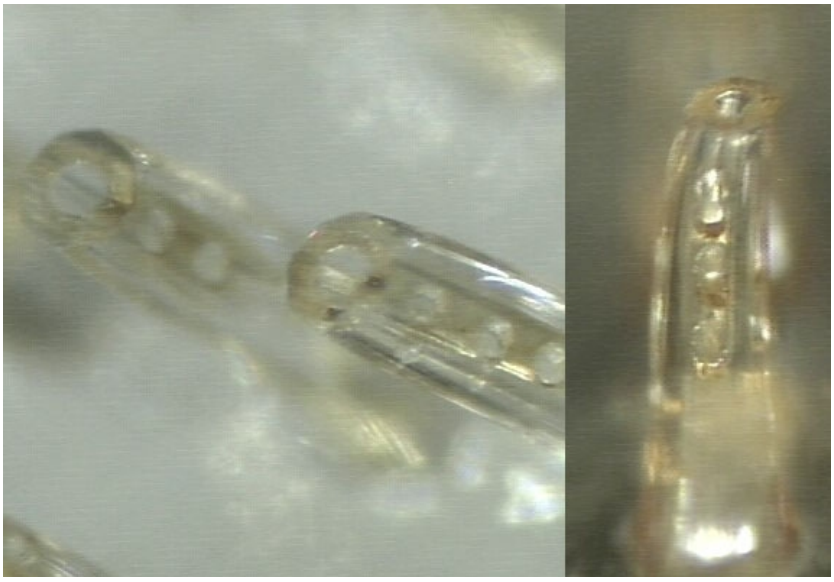

Figure 3.8 Towers with laser created side holes

Although the 3-D perfusion systems could be generated with the simplified fabrication technique, there was warping of the SU8 substrate that required additional steps to address this issue. Figure 3.9 shows the warping of the SU8 substrates. It was due to the gradient in the exposure of the substrate. As explained in Figure 3.5(c), the top part of the SU8 substrates was exposed to the entire 200mJ, but the bottom part was exposed with nearly zero amount of power. Unlike similar processes which were used for solid towers where the substrate was placed on a glass wafer, the substrate for this fluidic channel was made on top of the channels. The free standing substrates were warped during the developing and drying steps. To make the substrates flat, a metal sheet that had a center hole was place on the SU8 substrates to hold the flat shape. Then flood exposure and heating were continuously applied to make the substrate flat as shown in Figure 3.9.

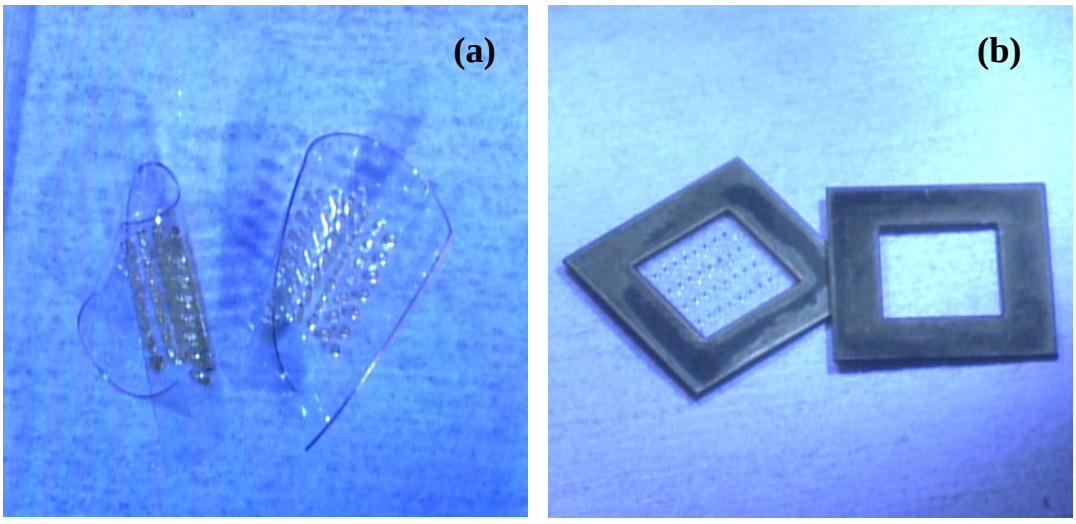

Figure 3.9 (a) Warped SU-8 substrates after releasing from glass substrates (b) Flattened SU-8 substrates with post baking with metal sheets

Despite of these modifications, it was difficult to make the substrates perfectly flat. This warping and additional post processing steps, therefore, lead to the search for alternate fabrication approaches, which are detailed in the following sections.

3.3.3 Modified Fabrication Process

Microfluidic systems normally have complicated and fine configurations inside the system but simple and large fluidic connections to the outside environment. As the number of connections between micro and macro systems is increased, flat substrates for microfluidic systems are necessary, especially for multilayer fluidic systems. To make the SU8 substrate flat, some fabrication steps were modified from the previous double exposure technique. The substrates and hollow towers were separately spin coated and exposed with sufficient power. The development, however, was done only once at the last step. It eliminated one step of post-baking and development as well as increasing the adhesion force between the SU8 substrates and the hollow towers. Figure 3.10 shows the fabrication sequence that began with patterned chromium on a glass mask as a temporary substrate. The mask pattern is a ring shape for the hollow tower. 100 μm thick SU8 2025 was spin-coated on the patterned chromium side of the mask enabling good contact between the SU-8 and the mask. After soft baking (2 hours at 95°C on a hotplate), the sample was exposed (800mJ/cm^2) to make SU-8 substrates. Although the SU8 substrate was the first pattern, it should be aligned to the hollow tower patterns that were on the chromium layer of the glass substrate. Since the second pattern of hollow towers was aligned with the first pattern of SU-8 substrate during patterning of the first layer, the

hollow towers can be exposed using the embedded chromium patterns which, by this point, were already aligned.

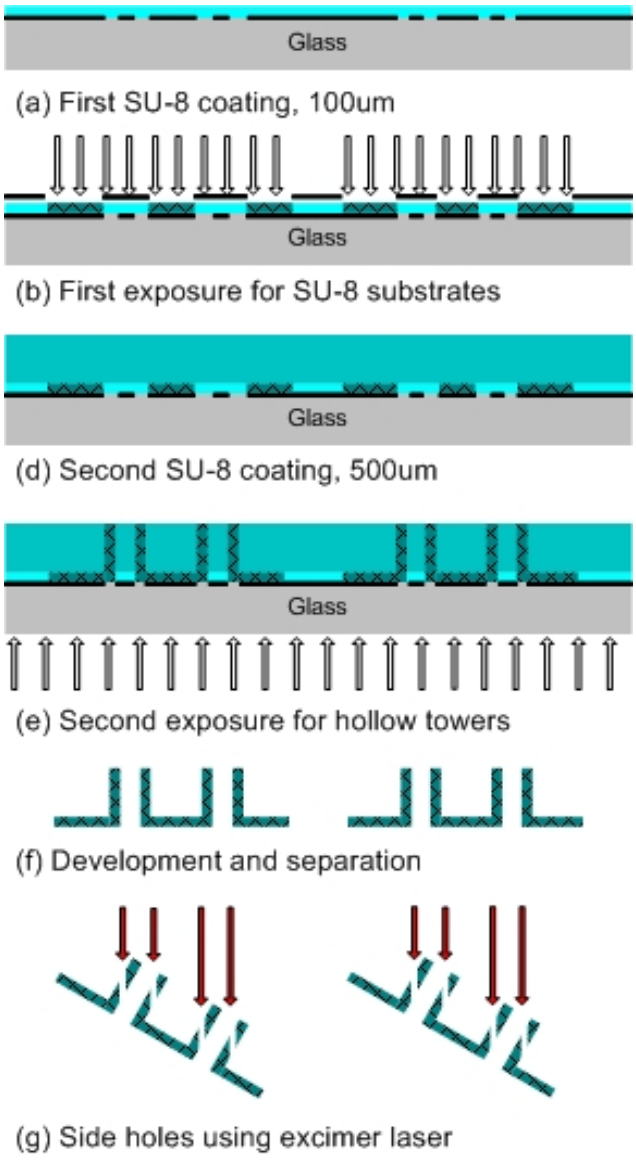

Figure 3.10 Fabrication sequence

Without post-exposure baking and developing the first layer, the second layer of SU8 was coated for the hollow towers to around 500 μm thickness. During soft baking of the second layer (22 hours at 95°C on a hotplate), the exposed first layer of SU8 was cross-linked. Then, backside exposure (5000mJ/cm^2) was performed through the chromium patterns on the glass substrates to make the hollow towers. After post baking (2 hours at 95°C on a hotplate), the sample was developed with PGMEA. After patterning the first layer of SU8 substrates, 500 μm vertical hollow towers should be aligned to the circle holes on SU8 substrates. However, the gap of 500 μm between the mask and the first pattern makes alignment practically impossible with current equipment which can not focus on two different points that are 500 μm apart. However, using the patterned chrominum substrates and backside exposure, the 500 μm thick hollow towers were generated on the SU8 substrates with perfect alignment. Even though the inclined hollow towers were still available using this alternative, vertical towers were generated for simplification of the design of the fluidic mechanism. Instead of inclined towers, the sample itself was tilted during laser ablation to make side ports. Figure 3.11(a) shows the vertical hollow towers with a flat substrate and Figure 3.11(b) shows the bottom view of the vertical towers and the through-holes can be seen clearly.

Figure 3.12 shows the side ports that were generated by excimer laser ablation. There are two side ports on the vertical towers that were bored while tilted. The top exit holes have a diameter of 120 μm and the diameter of the higher side ports is 100 μm and the diameter of lower side ports is 50 μm. The brighter color of lower side ports came from the through holes of the towers because the light source underneath the substrate was illuminated through the lower side holes. The diameters of two side ports were

chosen both for their ease of fabrication and conformity to fluidic design rules. The two side ports were calculated to be 100 μm for the upper holes and 75 μm for the lower holes. However, the tower arrays are a little too dense to make 75 μm diameter holes at the lower parts of the hollow towers since adjacent towers block the laser beam from reaching deep inside the arrays. 50 μm diameter holes, instead, were possible and thus generated without any deformation of the towers.

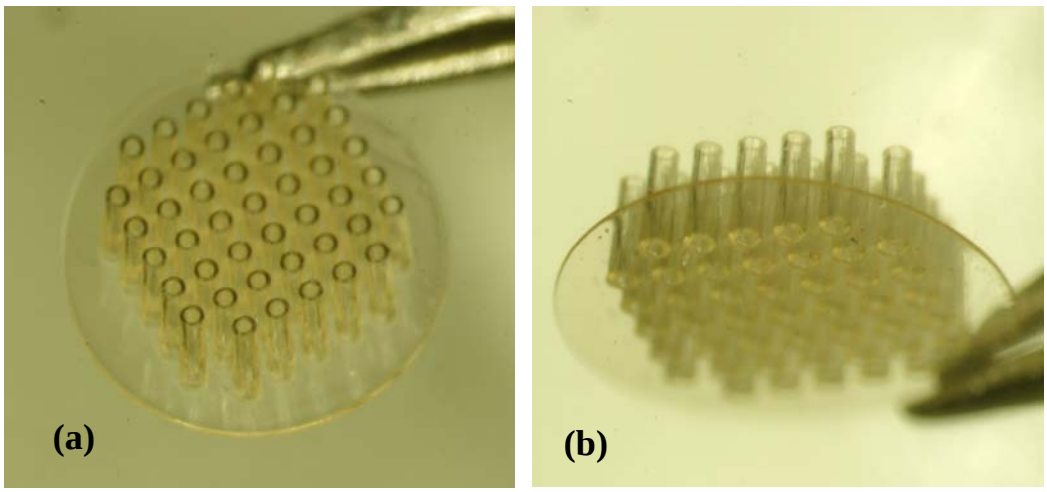

Figure 3.11 (a) Top view of vertical towers, (b) Bottom view of the towers (Through holes can be seen from this bottom view)

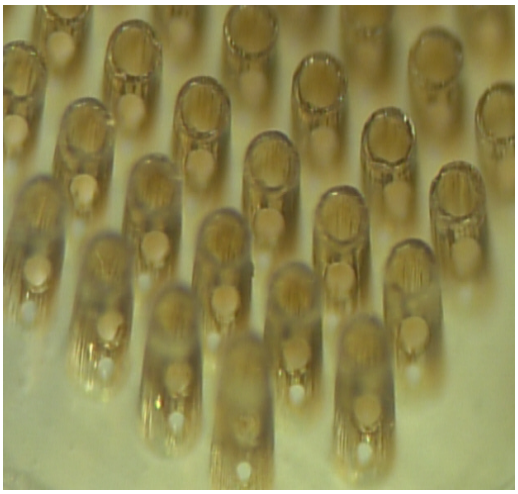

Figure 3.12 Laser-bored side holes on the hollow towers

3.3.4 Fluidic Measurement

The developed fluidic system utilizes both convection and diffusion to enhance the mixing within the chamber. Figure 3.13(a) shows the chamber and Figure 3.13(b) shows the integration of 3-D perfusion devices and the chamber. The perfusion chamber is fabricated using polydimethylsiloxane (PDMS) in a 3-step process: a 3-D mold is fabricated in wax using thermojet printing, the liquid PDMS is poured into the mold and finally, a cured 3-D replica is released from the mold [58]. The chamber is centrally located on the top of the manifold. The manifold is operated in a closed loop, via a syringe pump, such that the perfusate enters through the inlet port and leaves through the outlet port. This enables continuous infusion of nutrients into the cell and withdrawal of waste from it. Nutrients enter the chamber through the SU-8 substrate that contains a number of hollow towers including side openings. Waste leaves the chamber through the outlet channels within the enclosure walls surrounding the SU-8 substrate, and collects within an inclined pool outside the perfusion chamber before leaving the manifold through its outlet port. The top of the cell is covered by glass to enable flow visualization.

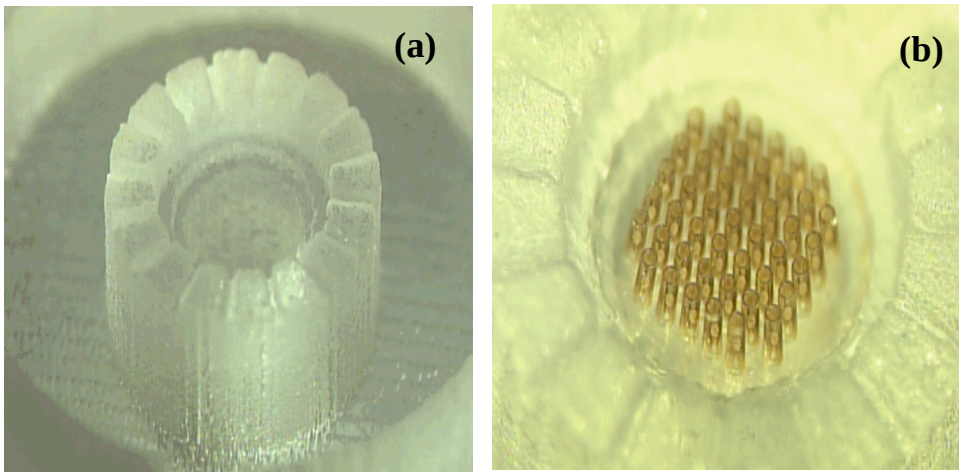

Figure 3.13 (a) a manifold for supplying fluid through the system (b) integration of 3-D perfusion devices and the chamber

Particle image velocimetry (PIV) has been used to investigate the fluidic performance of the system [59, 60]. In this research work, the fluidic measurement and analysis using PIV methods have been performed by Dr. Ari Glezer's lab in Georgia Tech. Flow within the system is investigated using an upright microscope using backward scatter illumination. In this imaging configuration the objective is used to deliver the light to the substrate and the reflected light gathered from 500nm, nile-red coated, polystyrene seeding particles that focus back onto the CCD camera through the objective lens. Velocity is measured using standard cross-correlation algorithms that obtain average particle displacement in a square spot size that measures 57.6 μm in size, and using a known time-delay between the images. Image processing algorithms are developed that exclude dimmer, out-of focus particles.

To investigate the induced flow within the perfusion chamber for an array of 45 hollow towers, the flow was imaged in the x-y plane at various z-heights from the planar SU-8 substrate, that upholds the towers, by moving it from the objective lens. Figure 3.14(a) show a conceptual view of the view plane that is placed at the height of the center of the upper side holes. Figure 3.14(b) is a close-up of the magenta colored view plane. Detailed fluid movement in this view plane is imaged by tracing the particles that pass by it. To compare the effect of the side holes, two different hollow towers were inspected using PIV measurement tools. First the hollow towers without the side ports (Figure 3.11) were tested and then the hollow towers including the side ports (Figure 3.12) were tested to check the effect of side ports. Although whole fluidic systems were imaged at every 10 μm in the z-direction, two different view planes at different heights were selected at heights of 480 μm and 620 μm. The 480 μm height view plane is placed in the center of

the upper side holes as shown in Figure 3.14(c), and the 620 μm height view plane is placed just over the hollow towers as shown in Figure 3.14(d).

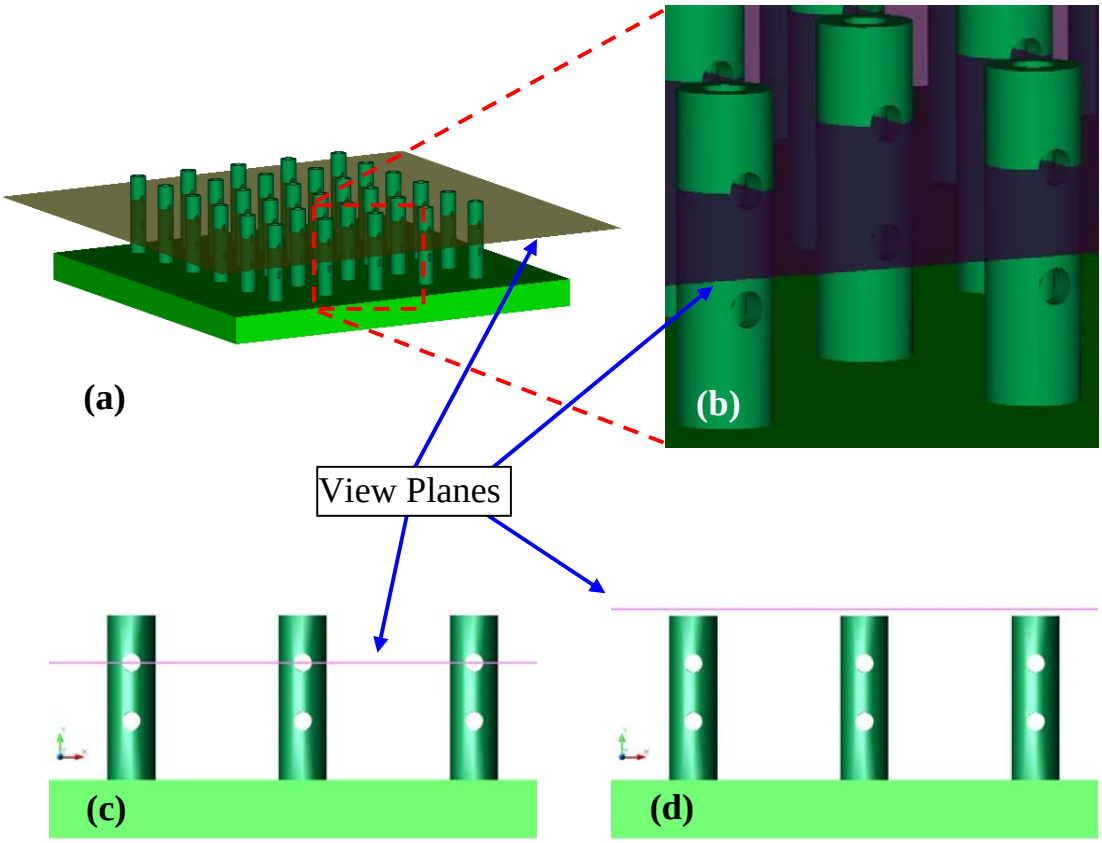

Figure 3.14 Conceptual views of the PIV view planes

Figure 3.15 shows the flow from the hollow towers without side ports. Nominal volume flow rate is 3 μl/min which yields the nominal jet ejection velocity of 140 μm/s (normal to the field of view) and the corresponding jet Reynolds number is 0.014, based on 100 μm tower openings. The flow is induced by discrete jets and their interactions as well as from convectively biasing the flow towards the outlet channels within the enclosure walls. In this configuration, however, the jets issue out of the top of the towers

where the outlet channels are also located so that the jets have little influence on the diffusion that takes place below the top of the towers.

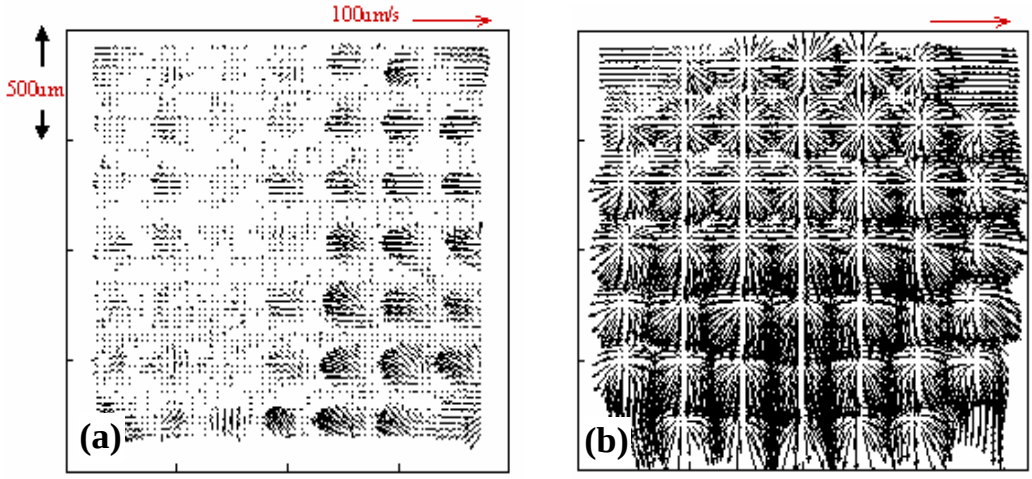

Figure 3.15 Hollow towers without side ports, (a) 480 μm, (b) 620 μm

3-D flow is only established near the top of the towers and is characterized by impingement of discrete jets on the top surface of the chamber and their subsequent radial turning towards the outlet channels. As shown in Figure 3.15(a), at 480 μm above the substrate, the magnitude of induced velocity in the x-y plane normal to the tower axis is small and in some cases influenced by imperfections in the attachment of the substrate to the manifold such that a small tilt of the substrate can bias the flow. In this case some of the jets issuing from the openings at the top of the towers vector downward. We can deduce that the dominant mode of mass transfer here is pure diffusion.

Above the top of the towers, 3-D flow takes place induced by discrete jets that are issuing normal to our field of view in the x-y plane and vector towards the outlet channels, as shown in Figure 3.15(b). Even the smallest imperfection in the fabrication of the

manifold or substrate or their subsequent attachment can bias the flow. For example, a slightly larger channel in the enclosure wall can bias the flow towards it. In general, in the sequence of images not shown here, the radial outflows from discrete jets merge and vector towards the outlet channels so that the magnitude of induced flow in the x-y plane appears higher towards the channels than at the center of the chamber. The overall appearance of the flow normal to the jet axis, above the top of the towers, increasingly begins to look like a radial outflow from the single center jet following its impingement on the top surface of the chamber. This is not surprising as jets closer to the enclosure walls start turning radially outward earlier, while those issuing closer to the center penetrate deeper and start turning in the vicinity of the top chamber surface.

For generating evenly perfused fluidic flow between towers, two side ports are introduced to the hollow towers. Assuming that the network was balanced so that the volume flow rate from each of the two side ports and the top port is equivalent, the overall volume flow rate of 10ul/min through the substrate yields 157μm/s of jet ejection velocity through the second side port, Reynolds number is 0.016 based on 100 μm openings of the second side port.

Clearly the presence of side ports increases the magnitude of the induced flow in the x-y plane as shown in Figure 3.16. Near the center of the second side ports, the flow corresponds to that of a number of discrete jets issuing towards the left upper corner of the perfusion chamber. Jet outflows are restricted by the presence of nearby towers - jets interact and merge, finding the path of minimum resistance enhanced by the miniature imperfections in the fabrication process that can vector the flow. Unless the fluidic network is successfully balanced, the volume flow rates from individual nozzles vary

along a single tower. While the jets issuing from the top ports were present, it appears that the presence of side ports near the top of the towers vectored the top jets, and the streamwise momentum of the top jets was substantially reduced.

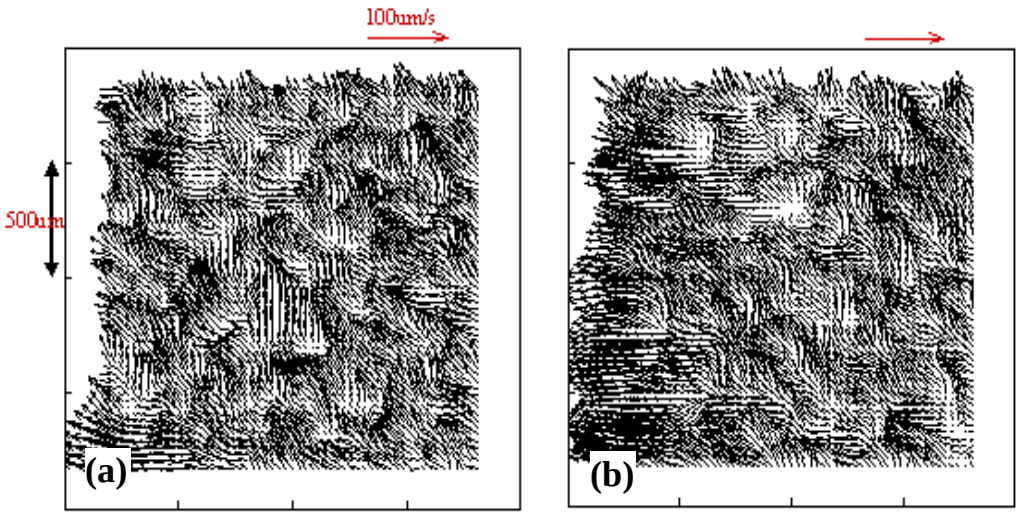

Figure 3.16 Hollow towers with side ports, (a) 480 μm, (b) 620 μm

Although the hollow towers with side ports can show better perfusing properties in comparison with the fluidic system without side ports, it is difficult to analyze the exact fluidic characteristic of the side ports because fluidic flows from adjacent towers in an array interact with one another. Therefore, fluidic flow from a single hollow tower will be investigated to validate the design principles.

Consider the case of a single tower which possesses five openings in addition to an inlet, as shown in Figure 3.17(c). If it is desired that the same volumetric flow rate issue from each of the outlets, the size of each outlet must be designed in accordance with the theory developed in section 3.3.1. Application of this theory, with a nominal input volumetric flow rate Q_0 of 0.04 μl/min results in a tower design with the dimensions of

Figure 3.17(c). Note that initial size parameters have been chosen within the fabrication-feasible range. Further note that although the volumetric velocities from each orifice are the same, the linear velocities are not. Since a linear velocity measurement (PIV) will be used to characterize the performance of the towers, it should be expected that unequal linear velocities will be seen at the orifice outlets.

For clear imaging of fluorescent nano particles, 0.3 μm thick titanium layer is coated on the entire structure as shown in Figure 3.17(b). Figure 3.17(c) shows the dimensions of the single hollow tower and velocities from side ports which are calculated using the equation in section 3.31. Nominal input volume flow rate is Q_o = 0.04 μl/min. A pump is operated in a continuous infusion/withdrawal mode. Velocity is measured using the PIV method via darkfield fluorescence in reflective mode. Fluorescent polystyrene beads (0.5 μm diameter) are used as tracer particles. Specific algorithms are developed to exclude out-of-focus particles. Standard cross-correlation algorithms are employed following the averaging of 6 appropriate particle images to increase the seeding density, thus allowing about 10 particles per spot size on the average. Velocity resolution is within 5% of the maximum velocity. On the average, the volume flow rate from the same z elevation side ports was found to be within 10% of the value predicted by the fluidic analysis. For an example, the calculated jet exit velocity from top side holes is 35 μm/s and measured jet velocities are ranged between 33 and 38μm/s.

Figure 3.18 shows the results of PIV measurements. The length of arrows interprets the amount of velocity. The calculated velocities from side ports at two different heights are drawn as arrows. Therefore, if the theory is an accurate predictor of the experimental results, the arrow length shown in the center of each PIV diagram (the

"reference arrow") should match the average length of the observed linear velocity arrow. The reference arrows indicating velocity at the exit ports are 35 μm/sec for top side ports and 71 μm/sec for bottom side ports. As shown in Figure 3.18(a), the velocity profile of bottom side ports is more widely spread than the top side profile. This is due to the higher speed and larger speed variance of bottom port flows.

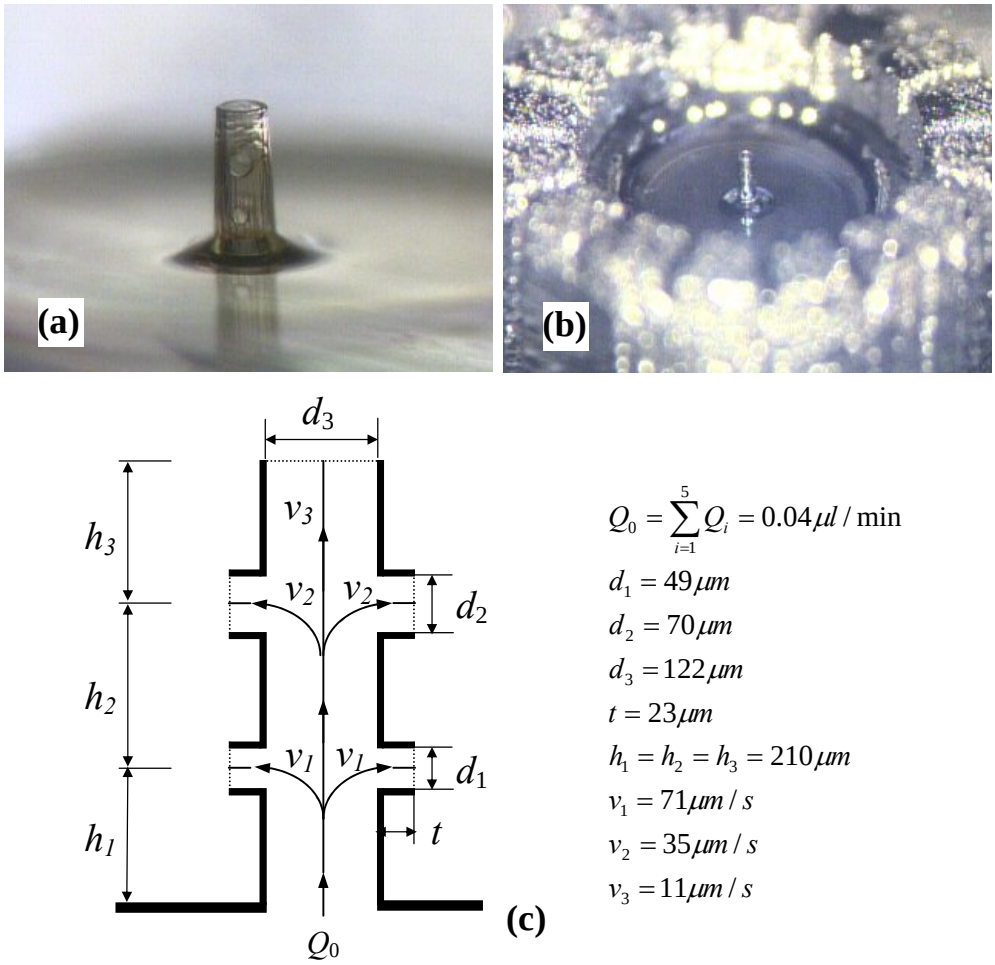

Figure 3.17 Single hollow tower for fluidic analysis

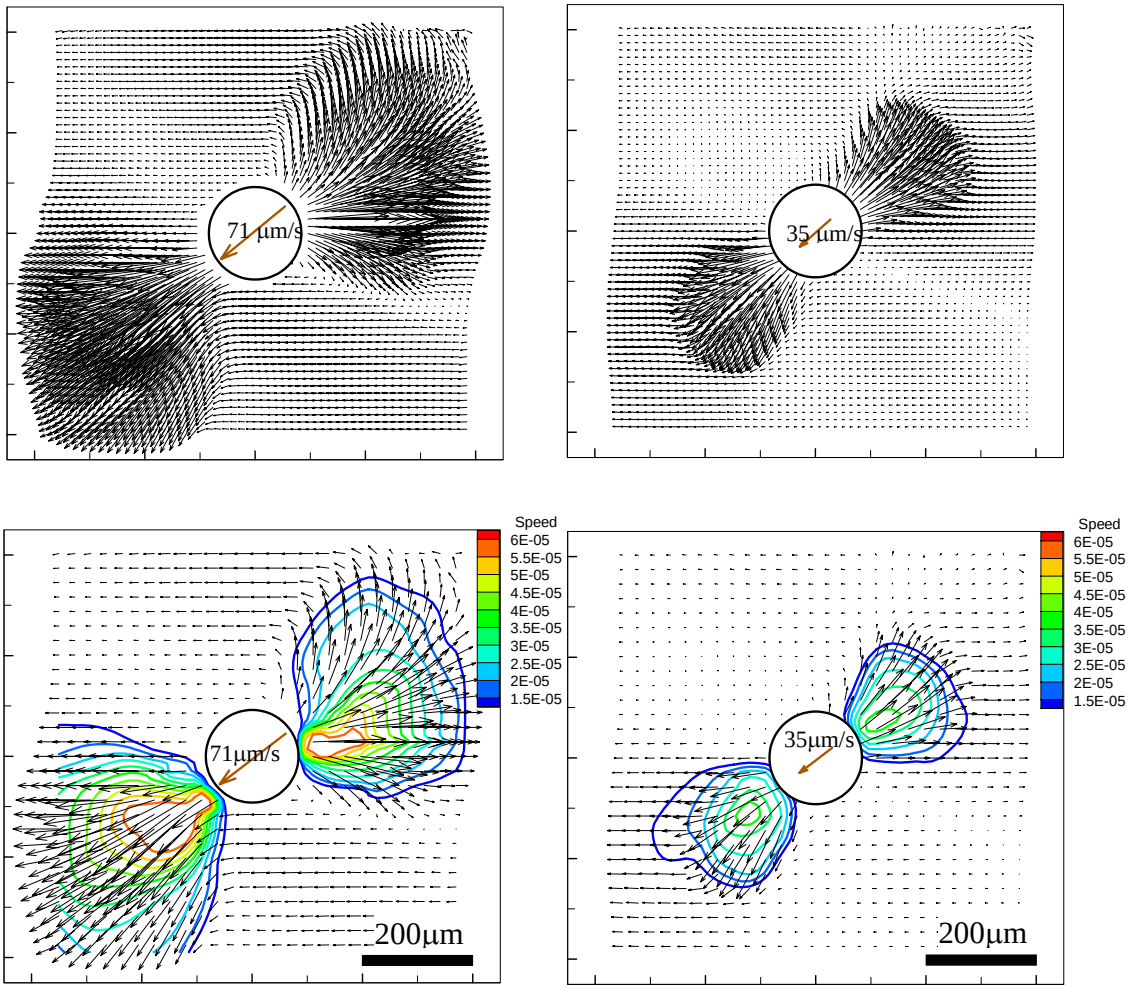

(a) Bottom side ports (d_1 = 49µm) (b) Top side ports (d_2 = 70µm)

Figure 3.18 Fluidic measurement using PIV method

The PIV fluidic measurements demonstrate the extent to which the presence of side ports affects the otherwise stagnant flow within the perfusion chamber. Contour plots of velocity reveal that small size ports in the vicinity of the bottom of the substrate obtain greater depth of penetration of delivered media than those at higher elevations.

This is not surprising, considering that fluidic sizing was performed to achieve even perfusion (i.e. equal volume flow rates coming from all exit ports). With a given volume flow rate of 0.008 μl/min per exit orifice, the contour plots also demonstrate that the spacing between the towers does not need to be less than about 250 μm. For example, the effect of the discharged fluid from the top (side) port can be felt at a distance that is over 250 μm downstream from the orifice. Further, to enhance the uniformity of media delivery within the volume, the tower array can be fabricated in a staggered grid, with side ports at one elevation pointing toward one direction and ports at the second elevation pointing toward another.

3.4 Solid Towers with Laser Ablated Channels

3.4.1 Fluidic Design

The hollow towers that were generated by previous methods consist of a long (500 ~ 700μm) center channel with a top hole developed by photolithography and side holes bored by excimer laser ablation. Since these hollow towers were made by photolithography, the top center hole was inevitable. It could not be closed because there need be an exit hole for the unexposed SU8 inside the channel when it was dissolved during the development step. Although it is possible to design the fluidic system for an evenly perfusing fluidic network with the top hole and side ports, open-top hollow towers have a limitation as a general purpose fluidic system. To get the same flow rate from every port, the diameter of the side ports should be different depending on the height. The different sizes of the side ports imply different structural and fluidic environments for the

cells. Since the size of the cells (rat brain neurons) are around 10 μm, it is better to design the fluidic system with 10 μm diameter side holes, including the top hole, to investigate cell responses to special drugs that come out from the top and side holes together.

Regarding the general design of 3-D fluidic systems, it is necessary to have a big center channel and relatively small peripheral ports. This requirement for fluidic system comes from the pressure drop of the main channels. If the main channels are too thin, the pressure difference that is required for the fluidic operation is increased by an order of four of the diameter as seen in equation (3) in section 3.1.1. So the main center diameter should be big as much as possible to yield an efficient fluidic design. If the pressure difference along the center channel is negligible and the pressure can be assumed to be the same at every inside surface of channels, the fluidic environment for side ports of different heights are the same at the inlet parts of the side port. Then, the design parameter of the system is only the diameter of the side ports. Therefore, the fluidic system that has a big center channel relative to the side ports can give us a big advantage from a fluidic design point of view. The fluidic environment can be controlled just by the diameter of the side ports, although the side ports are positioned at different height along the hollow towers. Bigger side ports produce higher flow rates regardless of the height.

3.4.2 Fabrication Processes

This requirement for a general fluidic design can be achieved by using the new methods of solid towers and laser ablation, which cannot be achievable using hollow towers and surface micromachining techniques. The solid towers could be generated by the same method presented in chapter 2.1 for 3-D scaffolds. The center channels and side ports were made by excimer laser ablation. Figure 3.19(a) shows the concept of laser

ablated center channels and side ports. The tilted direction of the laser beam for side ports can be easily implemented by leaning the substrates. Figure 3.19(b) shows the center channels that were generated inside the 500 μm tall solid towers with 550 μm thick SU8 substrates. Although the thickness of the SU-8 substrate is higher than necessary, the laser ablated center channels can be seen clearly with this thick substrate. This thick and strong substrate can be used for different applications using the same fabrication scheme. The laser beam used for ablation came from the bottom of the substrate and through the inside of the solid towers. The beam was shot with precisely controlled power settings and used to bore the center channel, after which, small side ports were generated using a smaller laser beam.

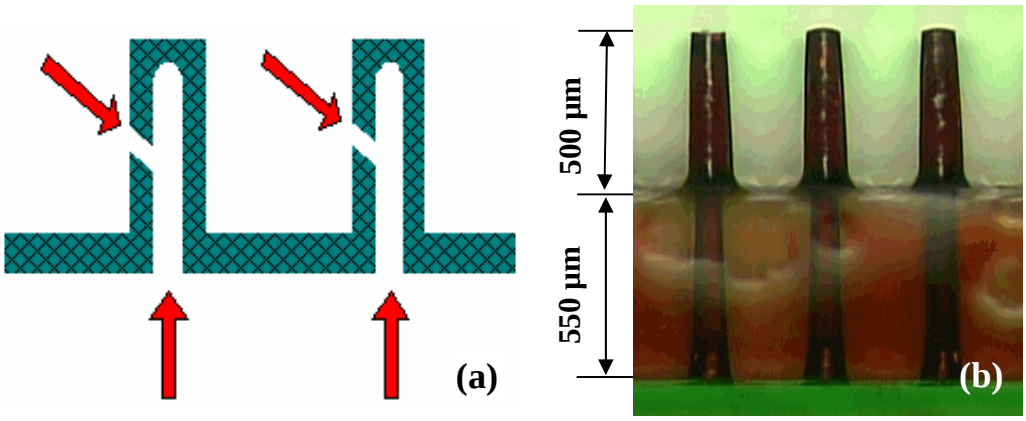

Figure 3.19 (a) Concept of laser patterned center channels and side holes,
(b) Towers with laser created center channels

To see the different heights of the inside center channels, red ink was used to fill in the entirety of the fluidic channels as shown in Figure 3.20 in which two towers have the same heights as the center channels. For example, the 300 μm depth center holes were generated using 500 pulses of laser beam, and 800 pulses were needed to make the 400 μm length channels as in Figure 3.20.

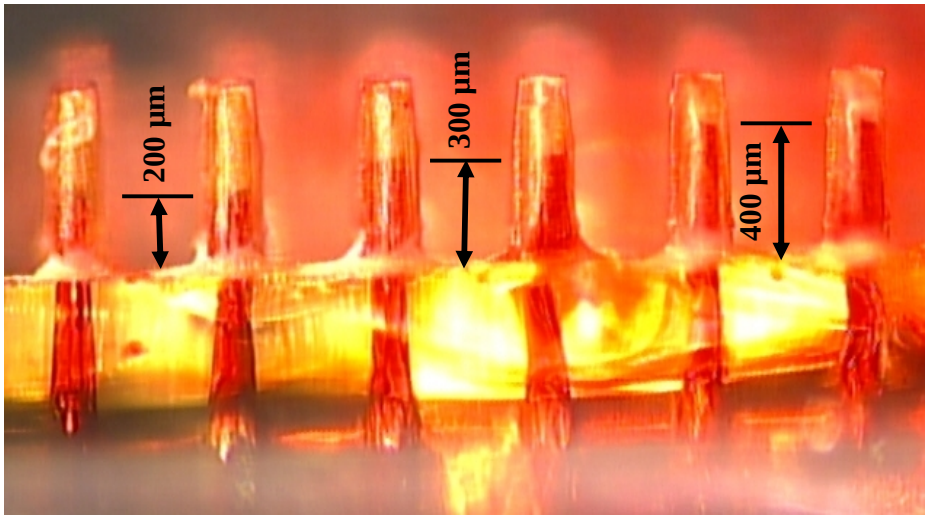

Figure 3.20 Different lengths of the center channels controlled by the power of the laser beam

The blurring of the image of the bottom substrate was due to the optically nonconformal epoxy glue that was used to seal the red ink inside the fluidic channels. Figure 3.21 shows the 9 µm diameter side holes on a solid tower that have center channels with widths of 110µm. Without large, opened, top holes, the modeling of the fluidic system with side ports is easier. Compared to the center channel, relatively small side ports can be generated even at the top. The flow rate from side ports can be higher than that from the top hole by using a bigger hole on the side. This had been restricted with hollow towers with top exit holes because the main flow was going toward the top hole when a high speed flow rate was applied. With a fluidic system with a closed top, 10µm diameter small holes are possible that are also restricted with hollow towers. These should have similar or bigger side holes to make the flow rate controllable through

the side ports. The small size of the fluidic outlet is suitable for use with cells that are the same size as the outlet or larger.

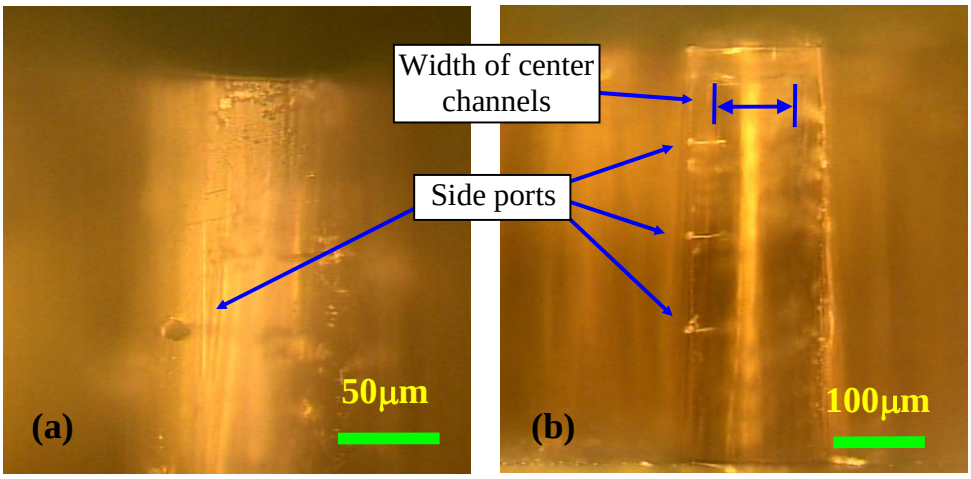

Figure 3.21 The side ports on the solid towers

3.4.3 Microfluidic Measurement

A single solid tower has been investigated for fluidic performance. The primary reason for this is that the fluidic flow from any given tower in an array of towers interacts with adjacent towers and therefore makes it difficult to isolate the effect of side ports from each tower. A PMMA (Polymethyl methacrylate) manifold was used to interface the tower and the syringe pump. A 2.5mm diameter reservoir and 2mm wide fluidic channel were patterned on a PMMA sheet using a CO2 laser, and a 2mm thick tube was connected in the channel as shown in Figure 3.22. The center channel and side ports inside the solid tower were generated using the same dimensions as in Figure 3.21.

Towers were created for fluidic tests that were 550μm in height, with 9μm diameter side holes, and a 110μm diameter center channel. Constant flow rates of 2μl/h and 100μl/h were chosen to compare the fluidic performance. Figure 3.23 shows the evenly perfusing fluidic flow from six side ports for both flow rates. Although the flow rate of 100μl/h exhibits a stronger and faster flow pattern than that of the 2μl/h flow rate, the same amount of perfusing flow can be observed from each side port. The rugged-looking surfaces under the towers were due to the glue used to hold the towers firmly onto the manifold.

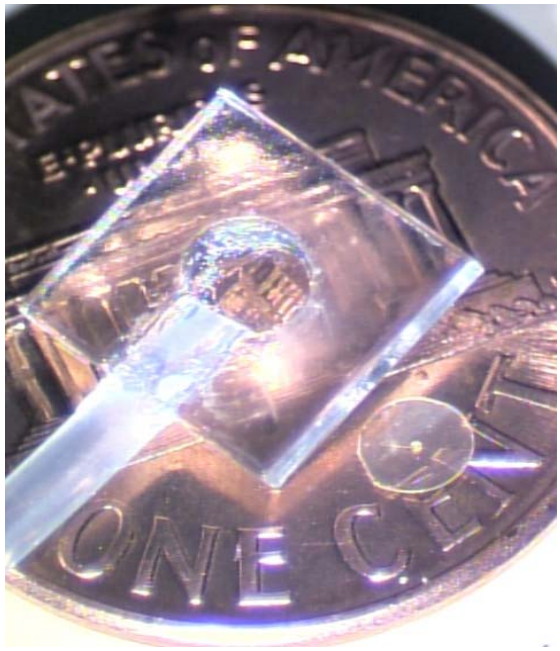

Figure 3.22 Single tower and its manifold pump connection shown next to a US penny

After 3sec 6sec 9sec

[Flow rate: 2ul/h]

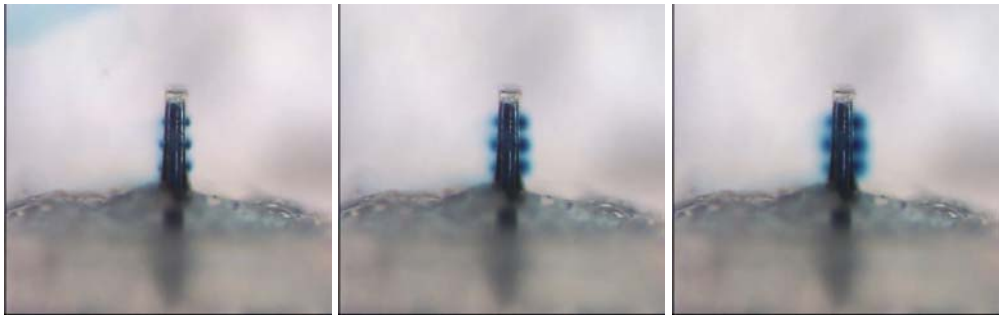

0.5sec 1sec 1.5sec

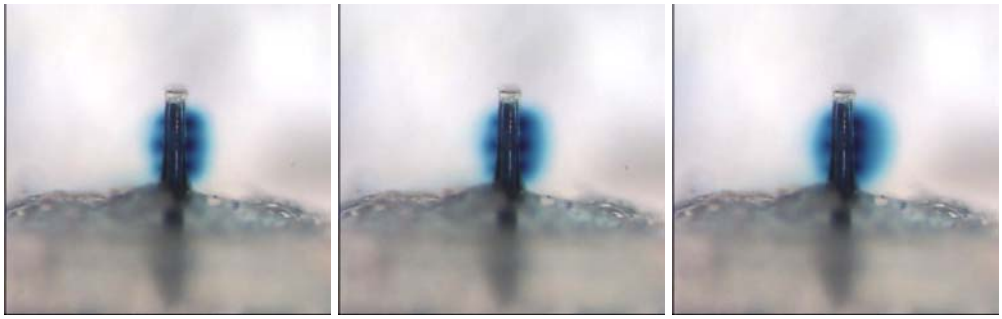

2sec 2.5sec 3sec

[Flow rate: 100ul/h]

Figure 3.23 Evenly perfusing flow from six side ports

CHAPTER 4

A 3-D MULTI-ELECTRODE ARRAY

4.1 3-D MEA on Solid Tower Arrays

4.1.1 Introduction to 3-D Electrodes Electroplated on Parylene Molds

In this research work, the primary goal of the 3-D neuronal interface systems is to detect electrical signals generated by brain neurons. As discussed in section 1.2, each neuron can communicate by propagating electrical signals within the network. The electrical signals, which manifest themselves as action potentials, can be recorded extracellularly as a voltage signal. For example, when some stimuli (such as touch, sound, light, and so on) activate neurons, the electrical potential inside mammalian neurons is changed from -70mV to 30mV in relation to the external side of neurons [61, 62]. Therefore, after development of the 3-D scaffolds and 3-D microfluidic systems as mentioned in previous chapters, the next step is to integrate 3-D electrodes at various heights within the array-tower structure. The process that produces 3-D electrodes is compatible with previous 3-D scaffolds and 3-D fluidic system. This process compatibility is important because all of the systems (structural, fluidic, electrical) are integrated together for the final 3-D neuronal interface system. Figure 4.1 shows the conceptual view of proposed 3-D electrodes on 3-D scaffolds. Green colored tower arrays are made of SU8 using the fabrication technology which was used for generating 3-D scaffolds. The yellow lines describe electrical traces used for the multi-electrode array. Because the electrodes are placed on the surface of tower structures at various heights, the electrical recording system will be truly three dimensional. The electrodes will be covered with platinum black. The entire surface, including electrical traces (but excluding

electrodes), will be covered by parylene for insulating electrodes and increasing biocompatibility [63-65].

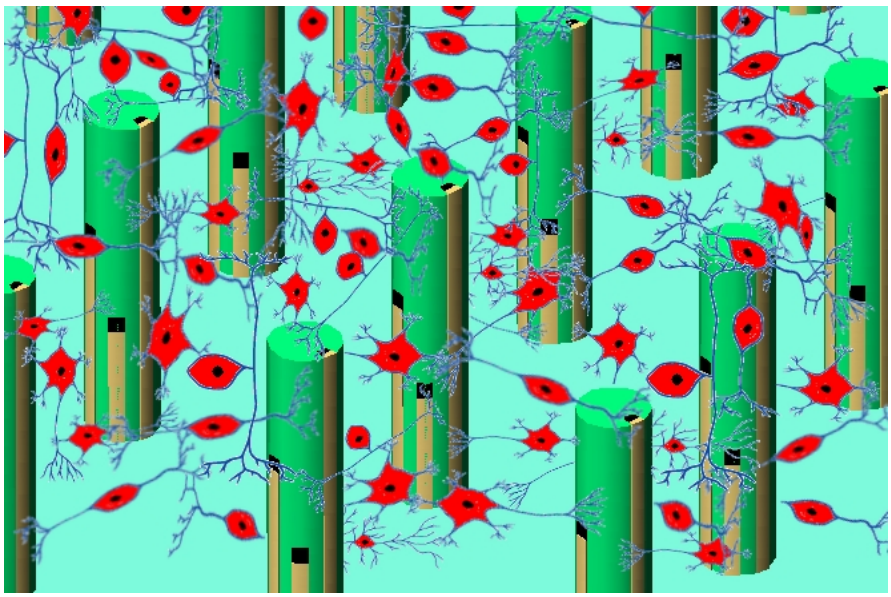

Figure 4.1 Conceptual view of a 3-D multi-electrode array

This chapter presents the 3-D multi-electrodes with a simplified fabrication method to make highly elevated electrical signal lines up to 700 μm above the height of the substrate. This configuration satisfies the requirement of high aspect ratio 3-D multi-electrode arrays (MEA) to detect electrical signals from deep 3-D networks of neurons [66]. This method, which generates thick electroplated metal lines on excimer laser patterned parylene molds, also provides excellent alternatives for traditional MEMS fabrication techniques. For example, this fabrication method could yield 3-D solenoid inductors and 3-D electrophoresis channels to augment the capabilities of the system. Although excimer laser patterning is a serial technique, it has been proven commercially viable in applications such as trimming and pad ablation [67-69].

In terms of micromachining technology, one challenging issue frequently encountered is patterning electrode lines on multi-level or deep sidewall structures. As seen in Figure 4.2, conventional photolithography cannot accurately produce patterns if the structures have differing elevations because of the diffraction of light.

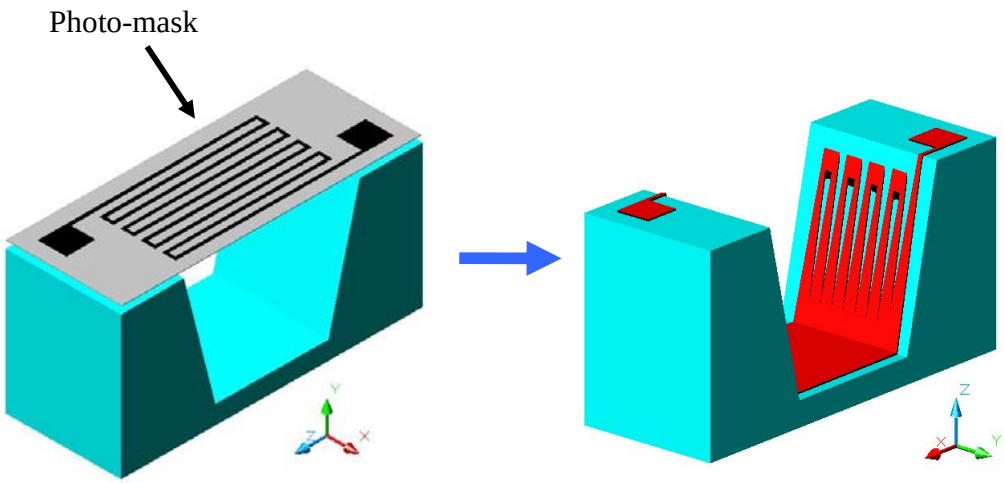

Figure 4.2 Merged lines using conventional photolithography

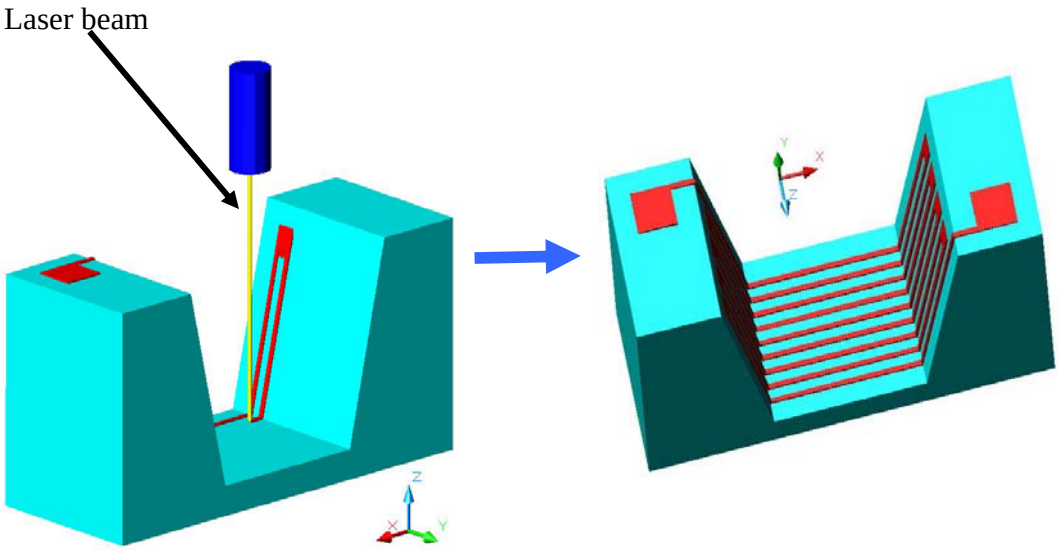

Figure 4.3 Straight lines using laser ablation

Although patterns are on an inclined surface and can be seen through the mask (as demonstrated in Figure 4.2), the light passing through the mask patterns will be expanded as the elevation is increased and patterned lines are merged together at the bottom. Figure 4.3 shows the concept of fabrication using laser ablation, which can make straight lines on multiple elevations. Directionality of the laser beam makes it possible to achieve practically straight patterns on the inclined sidewalls in addition to the bottom surface, which is several hundred microns below. The width of electrode on the 700 μm top surface of the tower is 30 μm, nearly identical to the 31 μm on the bottom-level substrate. 3-D multi-electrodes on various elevation surfaces and insulation of parylene coating are efficiently implemented by using the directionality of excimer lasers and the conformal coating of parylene. These fabrication techniques are independent of other processing steps and can be performed after finishing some complicated structures, such as the ones featured in this research work. Complex scaffolds and fluidic systems have been generated without preventing the addition of electrodes.

4.1.2 Characteristics of Parylene

To implement 3-D electrodes, some major equipment has been used in addition to the conventional MEMS fabrication facilities. One is an excimer laser which was explained in section 3.2.2, and the other is a parylene coating system. Parylene conformal coating technology, originally developed by Union Carbide, has been in commercial use for more than 25 years. Parylene (poly(p-xylylene)) is an insulating thermoplastic polymer film that has a high degree of chemical inertness, absence of pinholes and perfect conformity to the topography of the surface applied. This class of polymer has

been used for decades on a variety of applications – especially those involving the protection of electronic devices and circuitry.

Parylene coating process is best described as a vapor deposition polymerization process (VDP) (Figure 4.4). The dimer obtained by the direct pyrolysis of p-xylene is very stable compound. This dimer can be evaporized into vapor phase at around 170^{o}C. Then the dimers are pyrolyzed into monomers at around 650 ~ 700^{o}C. The monomer molecule is thermally stable, but kinetically very reactive toward polymerization with other molecules of its kind. On condensation it polymerizes spontaneously to produce a coating of high molecular weight, linear poly(p-xylylene).

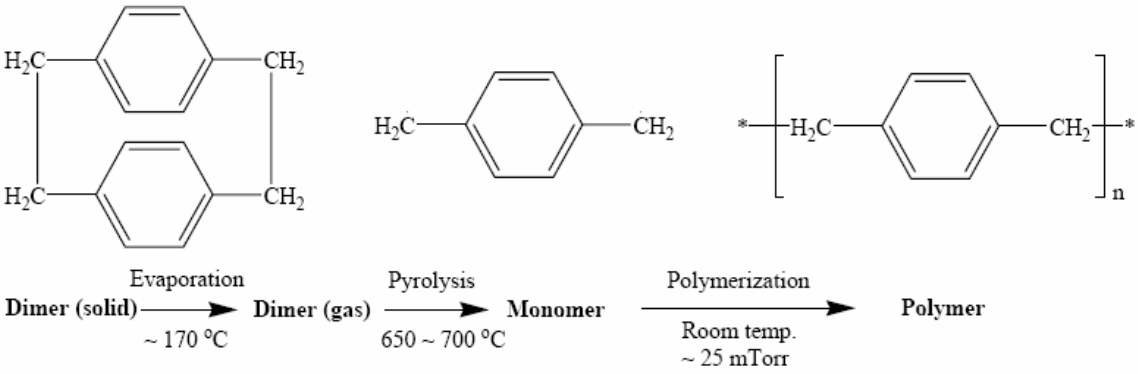

Figure 4.4 Parylene deposition process.

Substitutes can be attached to the ring positions of the dimer, di-p-xylylene (DPX). Although a variety of substituted dimers are known in the literature, at present only, DPXN, DPXC, and DPXD are commercially available, which give rise to Parylene N, Parylene C, and Parylene D, respectively. Parylene A, Parylene AM, and Parylene F will be also commercially available in a near future. Different functional groups produce different material properties. Figure 4.5 shows the molecular structures of different

parylenes. The physical processes of condensation and diffusion must be considered along with the p-xylylene polymerization chemistry for a proper understanding of what happens microscopically during vapor deposition polymerization. A gaseous monomer is transported to the location within the coating where it is to be consumed to produce polymer by an initial condensation, followed by diffusion. The monomer is consumed by initiation and propagation, in which existing polymer molecules are extended to a higher molecular weight. In steady-state VDP, both reactions proceed continuously inside polymeric coating, in the reaction zone just behind the growth interface. The concentration of monomer within the coating decreases approximately exponentially with distance from the growth interface. With this decrease in monomer concentration, the rates of initiation and propagation reactions also decrease. Under conditions prevailing during a typical deposition, the characteristic depth of the reaction zone is a few hundred nanometers, and the maximum concentration of monomer, ie., the concentration at the growth interface, is of the order of a few tenths percent by weight [26].

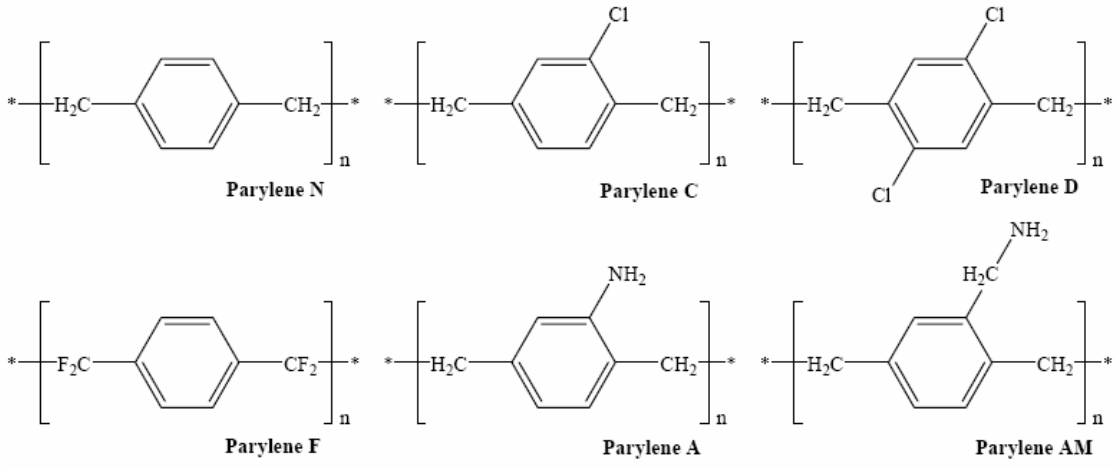

Figure 4.5 Molecular structures of parylenes

During the vapor deposition process, the polymer chain ends remain truly alive, ceasing to grow only when they are so far from the growth interface that fresh monomer can no longer reach them.

4.1.3 Fabrication Process

The fabrication processes were started with vertical and inclined SU-8 towers which were created using double exposure methods to get high aspect ratio structures [4]. Both conformal deposition of parylene and straight patterning of excimer laser ablation made it possible to generate fine electrode lines on multi-level structures. Figure 4.6 shows the fabrication sequence. After generating tower structures, 0.3 μm thick copper seed layer was deposited using DC sputerrer, which was followed by 1μm thick parylene deposition as shown in Figure 4.6(d). The copper and parylene deposition was achieved with conformal coating systems, which covered the entire surface including the sidewalls of towers. Conformal deposition was necessary to make these 3-D electrodes, which were formed on the surface of the towers. The excimer laser was used to generate electroplating molds on the parylene surface. The power of laser beam was just enough to burn 1 μm of parylene and spare the copper seed layer (which serves as a plating-base for electroplating 3-D electrodes.) The ablation rate of parylene is much higher than copper, so the selectivity for laser patterning parylene was easily achieved when parylene is coated on a copper layer.20 μ thick nickel electroplating was performed on the parylene mold which was made by laser ablation. The relatively thick metal electrodes (a few micrometers on commercial MEAs) can effectively decrease the impedance of

electrodes. Then the parylene mold and copper seed layer were removed using RIE and wet etching respectively.

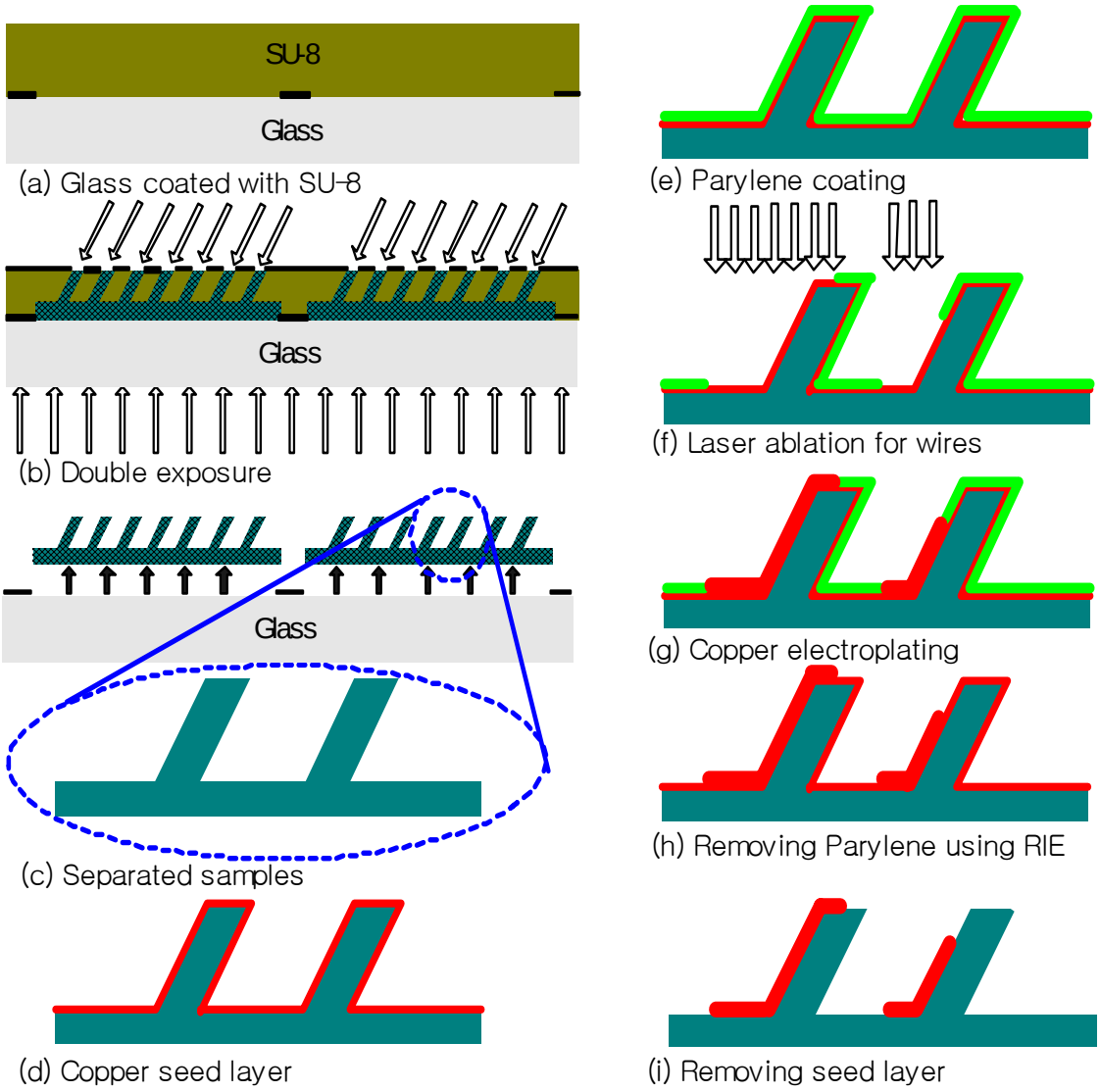

Figure 4.6 Fabrication sequence for electrodes on inclined surface

After generating 3-D electrodes, conformal parylene coating was used again for insulation of the 3-D electrodes. 25 μm thick parylene was deposited to decrease parasitic capacitance associated with electrical traces as well as increase biocompatibility (parylene biocompatibility examples). To open electrodes for recording and stimulating sites, excimer laser was used again. Platinum, a known biocompatible metal, was electroplated in the open holes. The open holes were first filled with smooth Pt deposits, followed by porous black structures to complete the electrode surface. Porous and smooth deposition were controlled by current density for electroplating. The porous structures increase the surface area which decreases impedance drastically. This micromachining technique using excimer of laser ablation with parylene molds offers fabrication simplification advantages over traditional photolithographic techniques. Various arrays of electrodes with electrode widths ranging from 5 μm to 30 μm and heights ranging from 200 μm to 700 μm were fabricated using the technique outlined above.

Figure 4.7 shows the straight multi-electrode lines patterned by laser ablation on vertical towers, which were generated by leaning the substrate about 30° for using the vertical laser beam. Figure 4.8 shows 3-D electrodes on inclined towers which were made without tilting the substrates. The inclined towers were generated by inclined exposure during photolithography steps. Although 16x16 array towers were used, only 60 towers were selected for generating 3-D electrodes to utilize a commercialized 60-pad interface system which is used to monitor cell culturing. Circular shapes of substrates were also generated as shown in Figure 4.9. The diameter of the disk is only 2.7mm; the small substrate makes it possible to decrease the thickness of substrate without any deformation of the structures.

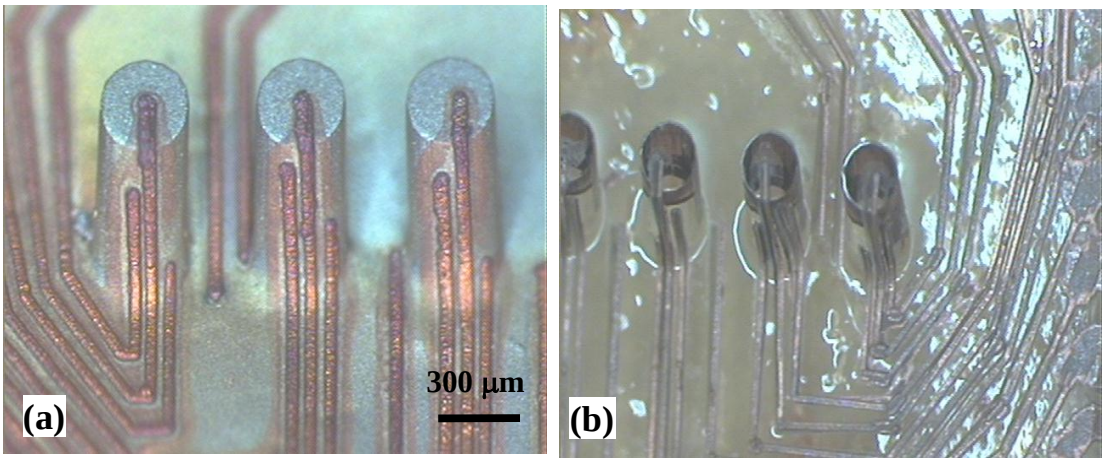

Figure 4.7 Electrodes on vertical towers (a) before removing a copper seed layer (b) after removing the seed layer

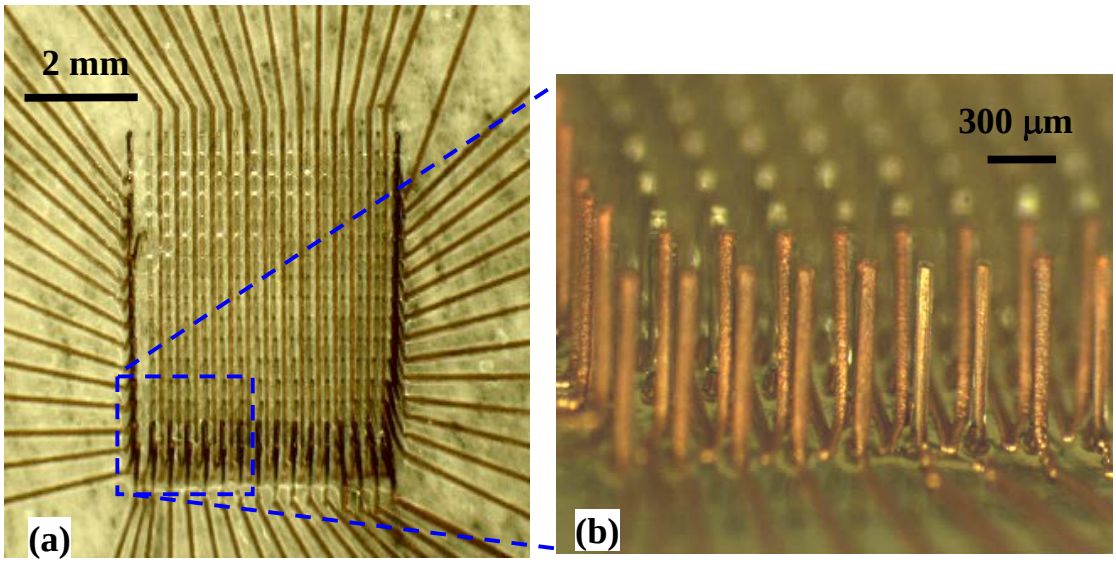

Figure 4.8 Electrodes on inclined tower structures (a) top view (b) perspective view on a close-up corner

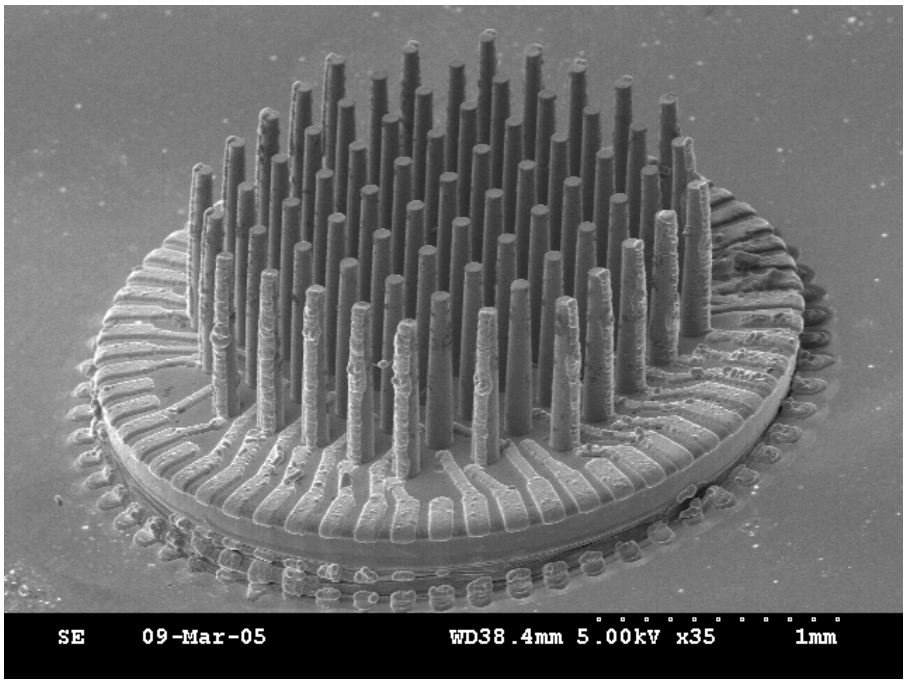

Figure 4.9 SEM picture of 3-D Electrodes on a circular SU-8 substrate

Small and thin substrates have some advantages in mass production; among them is that biocompatibility is improved by decreasing the amount of SU-8. To get a clear view of substrates and electrodes in the SEM image, the copper seed layer was not removed on the structures of Figure 4.9. The 3-D electrodes on SU-8 towers in which parylene and copper seed layer were removed are shown in Figure 4.10. The 3-D electrodes on a small 2.7mm diameter circular structure were connected using wire bonding system as shown in Figure 4.11. Although all fabrication procedures can be implemented on two inch square glass substrates, these two structures (SU-8 towers with electrodes and feed lines on glass substrates) were generated respectively and were packaged together in the final steps for some practical and efficient considerations. Because only 1/250 area of two inch square of glass substrates is covered by 1mm thick

SU-8, coating the entire surface with SU-8 is too much of a waste of resources. Furthermore, integrated the substrates in the final stages is necessary because the thermal mismatches between SU-8 and glass would likely cause bad adhesion between substrates during the ten different processing steps.

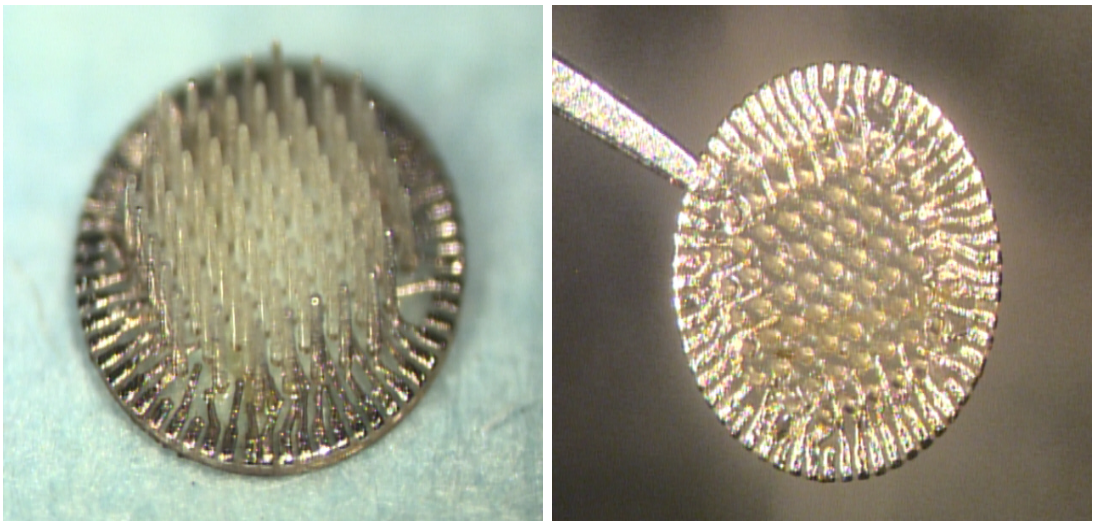

Figure 4.10 3-D Electrodes on a circular SU-8 substrate after removing a copper seed layer and parylene molds

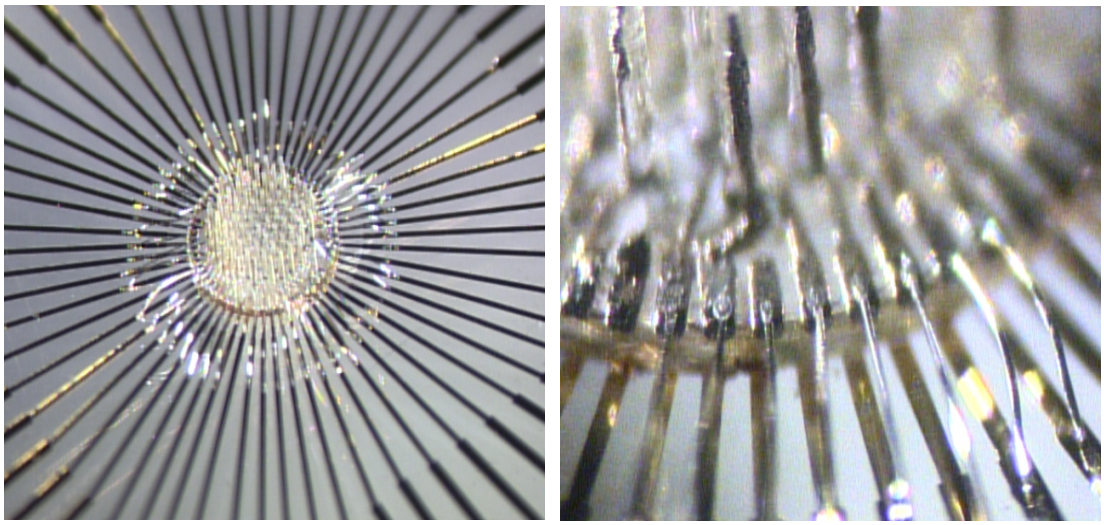

Figure 4.11 3-D Electrodes on a circular SU-8 substrate after removing a copper seed layer and parylene molds

Figure 4.12(a) shows the 3-D electrodes wire bonded to the feed lines on a glass substrate. A 5 mm tall polycarbonate 'cell culture' ring was added as shown in Figures 4.12(b). PDMS (Sylgard 184) was used to glue the ring on the glass substrate; PDMS is a well known biocompatible material. Twenty five microns of parylene were coated on the whole surface to hold the ring firmly and insulate all open electrodes. For the final step of whole process the tips of 3-D electrodes were opened using excimer laser and electroplated with platinum black as shown in Figure 4.13. The open site of electrode rests 600 μm high atop one of the SU-8 towers. Figure 4.13(a) shows the smooth and shiny platinum surface which was used to initially fill the 25 μ depth parylene hole and Figure 4.13(b) shows the platinum black deposited on top the smooth platinum. If the parylene holes are dried, air trapped inside the holes block the electroplating solution. So the pictures of electrodes in Figure 4.13 were taken inside plating solution.

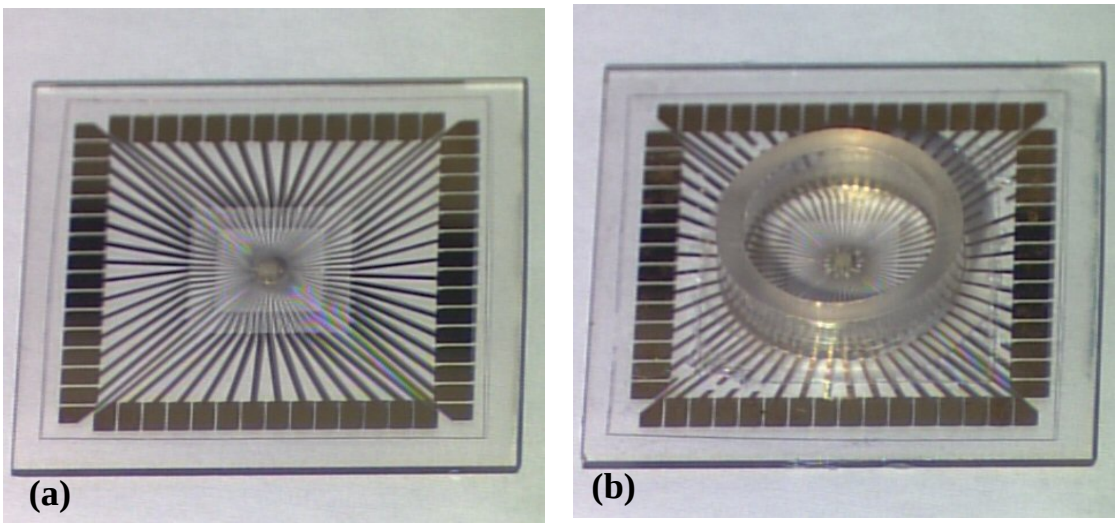

Figure 4.12 3-D Electrodes on a circular SU-8 substrate after removing a copper seed layer and parylene molds

The recording sites were placed on four different heights (100 μm, 300 μm, 400 μm, and 500 μm) to investigate 3-D cultured neuronal networks as shown in Figure 4.14. These finished 3-D electrodes have been tested and explained in the following section.

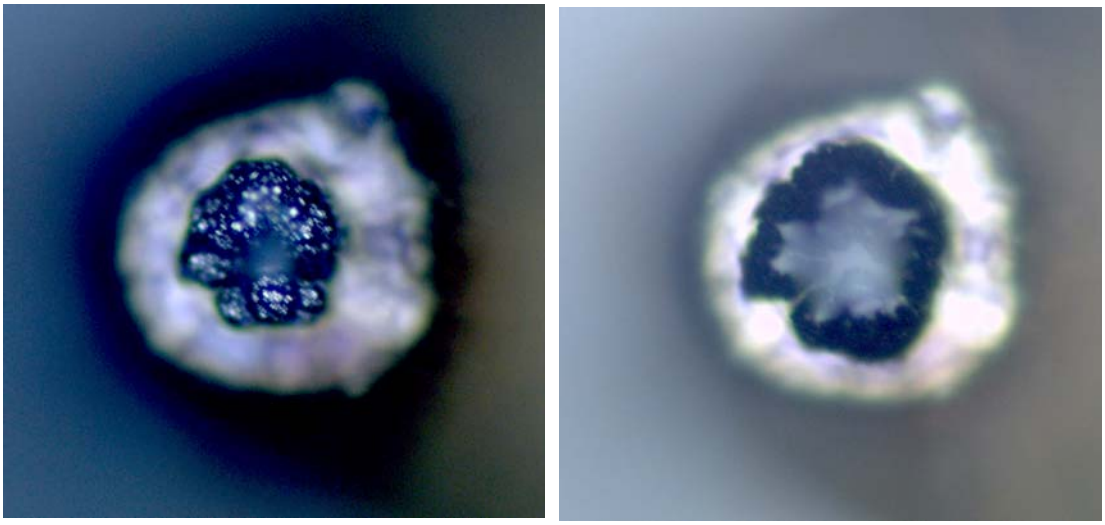

Figure 4.13 3-D Electrodes on a circular SU-8 substrate after removing a copper seed layer and parylene molds

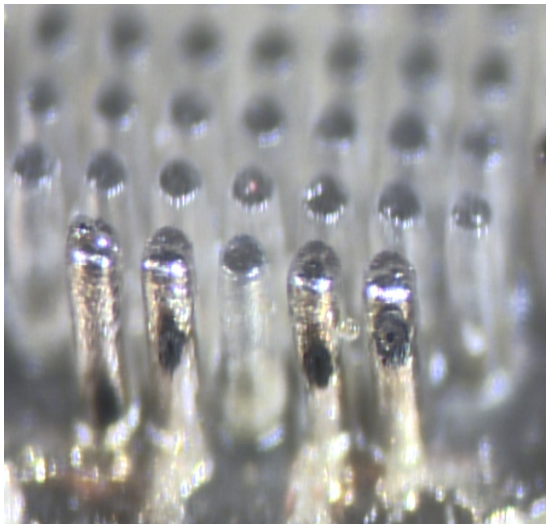

Figure 4.14 3-D Electrodes on a circular SU-8 substrate after removing a copper seed layer and parylene molds

4.2 Stimulation and Recording of 3-D MEA

4.2.1 Design of the Electronic Interface System

Before detailed explanations of the electrical experiments, it should be noted that these electrical stimulation and recording with 3-D MEA have been performed by Dr. Stephen DeWeerth lab at Georgia Tech.

Electrical stimulation is a common technique used to evoke cellular responses in neuronal cultures. Studying the role of stimuli in shaping neuronal development and connectivity is an important, ongoing problem in neuroscience. The use of MEAs offers extracellular electronic interfacing with fine spatial resolution, as a typical MEA has 60 electrodes at 200μm spacing. Efforts to extend MEA technology to 3-D configurations promises to further improve spatial detail. Taking full advantage of this resolution requires an easily scalable electronic system capable of both providing stimuli and recording neural activity at each electrode [70-73].

Significant technological challenges complicate the design of electronics for extracellular interfacing. Large signal losses are associated with extracellular recordings. The extracellular electrodes do not measure membrane potentials directly; rather, they record the electric field induced by ionic channel currents. This electric field decreases with distance from the cell, so the voltages present at the electrode are in the microvolt range, even though membrane potentials are in the millivolt range. Signal loss also takes place in the reverse path, so that extracellular stimulation requires voltages at the electrode that are many orders of magnitude larger than those due to cellular electrical activity due to signal losses from the cell membrane to the electronics, recording

meaningful signals with extracellular electrodes requires high performance amplifiers – that is, high gain and minimal input referred noise.

The stimulation voltages overwhelm the sensitive recording system, creating an effect known as the stimulation artifact. The stimulus artifact is particularly troubling because its long duration interferes with attempts to study the immediate response of neural cultures to stimulation. During the duration of the stimulation artifact, which can be on the order of 100ms, recording cellular activity becomes impossible. As neurons respond to stimuli within a few milliseconds, the loss of recording functionality for the entire duration of the artifact is unacceptable; thus, it is necessary to reduce the duration of the artifact [74].

The electronics system consists of stimulation, recording, and artifact suppression circuitry. Separate instances of these circuits are fabricated for each electrode, allowing the experimenter to use any electrode for stimulation and recording. Stimulation devices vary in the types of stimuli that they produce. The types of stimuli generally fall into two categories: voltage-control and current-control. Literature suggests that biphasic voltage stimulation is the most effective and least likely to cause electrochemical damage to the electrode [75]. With these requirements, the stimulation circuitry for biphasic voltage stimulation is designed, which gives the experimenter independent control of voltage levels and stimulus polarity.

Evaluation of the experimental functionality requires integration of the stimulation and recording system into a complete system with an MEA and a data acquisition system. The culture dish of the MEA contains an electrolytic medium. As a demonstration of the artifact suppression, the stimulation circuitry is activated twice –

first with the suppression circuitry inactive, then with the suppression active. The stimulation pattern begins with a 200 μs pulse of +0.5V, and finished with a 200 μs pulse of -0.5V. The electrode voltage at both the stimulation electrode and neighboring electrode are recorded. Without use of the suppression circuitry, the stimulation electrode voltage saturates the recording preamplifiers for over 30ms, as shown in Figure 4.15(a).

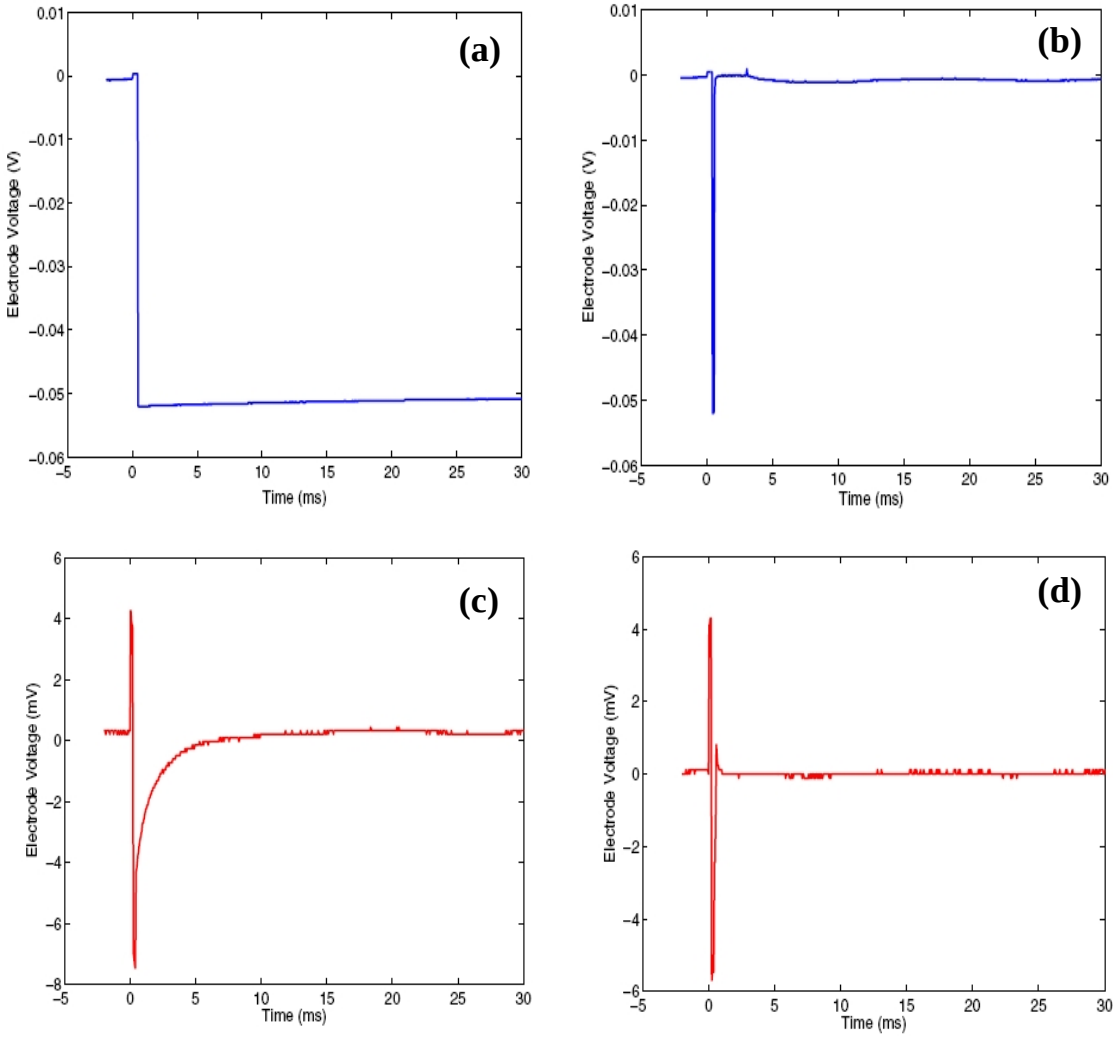

Figure 4.15 Results of artifact suppression experiments

The artifact is so large that it is noticeable even on a neighboring electrode (see Figure 4.15(c)). Use of the suppression circuitry results in significant reductions to the artifact in the stimulation electrode as well as the neighboring electrode. Briefly discharging the electrode after stimulation returns the stimulation electrode (see Figure 4.15(b)) and the neighboring electrode (see Figure 4.15(d)) to usable states within 3 ms. These experiments verify the effectiveness of the artifact suppression circuitry.

In order to verify that trapped charge causes the artifacts, stimulation systems are modeled. The model uses nonlinear equations that mimic the underlying physics of the system. The model stimulation source is an ideal voltage source in series with a time dependent resistance that models the stimulation switch. A physical system is also used to generate real artifacts. The physical system serves as the reference that the model systems attempt to reproduce. The models demonstrate behavior qualitatively similar to observed artifacts, thus providing a tool for development of integrated circuits for stimulation and recording. A SIMULINK model is used to consider the electrode as an interface capacitance, C_I (V), charge transfer current source, I_t (V), and spreading resistance, R_S, as shown in Figures 4.16. The nonlinear components follow the formulas:

$$C_I = A\frac{\epsilon_r \epsilon_0}{d_{OHP}} + \frac{\epsilon_r \epsilon_o}{L_D}\cosh\left(\frac{zV}{2U_t}\right) \quad (1)$$

where A is the area of the electrode, εrεo is the permittivity of the electrolyte, LD is the Debeye length, z is the valence of the ions in solution, d_{OHP} is the distance from the outer Helmholtz plane to the electrode, and U_t is the thermal voltage;

$$I_t = AJ_0 \left(\exp\left[\frac{(1-\beta)\, z\eta_t}{U_t}\right] - \exp\left[\frac{-\beta z \eta_t}{U_t}\right] \right) \tag{2}$$

where J_0 is the exchange current density of the electrode, β is a symmetry factor reflecting the energy barrier differences between oxidation and reduction, and η_t is the difference between the applied voltage and the equilibrium voltage; and

$$R_S = \frac{\rho \, \ln\left(4\frac{l}{w}\right)}{\pi l} \tag{3}$$

where ρ is the resistivity of the electrolyte, *w* is the width the electrode, and *l* is the length of the electrode.

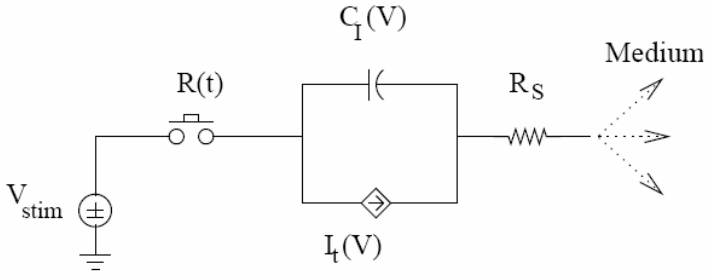

Figure 4.16 The nonlinear model of the electrode and stimulation voltage. The electrode model consists of a nonlinear interface capacitance, $C_I(V)$, a nonlinear charge transger, $I_t(V)$, and a linear spreading resistance, R_S. The model of the stimulation switch is a time dependent resister, R(t).

Generation of a model artifact is as follows: First, the variable resistor, R(t), assumes a low value, simulating connecting the stimulation voltage. Next, the stimulation voltage source creates a biphasic pulse. Finally, the variable resistor assumes high value, so that the only discharge path for charge through the electrode itself. Figure 4.17(b)

shows the generated artifact, which is very similar to the measured artifact of Figure 4.17(a).

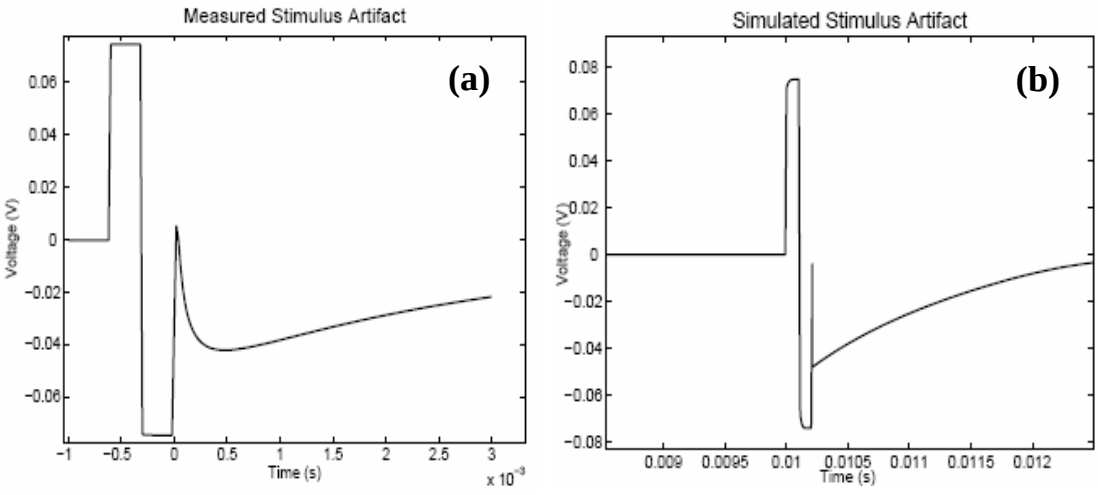

Figure 4.17 (a) Artifact generated by the physical system. (b) Predicted artifact from the nonlinear model

4.2.2 Electrical Measurement of 3-D MEA

To investigate the electrical functionality of the generated 3-D MEA, stimulation and recording have been done with the electronic system explained in the previous section. The commercial MEA60 from Multichannel system was also tested to compare the results. Active artifact suppression circuitry was employed to stimulate and record from a stimulating electrode, while passive recording was preformed on a neighboring electrode. Figure 4.18 shows the control panel which reports the stimulation and recording results and the input values they depend on. The input window marked by (1) is used to control the recording amplifiers. Artifact rejection timing is performed by editing the value of the input widow (2). Stimulation timing information is controlled by using input window (3). A graph displayed on window (4) is stimulation out. And window (5)

draws the output on stimulation channel (note: recording amplifiers are turned off during application of stimulation on the stimulating channel only). Window (6) shows the output on the neighboring channel; recording amplifiers are left on during stimulation.

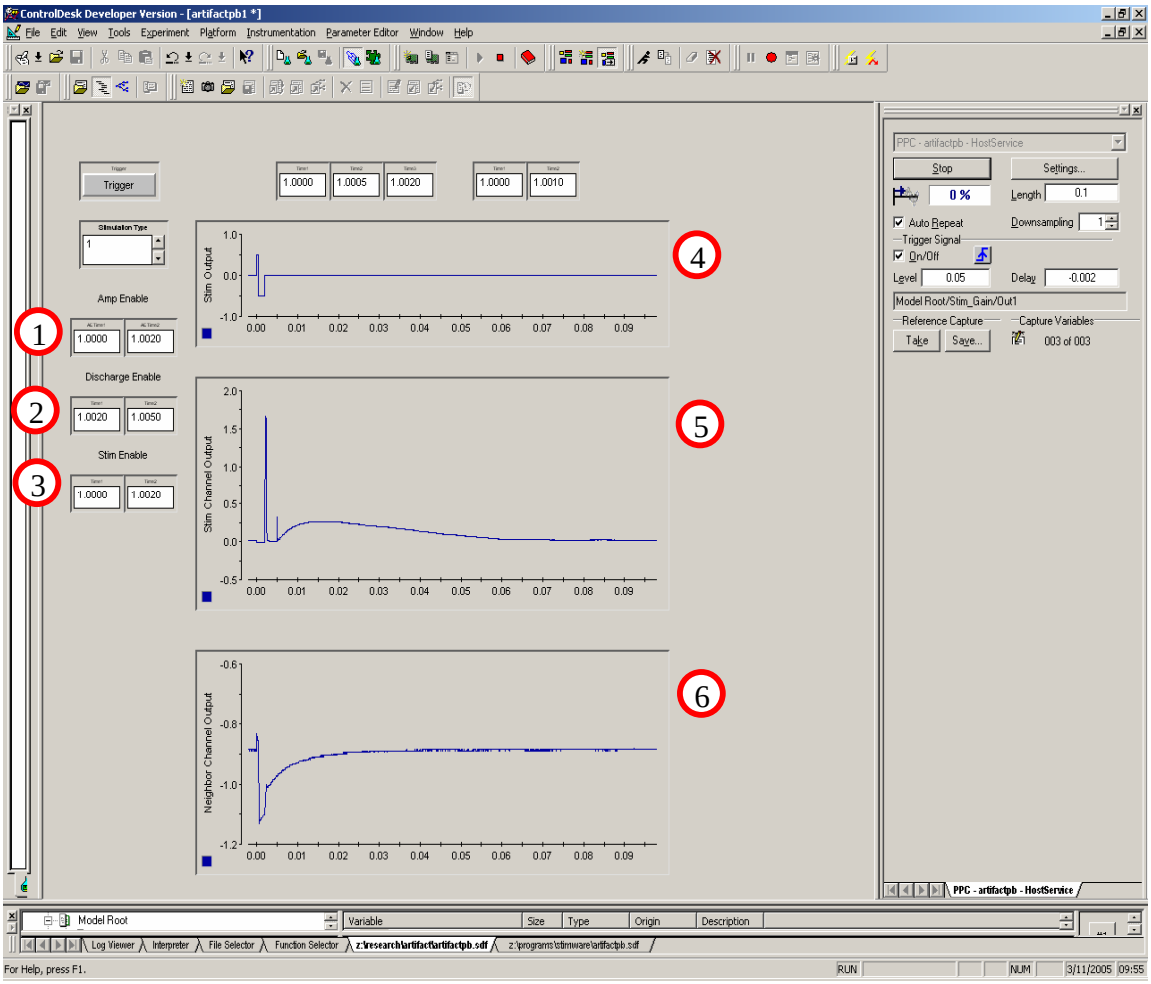

Figure 4.18 Control panel for stimulation and recording on multi electrodes.

Figure 4.19(a) shows the stimulation and recording results from a commercial MEA (MEA60, Multichannel systems), which were generated using stimulation artifact suppression. Figure 4.19(b) shows the stimulation artifact and the delay effect on the

recording channel. These pictures were generated by the control tool shown in Figure 4.18. And the graph-types are identical to graph numbers (4), (5), and (6).

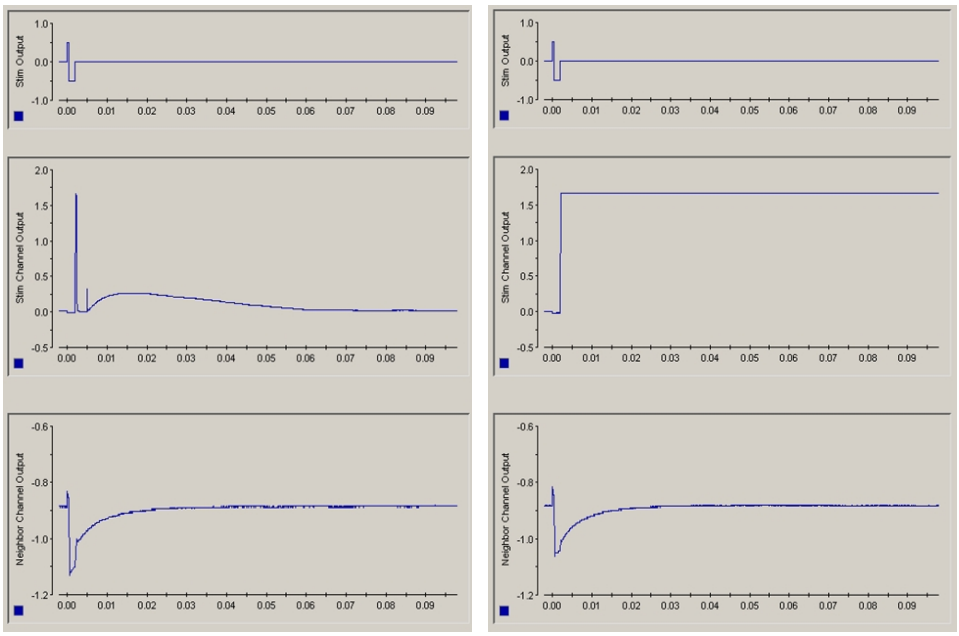

Figure 4.19 Results of stimulation and recording on MEA60.

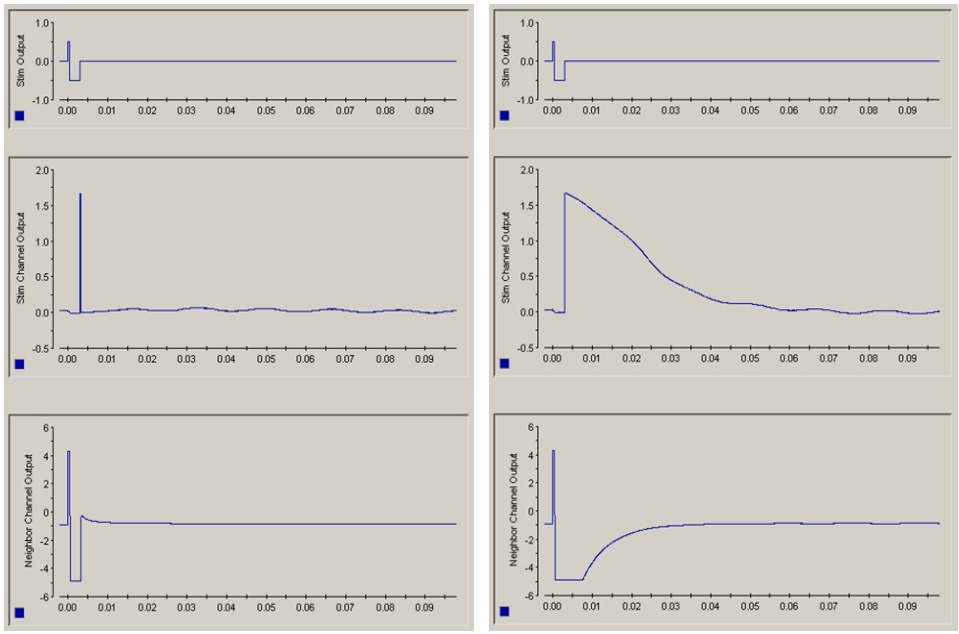

Figure 4.20 Results of stimulation and recording of 3-D MEA

Figure 4.20(a) shows the stimulation and recording results of the fabricated 3-D MEA, which was investigated with stimulation artifact suppression. Figure 4.20(b) shows the results which were generated with the stimulation artifact present. Compared with the results in Figure 4.19(a), the recording results of 3-D MEA in Figure 4.20(a) clearly demonstrate and improvement over the commercial system. Note that the original triggered signal was more faithfully reproduced on the neighboring channel in the 3D MEA.

The electrical improvements of the 3-D MEA over a commercial MEA has come from the flexibility of the design of the 3-D MEA system. Since electroplated metal lines are used for electrodes, 20 μm thick metal pattern was possible which could decrease the impedance of electrodes. The open areas of electrodes are also coated with platinum black, which form a porous structure that effectively decreases the impedance by one order of magnitude again. The parylene insulation layer coating the entire surface is 25 μm thick and removes any parasitic capacitance drastically.

Figure 4.21 shows an electrode model that was used to relate the effect of a stimulus to the impedance of the electrode. As a first order approximation, the maximum voltage produced in the media from a biphasic pulse can be shown to be

$$-V\max \approx \frac{-R_m}{R_s + R_m}\Delta V\left(1 - \frac{\Delta t}{2C_I\left(R_m + R_s\right)}\right)$$

where R_M is the resistance of the medium, R_S is the spreading resistance, and C_I is the interfacial capacitance.

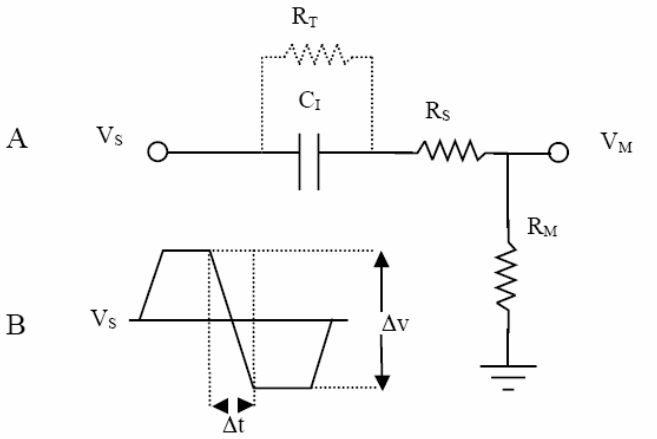

Figure 4.21 A) Circuit model for the microelectrode. The transfer resistance, R_T, is assumed to be infinite. R_S represents the spreading resistance. C_I is the interfacial capacitance, and R_M is the resistance of the media. B) Biphasic waveform applied at V_S

The spreading resistance is fixed by the base area of the electrode. Decreasing the impedance has the effect of increasing capacitance, thereby allowing for a reduction in ΔV without compromising the magnitude of V_{max} [76]. The results of impedance measurement of the 3-D MEA and the commercial MEA60 are shown in Figure 4.22. Although the open area of electrodes of 3-D MEA is 20 times bigger than the MEA60, the 50 times smaller impedance of the 3-D MEA can explain the big improvement on electrical functionality of the 3-D MEA.

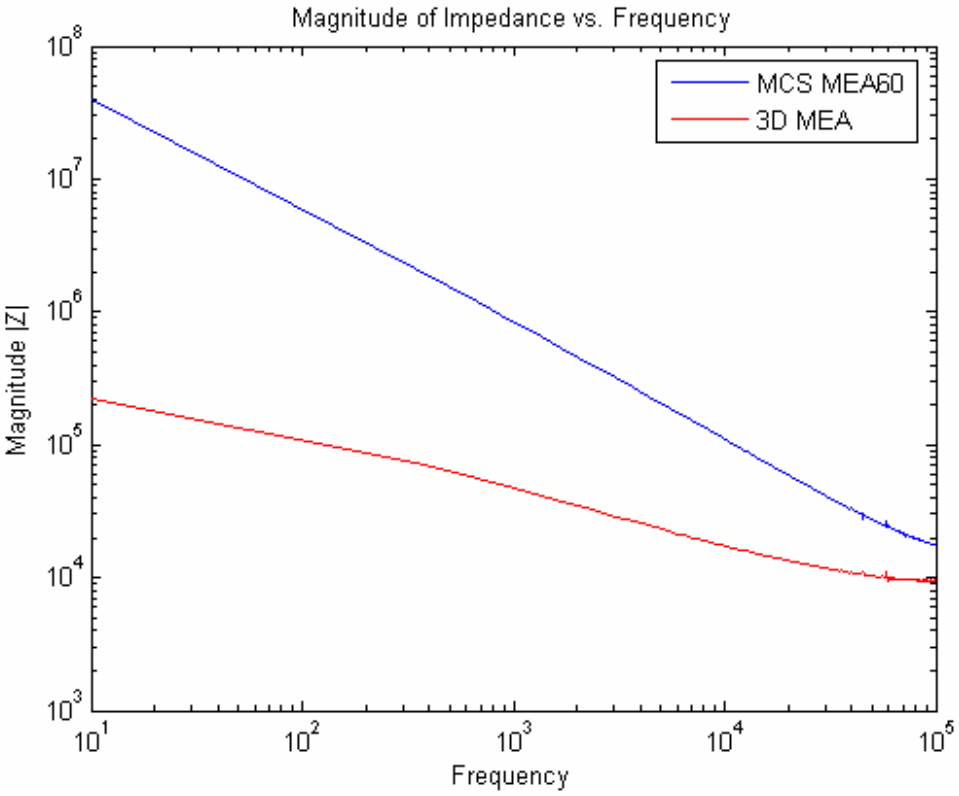

Figure 4.22 Impedance measurement of (a) electrodes of 3-D MEA (b) MEA60

CHAPTER 5

MICRONEEDLE ARRAYS

5.1 Introduction

So far, 3-D scaffolds, fluidic channels, and electrodes have been introduced for investigating 3-D neuronal culturing systems. Although cell culturing technology has been routinely used in basic biological experiments, there is a strong desire for alternative methods for *in vitro* study in neuroscience research fields. Note that it is possible to culture brain slices themselves. The advantage of culturing brain slices is the fast responses we can get from neurons since neurons inside brain slices are intact and can still generate the action potentials even after the brain is separated from body and cut into a small pieces [77-81]. Normally, the cultured neurons that are dissected mechanically and dissociated chemically from the brain can generate electrical signals 15 days after culturing. It takes that amount of time for the removed neurites from neurons to fully grow again and form networks between neurons in the cultured environment. Theoretically, it is possible to detect the action potentials from the neurons inside the brain slices just after starting the culturing because the living neurons are used immediately after dissection. Brain slice culturing also support a real *in vivo* biological environment that is not possible with any other *in vitro* research technology and the *in vitro* biological experiment should follow the *in vivo* experiments as closely in time as possible. Although it is possible to get some data from *in vitro* experiments alone, if the *in vitro* environments are much different from real environments, the strength of the data is considered less reliable due to its lack of correlation to an actual biological system.

The major hurdle in brain slice research is in extending the duration of the culturing. For chronic studies, it has been reported that it was possible to keep cultured cells networks alive for over a year. However, this is difficult for brain slice culturing. In cultured cell networks, nutrients can be applied on the culturing dish with pipettes and these can reach directly to neurons. On the other hand, it is difficult to supply nutrients to the neurons deep inside brain slices because the living tissue of the brain slices is a strong barrier for any chemical to penetrate inside of them.

There are two structural requirements -fluidic channel, sharp needle- to keep brain slices alive and be able to detect some electrical signals from them. The fluidic channels are useful for specific drug delivery applications but they are not necessary in cultured cell networks since nutrients can be directly applied on the culturing dish with pipettes. However, they are necessary for brain slice culturing since the capillary vessel inside the brain do not function any more and the nutrients applied to the outside of the brain slices cannot reach the neurons. The other requirement for brain slice culturing is the needle shaped structures to insert the devices into the brain slices, the 3-D MEA can be broken or the brain slice tissues can be damaged without sharp tips. To satisfy these requirements, a microneedle array that includes 3-D electrodes and fluidic channels is developed in this research.

Even though this microneedle was designed for brain slice culturing, there already exists a major research field called transdermal drug delivery (TDD) that uses microneedle arrays. Some TDD microneedle structures that are modified for brain slices are also presented in this chapter. This transformation was possible by little modification

of the pre-existing microneedle arrays since the device for brain slices has already been developed for insertion into tissue and applying liquid inside tissue.

5.2 Requirements of Microneedle Arrays

The first structural requirement of microneedles is a sharp tip to penetrate into the outer tissue of the brain slices. The sharper the structures are, the safer they are, especially for preventing damage to the microneedles and the tissues together. Several different examples of sharp microneedles have already been demonstrated in the literature. However, thin body, side opening and economical structures are still required even for TDD applications [82-86]. In this research work, a microneedle array that satisfies these requirements is presented. This technology can be combined with the 3-D fabrication techniques that were demonstrated in previous chapters. This combination of 3-D fabrication methods now serves as a powerful set of tools for the fabrication of various kinds of 3-D microstructures.

The sharp tip of SU-8 microneedles can be generated from tapered SU-8 solid towers using RIE etching [87, 88]. The solid towers were made by the same techniques that were used for 3-D scaffolds in chapter two. Because the height of the solid towers is up to 1mm including the substrate, it is already out of the range of standard photolithography tools used to make straight vertical structures seen in most examples of surface micromachining. The major reason of this tapered shape is due to diffraction of the UV light after it passes through the mask patterns [89]. Since the size of the mask patterns ranges from 20 ~ 100μm and the thickness of SU-8 pattern is 1mm, the aspect ratio can be up to 50:1. Although it is still possible to create patterns with these

thicknesses and aspect ratios by controlling the exposure energy, it is almost impossible to make perfectly vertical towers using such conventional methods. However, for developing the microneedle arrays, tapered structures of SU-8 were ultimately used. Relatively short RIE etching can make sharp SU-8 needles from tapered towers structures. Although some silicon microneedles have been created using similar techniques, the running time for etching silicon needles is around 30 times longer than the etching time for SU-8 needles (5~ 10min). Figure 5.1 shows the sharp tip of the microneedle array.

The second challenge in developing microneedle arrays was the implementation of the side open holes [90-92]. Because the purpose of this microneedle is insertion into the skin or brain slices, the open positions of fluidic ports must be placed on the side walls, otherwise shorn tissue may clog the channels and prevent the proper functioning of the fluidic systems. In this research work, the fluidic channels and the side openings can be generated easily by excimer laser boring which was demonstrated in section 3.14.

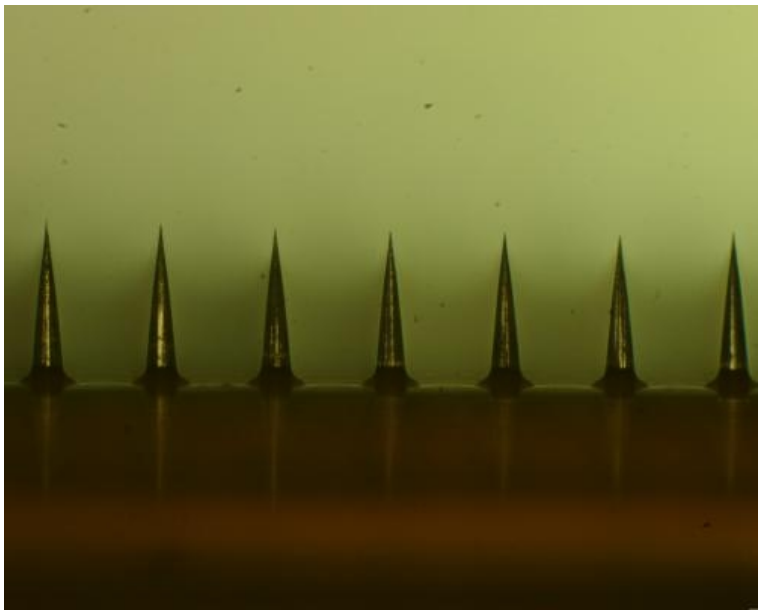

Figure 5.1 Sharp SU-8 microneedles

By drilling the hollow needle bore off center, side openings of fluidic channels are implemented and tip sharpness is also retained. In Figure 5.2, scanning electron micrograph images show a section of a hollow microneedle array with sharp tips and side-openings.

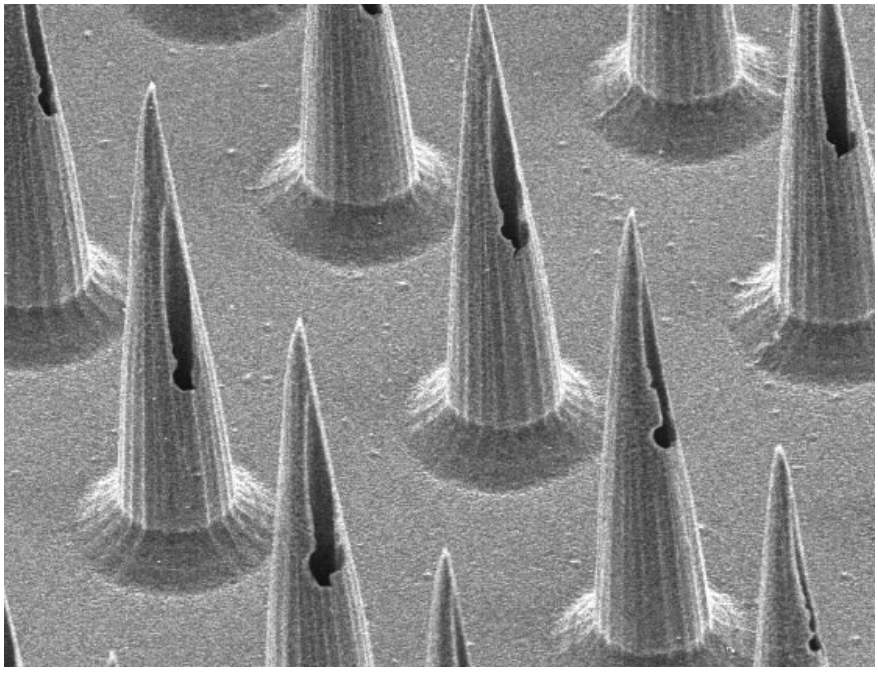

Figure 5.2 Side opening of fluidic channels

The other requirements for practical and reliable microneedles are strong structures and economical fabrication processes. Although SU-8 needles are weaker than the silicon needle, silicon microneedles are also not proved to be as safe for use in humans due to their brittle nature. To make microneedle structures strong enough to penetrate into the skin and brain slices, metal coatings on microneedles are necessary. In this research work, electroplated nickel is coated on SU-8 microneedles to provide

structural support [93]. Furthermore, the fabrication processes of SU-8 microneedles are so economical that it might be possible relatively easy to transition to commercialization of such microneedles.

5.3 Microneedle Arrays for Brain Slice Cultures

To investigate cultured networks of brain slices using microneedle arrays that were described in the previous section, one additional functional explanation is still necessary. Since the primary goal of the neuronal interface system is to detect electrical signals from brain neurons, these microneedle arrays should have 3-D electrodes on the surface of the microneedles themselves to pick up the signals. The 3-D electrodes can be combined with microneedle arrays using the same method as was used for the 3-D cell culturing system described in chapter 4. The only difference between these two systems is the solid tower shape versus the needle shape in the base structures. Therefore, only the fabrication techniques for making sharp needles and hollow channels are described in this chapter. Figure 5.3 shows the conceptual view of the 3-D microneedle array that has electrical and fluidic functionalities.

The fabrication steps for SU-8 microneedles are composed of four major steps: generating high aspect ratio SU-8 tapered towers, sharpening the tips of the microneedles, laser drilling for the drug delivery channels, and making 3-D electrodes on the needle structures. Figure 5.4 shows the fabrication sequence. A glass plate including chromium patterns was used as a temporary substrate.

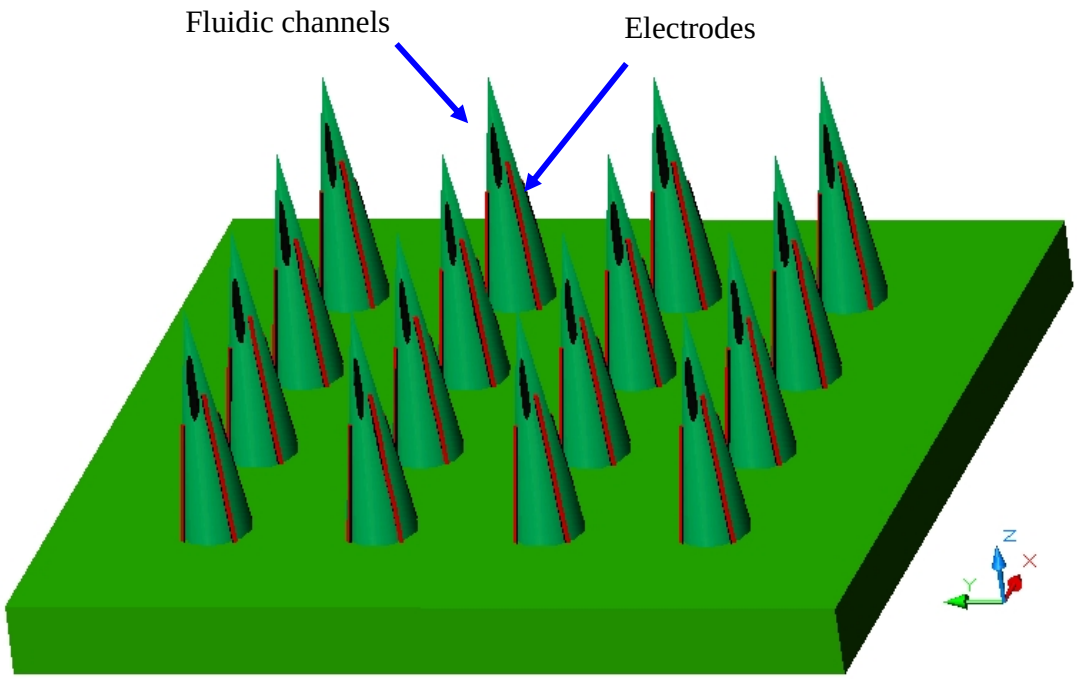

Figure 5.3 Conceptual view of microneedle arrays for brain slice culture

The mask patterns were circle arrays for the towers. 100 μm thick SU8 2025 was spin-coated on the patterned chromium side of the glass, which can remove the air gap between a mask and a sample and generate shapes that are closer to the mask patterns. After soft baking (2 hours at 95°C on a hotplate), the sample was exposed (800mJ/cm2) to make SU8 substrates. Without post-exposure baking and developing of the first layer, the second layer of SU8 was coated for the towers to around 600 μm thickness. During soft baking of the second layer, the exposed first layer of SU8 was cross-linked. Skipping the post-exposure baking and development for the first SU-8 layer not only saves processing time but also increases the adhesion force between the first SU-8 substrates and the second SU-8 towers.

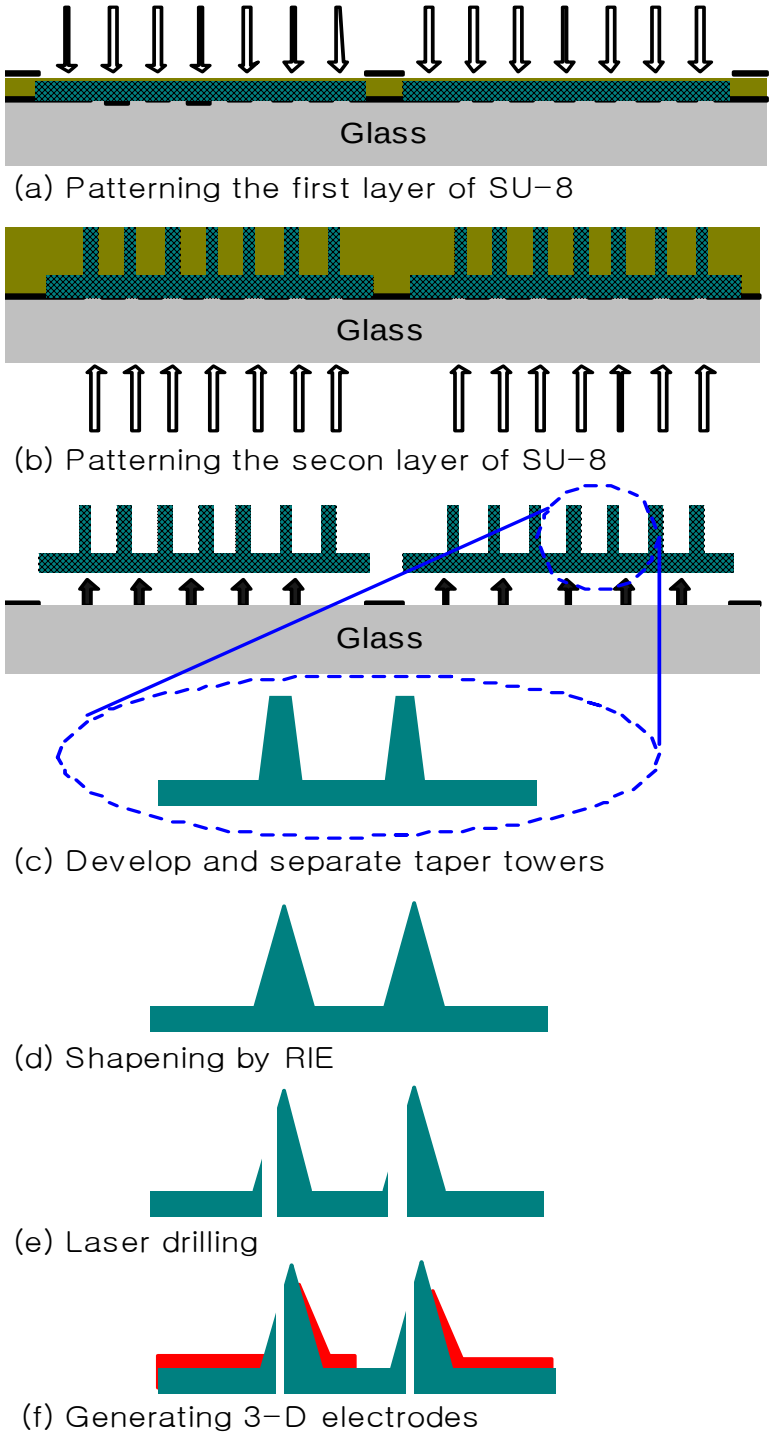

Figure 5.4 Fabrication sequence

Backside exposure (5000mJ/cm2) was performed to make the towers after soft baking the second layer of SU-8 through the chromium patterns on the glass substrates. After post baking (2 hours at 95°C on a hotplate), the sample was developed with PGMEA. With this single development, both the first and the second layers of SU-8 are patterned together. Even the unexposed parts of the first SU-8 layer were dissolved in PGMEA. Using the patterned chromium substrates and the backside exposure, the 600 μm thick hollow towers were generated on the SU8 substrates without any adhesion problems. With the back side exposure, the towers were developed as a taper shape. The angle of the tapered towers can be controlled by the amount of exposure energy during photolithography. After generating the tapered pillar structures, the sharp tips of the microneedles were made using the reactive ion etcher (700 series wafer/batch Plasma Processing System, Plasma Therm Inc). The sharp shapes of the tips were generated by isotropic etching on the tapered towers with the following conditions: gas ratio, CHF3(10sccm)/O2(100sccm), pressure, 1000mTorr, and power, 100W. The high pressure was selected to increase the degree of isotropy during etching and the lateral etching rate. The power level was kept low enough to control the etching speed and make smooth surfaces on the microneedle arrays. The etching rate of SU-8 with the above conditions was 2μm/min. Figure 5.5 shows the etching status at every minute. Figure 5.5(a) shows the tapered towers just after the photolithography processes. Figure 5.5(c) ~ (n) show the process of sharpening the SU-8 needles by increasing the RIE running time. Because the RIE etching processes were checked every minute, the practical etching rate was different from these ten minute etching tests, due to the fact that the gas stabilization time inside RIE chamber for each cycle was more than one minute.

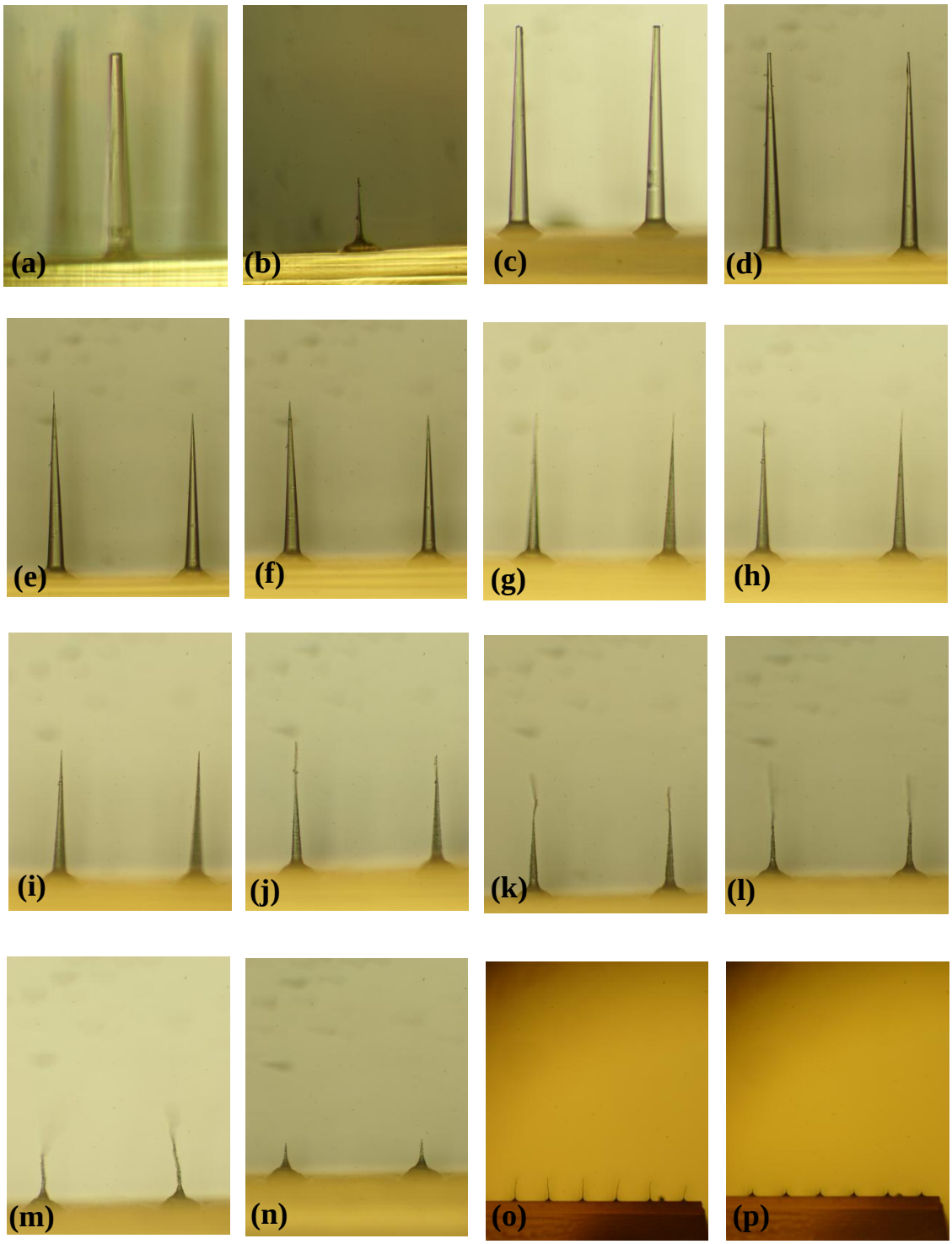

Figure 5.5 RIE etching procedure

Usually the recommended processing time for RIE is more than ten minutes to get a conformal etching rate. The needle structures in Figure 5.5(b) were etched for five minutes without interruption and it produced a shape that was almost the same shape as that in Figure 5.5(l), which was done for 9 minutes including restarting every minute after taking pictures. An additional advantage of this RIE etched SU-8 needles is the relative ease with which height of needles can be controlled by controlling the etching time. RIE etching can control not only the sharpness of the SU-8 needles but also the height of the needles. As shown in Figure 5.5(b) ~ (m), the height of the needles proceeded inversely proportional to the sharpest tip. Further RIE etching after creating sharp tips generated residues on the tips as shown in Figure 5.5(m),(o), and the residues could be easily removed by 10 seconds of sonication as in Figure 5.5(n),(p).

Although the height of the needles can be controlled by the thickness of the spin-coated SU8, the RIE etching time used for generating the sharp tip is an alternative parameter to modify to control the height of the needles. It provides greater flexibility in the design of structures with the possibility of modification after finishing the photolithography steps.

After making the sharp SU-8 needles, the next step was laser drilling the holes through the microneedles and base substrate, oriented off-center but parallel to the microneedle axis. This created holes that serve as the microfluidic needle bores for injection or infusion, which terminate in side-opened holes along the needle shaft below the needle tip. Directionality of the laser and high ablation rate of SU-8 with excimer laser make it possible to generate 600 μm length 20 μm diameter channels inside SU-8 needles. Laser ablation was done with two different beam spots. First, 100 μm diameter

laser beam was used for boring big holes which are started from the bottom of substrate and to just below the bottom of the needles as shown in the Figure 5.6(a). After that, the 20 μm smaller laser beam was used to make the fluidic channel inside the needles. This two steps laser ablation process has been used both for increasing the fluidic efficiency and also to enhance the economic feasibility of the fabrication. If the small channels begin from the bottom of the substrate, the fluidic resistance is increased as the thickness of the substrate that can be removed. Two times the fluidic resistance requires two times the fluidic pressure to apply drugs and is a big barrier in designing fluidic systems. Although the two steps laser ablation process increases the processing time, the shorter length of the ablation saves power in the laser system. There is an optimal length of the ablated channel given a beam of a certain size that was empirically derived.

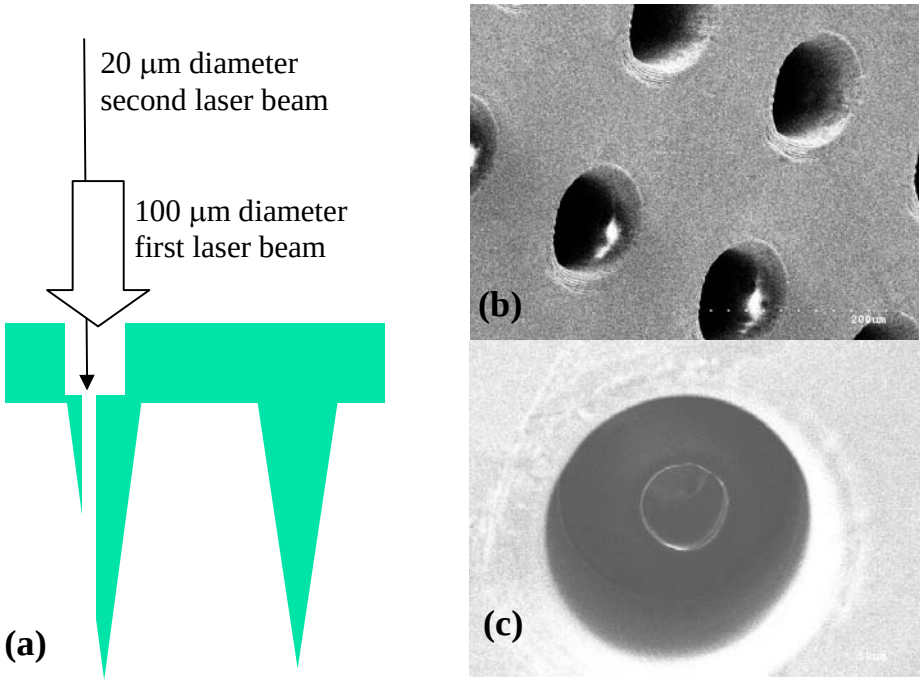

Figure 5.6 Two steps of inlet of fluidic channels

For example, a 50 μm diameter laser beam can make holes linearly up to 500 μm in depth. For a diameter of 500 μm, 100 pulses of the laser beam creates 100 μm deep holes. The ablated length decreases abruptly over a depth of 500 μm. 1000 pulses made 500 μm deep holes, but 1500 pulses made holes that were just 550 μm deep and 2000 pulses made 570 μm deep.

After finding a reliable recipe for creating sharp needles and micro fluidic channels, tower arrays on 2.7 mm diameter circular disks were generated for brain slice culture systems. Figure 5.7(a) shows the microneedle arrays on circular SU-8 substrates. Figure 5.7(b) shows the fluidic channels inside the microneedles. The green light was illuminated from the backside to provide a clear view of the laser ablated fluidic channels.

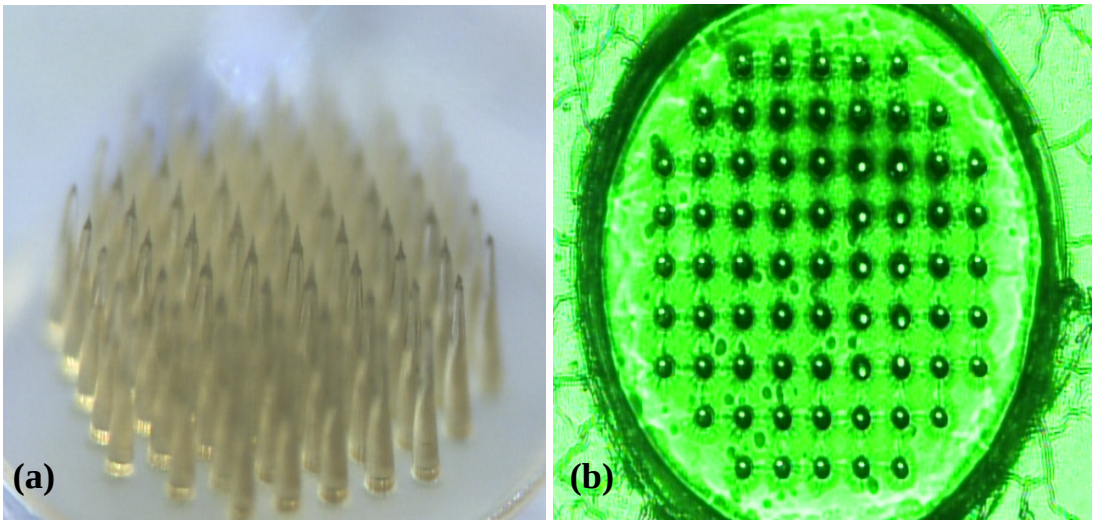

Figure 5.7 (a) Microneedle arrays on circular SU-8 substrates (b) Fluidic channels inside microneedles

Figure 5.8 shows insertion test of microneedle array with 500 μm thick brain slices. Figure 5.8(d) show the tip of the microneedles which pierced through the brain slices. Currently, gold coated and parylene coated microneedles have been investigated for biocompatibility and strength test of the structures have been performed.

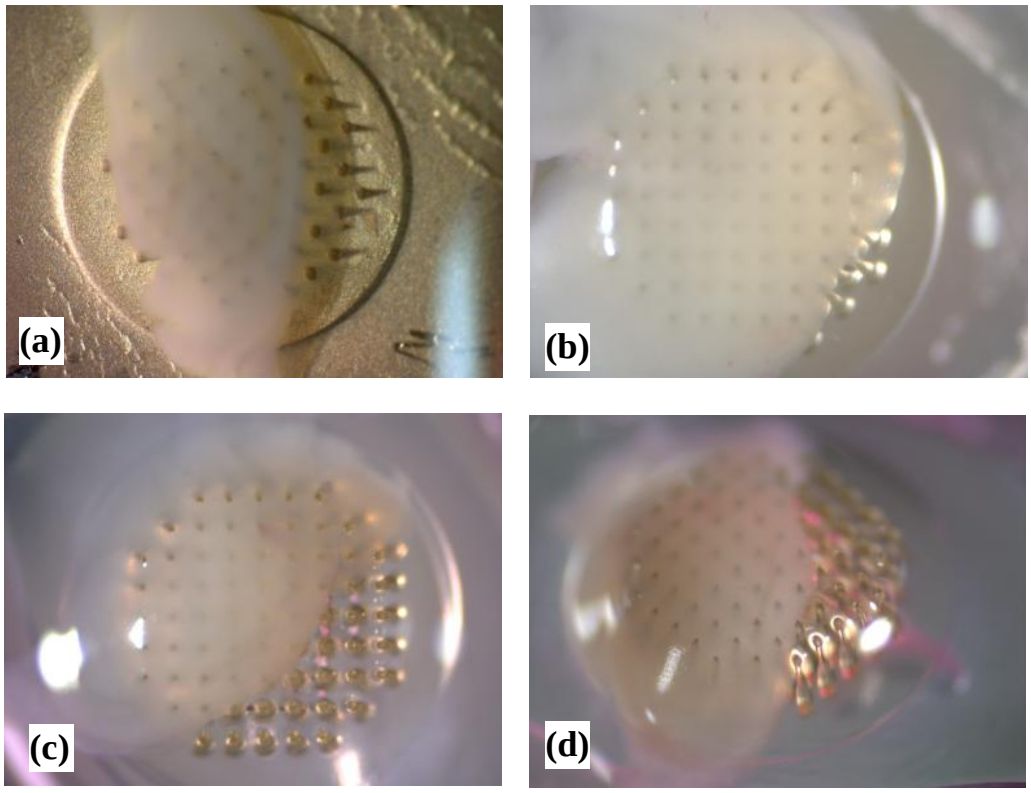

Figure 5.8 Insertion test of microneedle array (a) gold coated needle (b) parylene coated needle (c) bare SU-8 needle (d) perspective view of (c)

5.4 Brain Slice Culture

Initial brain slice cultures were performed on the fabricated hollow needle array at Dr. Bruno Frazier's lab in Georgia Tech. The needle array as shown in Figure 5.7 was connected to a PMMA manifold and flow tubing. The manifold has a large reservoir to apply equal pressure drop to each hollow needle. A 35 mm diameter Polystyrene Petri dish is also combined to supply enough nutrients to the surface of brain slices. Figure 5.9(a) shows the assembled microneedle array and Figure 5.9(b) shows the conceptual side view of the system.

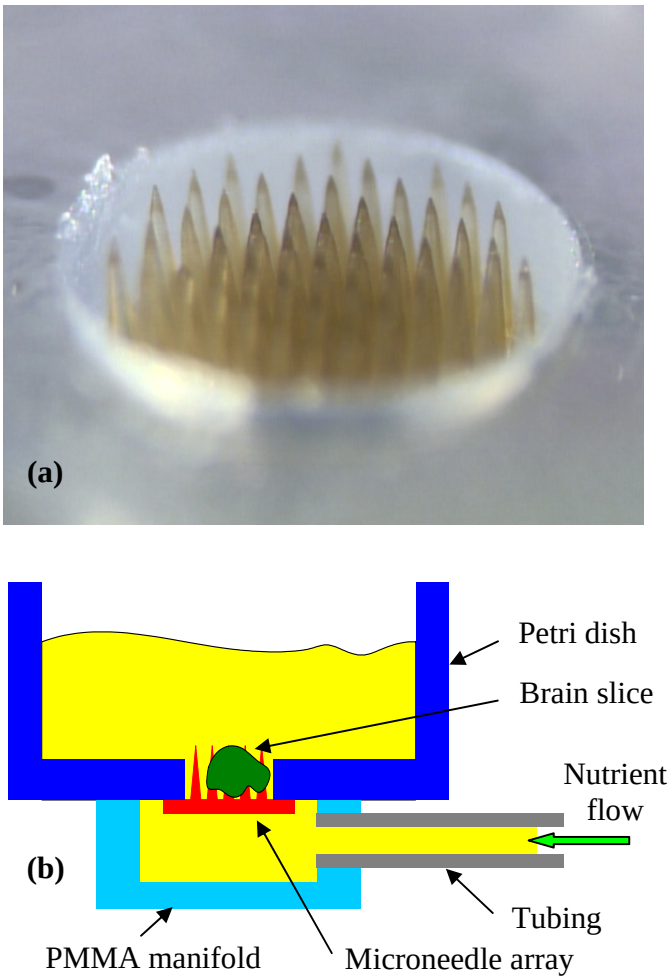

Figure 5.9 Fluidic perfusing system for brain slice culturing

Day 9 Sprague Dawley rat pups are anesthetized with halothane, and decapitated. The hippocampi from both sides are isolated and simultaneously sectioned into 400 μm thick slices using a McIlwain tissue chopper. The time from decapitation to tissue isolation is less than 15 min. The tissue is then placed in 5 ml of media in a Petri dish, which has been kept on ice. The composition of media is described in Table 5.1 [94, 95]. The slices are separated in the Petri dish and individually transferred to the system in which they will be cultured.

Table 5.1 Cell Growth Media

COMPONENTS	AMOUNT
Inactivated horse serum	25%
Hanks' balanced salt solution	25%
Optimem media	50%
D-glucose	25mM
L-glutamine	1mM
Penicillin/Streptomycin	2%

Upchurch "nanochem" fittings, Teflon tubing and a BD polypropylene syringe are used for fluidic connection. The system is flushed with EtOH, and then sterile water, then growth media for 30 min each using a syringe pump (flow rate of 1 ml/hr) under UV exposure in the laminar flow hood. In between the sterile water and growth media flushing, the sample piece is incubated for 2 hrs. The whole system is consecutively flushed with ethanol, sterile water and poly-L-lysine (PLL). PLL coating is used to promote cell attachment on the SU-8 structures. Then, the device is aseptically connected

to a syringe with media and perfused until the media is seen flowing out of the needles. After filling the whole fluidic channels with the media, a hippocampal slice is gently laid on the array. The flow rate of growth media which is controlled by a syringe pump is 20 μl/hr, which is about 500 ul/24 hr. The flow rate of growth media was not optimized. Brain slice cultures have been incubated in the incubator (36 deg C, 5% CO2) for four hours. Although it is a short term experiment, it is still useful for electrical stimulation and recording experiments. The dissociated cell culturing requires more than two weeks for growing whole neurites from the dissociated cells. However, the brain slice culture can generate electrical action potential just after starting the culture because a brain slice is a living organism and neurites are already well grown.

After 3.5 hours of culturing, Hoechst and Propidium Iodide dyes are used to image the dead and living cells. Hoechst (blue) stains the nucleic acid of all cells, Propidium Iodide (red) stains only the nucleic acid of dead cells. Therefore, the dead cells are red and live cells are blue. Hoechst (1/5,000 dil) and PI (3 μM) are diluted in media and poured on top of the slice, incubated in the incubator (36 deg C, 5% CO2) for 60 min. Before imaging, the slice is rinsed with D-PBS. Confocal microscopy is used for imaging of the brain slices where multiple z-stacks of the slice have been taken and then reassembled to present a 3-D view of the entire slice. Figure 5.10 shows the images which are taken from the cultured brain slices using a confocal microscope. Figure 5.10(a) shows the brain slice which was cultured without fluidic perfusion inside the tissue. 920 μm x 920 μm window images are taken at every 10 μm elevation through the slice - scans are shown as ”film strips” in 10 μm intervals between the top and bottom of the slice.

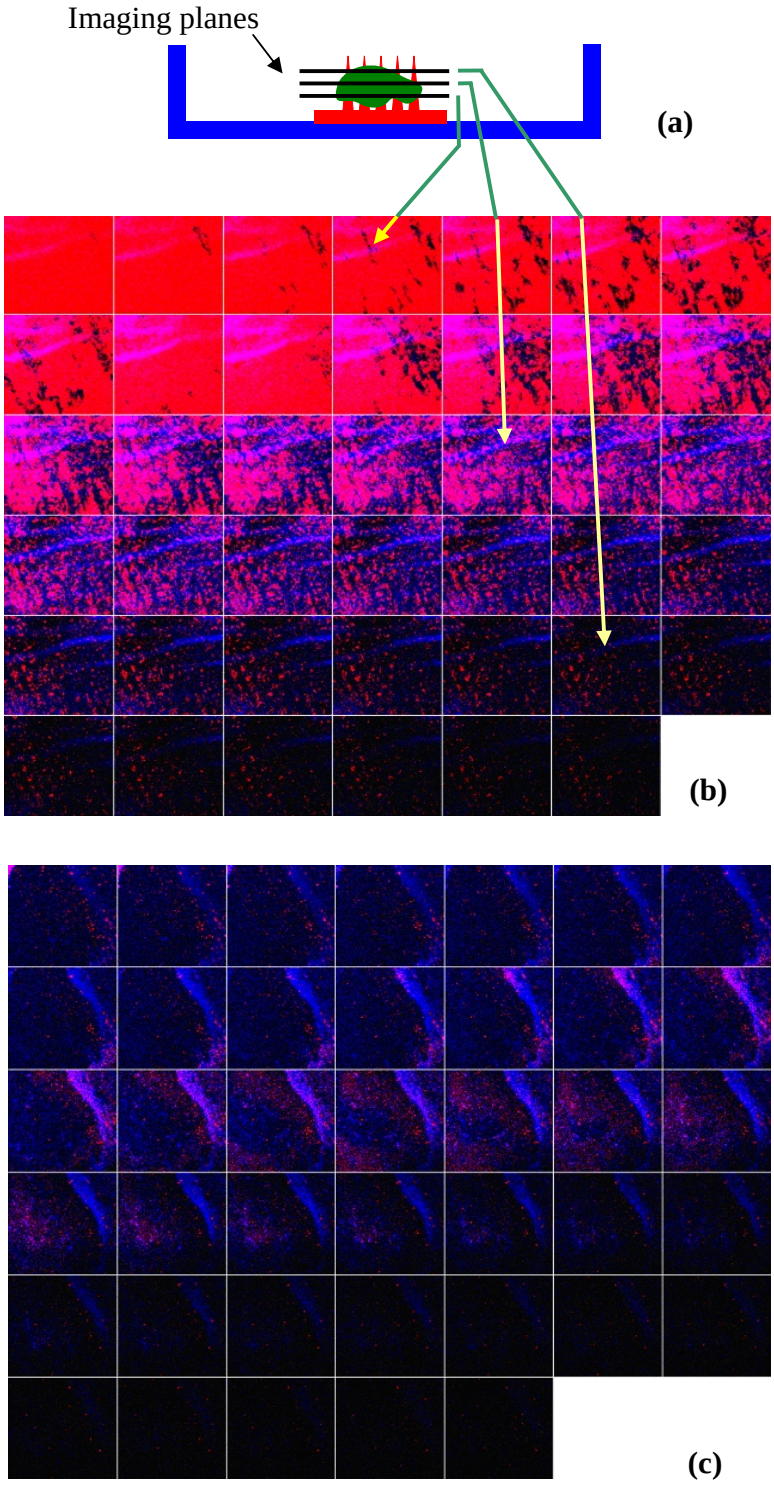

Figure 5.10 (a) Conceptual side view of a culturing dish with imaging planes (b) Confocal microscope images from non-perfused tissue (c) perfused tissue

41 cuts of pictures were taken of the brain slice, from the bottom to a height of 400 μm. After four hours, almost all cells in the brain slices die without a growth media perfusing system, although the slice was soaked in the media. Figure 5.10(b) shows the images which were taken from the brain slices that were cultured with a fluidic perfusing system. By comparing both results, the growth media perfusing system shows a marked improvement in the cell survival rate, even in these preliminary experiments. As the next step, long term slice culturing and adhesion properties between cells and microneedle array have been investigated.

5.5 Microneedle Arrays for Transdermal Drug Delivery

The perfusion of nutrient into brain slice tissue is reminiscent of the problem of transdermal drug delivery (TDD), namely, “perfusion” of drug across the stratum corneum and into deeper layers of skin. Since the devices used for brain slice perfusion are structurally similar to those previously utilized for TDD, the structures were evaluated for this alternative applications. TDD systems have been attractive dosage methods as new promising drugs have been developed which are not suitable with conventional dosage forms. TDD systems are also more patient-friendly methods than oral dosage and injection. Arrays of hollow microneedles have been proposed to achieve painless injection and infusion of drug solutions into the skin. Using the tools of microfabrication, a variety of hollow microneedle designs have been developed and a limited number have been demonstrated to deliver drug into skin. Most hollow microneedles have been fabricated out of silicon, which is not yet known to be safe for human use. Some have been fabricated out of metal, which can provide strong needles

made of FDA-approved materials. The requirements of microneedles for TDD might be met by a small modification of current microneedles for brain slices, which uses sharp-tipped, solid, polymer microneedles as a core structure that is coated with metal to provide added strength.

The only additional requirement over the microneedles of the previous section is the addition of metal coating. The needle arrays were coated with nickel by electroplating to increase their mechanical strength which was enough to penetrate the hard stratum corneum of skin. To test the ability of side-opening, hollow microneedles to insert into skin, microneedle arrays were attached to a vertical micropositioner that pressed the microneedles against and into pig cadaver skin. The needles were left inserted within the skin for 10 min, after which they were removed and a solution of Trypan Blue was placed onto the insertion location to facilitate imaging needle penetration sites. After 5 min, the dye was washed off the skin surface and the skin was imaged using bright field microscopy.

Using the microneedle design and fabrication method which explained in previous sections, hollow polymer microneedles were made with a metal (gold and nickel) coating and off-axis side openings, as shown in Figure 5.11. Each array contains 69 individual needles measuring 570 μm in height 120 μm in base diameter, and tapering to a sharp tip as shown in Figure 5.12. The position of the side-opening hole could be moved to different heights along the needle shaft and the size of the hole could be varied by changing laser drilling parameters. The shape of the hole was an oblong oval shape, which was inherent to the microneedle fabrication method.

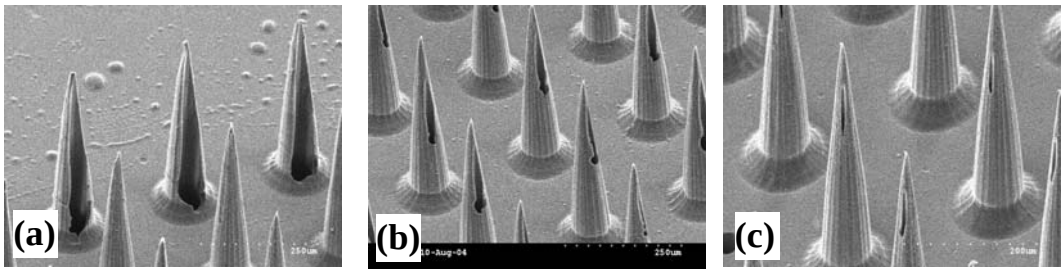

Figure 5.11 Metal coated microneedle array with different size of diameter of side openings: (a) 50 μm (b) 20 μm (c) 10 μm

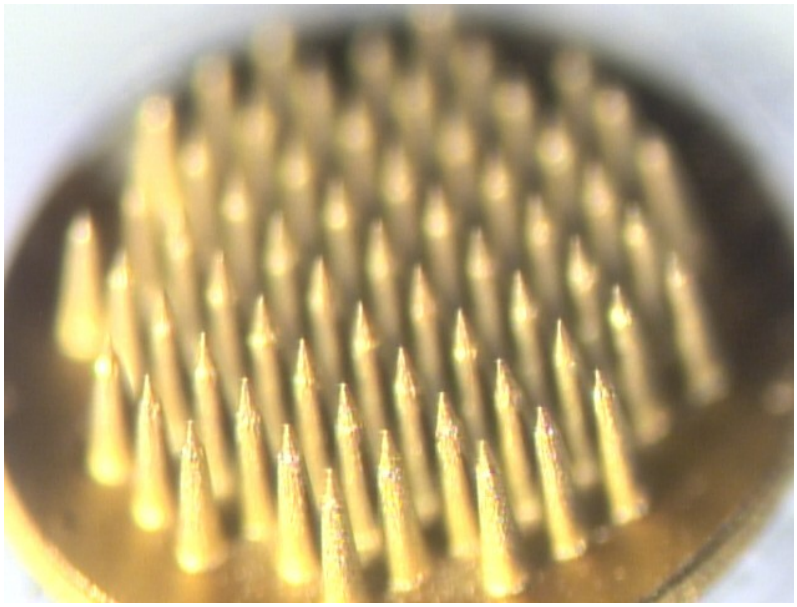

Figure 5.12 metal coated microneedle array

These microneedles were designed to have a polymer core with a metal coating that would provide mechanical strength. To determine if these microneedles were sufficiently strong, they were inserted into pig cadaver skin. After removing them, the microneedles were examined by brightfield microscopy and found to remain intact. The skin was also exposed to a blue dye, which stained sites of microneedle penetration after

excess dye was wiped off the skin surface. Figure 5.13 provides an image of the skin surface, which indicates that essentially all microneedles were inserted into the skin to create pathways for transdermal penetration. For drug delivery applications, microneedles need to be interfaced with a pump or syringe for injection or infusion. Figure 5.14 shows a 69-needle array of microneedles coupled with a liquid manifold and pump connection. This system could be used for transdermal drug delivery as well as other microfluidic applications.

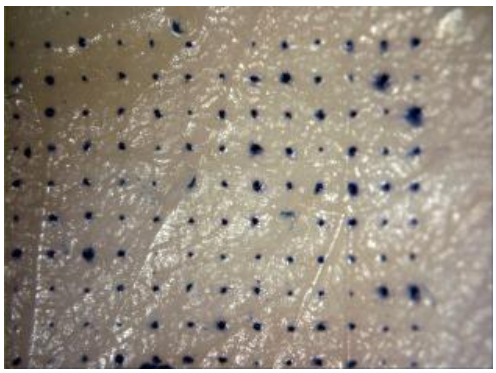

Figure 5.13 Surface of porcine skin after insertion and removal of microneedles *in vitro*

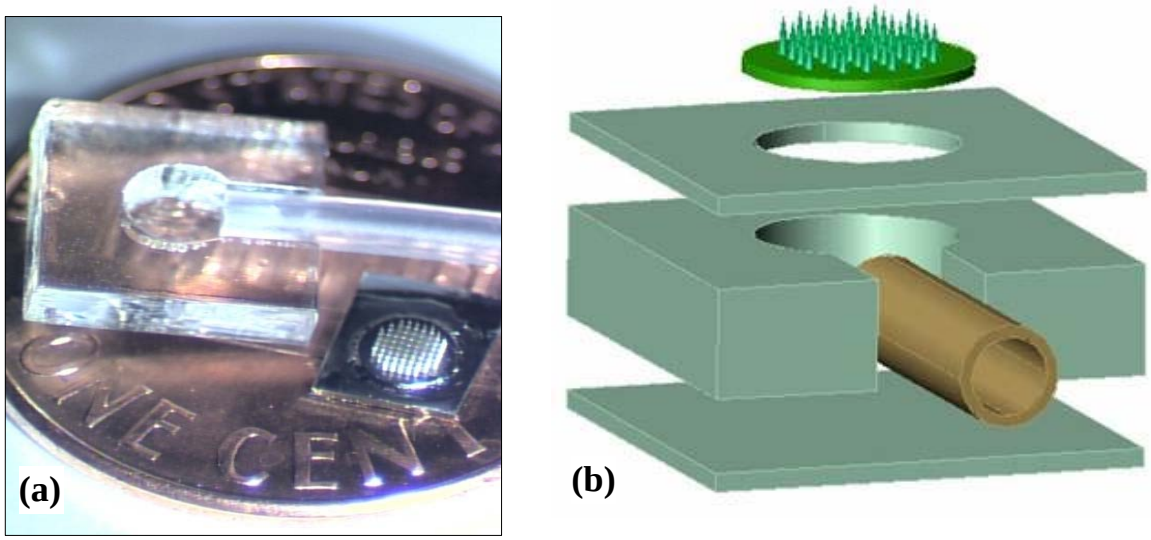

Figure 5.14 (a) A microneedle array and its manifold pump connection shown next to a US penny. (b) Schematic design of the microneedle array with manifold pump connection.

CHAPTER 6

CONCLUISIONS

6.1 Summary

The ultimate goal of this research is to implement 3-D *in vitro* neuronal interfacing systems which have electrical and fluidic functionalities. Two different applications were chosen for these systems: cell cultured networks and brain slice culturing. To address neurons inside 3-D cultured networks and brain slices, high aspect ratio SU-8 towers and microneedles were generated. 3-D multi-electrodes and 3-D micro-fluidic systems were combined with those base structures.

This research began with developing 3-D scaffolds which were the fundamental structures to implement additional electrical and fluidic structures on. The scaffolds facilitate the development of focal contacts by which the cells can adhere to the substrate and provide structural pathways by which the cells can make synaptic connections to each other. Two different types of scaffold structures have been fabricated. The first scaffolding scheme employed a double exposure technique that embeds SU-8 towers into an SU-8 substrate. Structures over 700 μm tall with aspect ratios as high as 35:1 have been fabricated. Arrays of 8 x 8 and 16 x 16 towers with tower diameters ranging from 20 μm to 200 μm and edge-to-edge tower spacing ranging from 100 μm to 225 μm were successfully fabricated for 3-D cell culturing.

The second scaffolding mechanism introduced interconnects between towers for the purpose of mechanically supporting 3-D cell cultures and facilitating 3-D synaptic connections. Several dimensions of towers and cross-connects have been tested to find

optimal structures of scaffolds for cell culturing. Towers with heights of 500 to 700 μm and diameters of 50 to 250 μm were used for neuronal culturing first. Then, to promote 3-D culturing, cross-connects with widths of 20 to 100 μm were combined with towers.

Constructing microfluidic channels on 3-D scaffolds was the next goal of this research. The fluidic systems were combined for fine control of the cellular microenvironment by means of diffusive and convective fluidic processes. Hollow towers with three-layer side ports were developed by using double exposure techniques and excimer laser ablation. Because no micro-assembly is required, these simplified fabrication methods save several steps in the fabrication of microfluidic channels compared to conventional micro-machining technologies.

The 3-D multi-electrode arrays were also combined with 3-D scaffolds that were capable of monitoring electrical activities and the cellular impedances of neurons which would be attached to the electrodes. The electrical functionality of 3-D electrodes was demonstrated by setting stimulation at one electrode and recording it at a neighboring electrode. The results were compared with commercial MEA and showed reasonable improvement by electrode design.

The alterative approach of this research work, investigation of 3-D *in vitro* neuronal networks, is to fabricate a microneedle array for monitoring brain slices, which will directly detect electrical signals from living brain slices. Although the microneedle array is targeting different 3-D neuronal networks, it also has three components and the fabrication steps are the same as those for the 3-D MEA. The only structural difference is the sharp, needle-like shapes of the scaffold for penetrating the brain slices. To generate the sharp tip, isotropic reactive ion etching (RIE) is performed on tapered SU-8 towers.

High aspect ratio tower structures can be effectively generated with SU-8 and tapered shapes are created by backside exposure.

These microneedle arrays have also been tested for transdermal drug delivery systems with little modification from the previous version. To penetrate the hard stratum corneum of skin, the microneedles arrays were effectively coated with electroplated nickel to make strong structures. The modified microneedle array could be upgraded up to commercialized devices with fluidic applying manifolds, because of its practical fabrication methods and efficient structures.

The resulting neuronal interface systems will enable a new field of neurobiological research, in which the collective properties of 3-D neuronal circuits can be observed and manipulated with unprecedented detail and precision, and at a level of control not possible in living animals.

6.2 Suggestions for Future Work

The 3-D scaffolds were combined with 3-D microfluidic systems and 3-D multi-electrode arrays respectively. The 3-D fabrication techniques demonstrated for each structure are independent of each other. Therefore, it is possible to make each structure working separately regardless of the other structure. Given the independent fabrication technologies of these three systems, 3-D scaffolds, 3-D microfluidic systems, and 3-D multi-electrode arrays, it seems to be very plausible to integrate all into the final system in the future. Finally, the optimal 3-D cell culturing protocols for such systems need to be determined. Further biological experiments on these structures will undoubtedly suggest future modification of the mechanical structures as well as biocompatible material

alternatives. Although the developed 3-D systems have shown the possibility of 3-D neuronal culturing, there is still room for modification of the structural design and for exploration of different shapes of scaffold structures. Therefore, reliable and denser 3-D cell culturing might well be further explored before integration of all structures.

Although brain slice culturing using microneedle arrays is an attractive alternative, there could be some biocompatibility issues. Since the 3-D cell culturing systems are covered by biocompatible materials like parylene and platinum black, it might be not a critical problem to prove the biocompatibility of the material inside structures. However, the microneedle arrays including fluidic channels could deliver some toxic materials through fluidic channels, which may come from inside SU-8 structures and manifold materials. Therefore, to generate reliable microneedle arrays for brain slice cultures, robust biocompatible tests of SU-8 should be done or micromolding techniques which can replace the SU-8 structures by biocompatible materials can be considered for further studies.

REFERENCES

[1] D. A. Borkholder, "Cell Based Biosensors Using Microelectrodes," Ph.D. Dissertation, Stanford University, CA, 1998.

[2] J. C. Chang, G. J. Brewer, and B. C. Wheeler, "Microelectrode Array Recordings of Patterned Hippocampal Neurons for Four Weeks," *Biomedical Microdevices*, vol. 2, pp. 245-253, 2001.

[3] Y. Jimbo, N. Kasai, K. Torimitsu, T. Tateno, and H. Robinson, "A system for MEA-based multisite stimulation," *IEEE Trans. Biomed. Eng.*, vol. 50, pp. 241-248, 2003.

[4] W. Li, K. G. Danielson, P. G. Alexander, and R. S. Tuan, "Biological response of chondrocytes cultured in three-dimensional nanofibrous poly(-caprolactone) scaffolds," *Journal of Biomedical Materials Research Part A*, vol. 67A, pp. 1105-1114, 2003.

[5] V. A. Liu and S. N. Bhatia, "Three-Dimensional Photopatterning of Hydrogels Containing Living Cells," *Biomedical Microdevices*, vol. 4, pp. 257-266, 2002.

[6] L. Won, N. Bubula, and A. Heller, "Fetal exposure to methamphetamine in utero stimulates development of serotonergic neurons in three-dimensional reaggregate tissue culture," *Synapse*, vol. 43, pp. 139-144, 2002.

[7] D. W. DuBois, A. R. Parrish, J. P. Trzeciakowski, and G. D. Frye, "Binge ethanol exposure delays development of GABAergic miniature postsynaptic currents in septal neurons," *Developmental Brain Research*, vol. 152, pp. 199-212, 2004.

[8] K. Cheung, T. Kubow, and L. P. Lee, "Individually addressable planar patch clamp array," *2nd Annual International IEEE-EMB Special Topic Conference on Microtechnologies in Medicine & Biology*, 2002.

[9] F. Greve, J. Lichtenberg, H. Hall, A. Hierlemann, and H. Baltes, "Physical Immobilization and Polymeric Microchannel Networks to Achieve Defined Neuronal Network Structures," *7th lnternational Conference on Miniaturized Chemical and Biochemical Analysts Systems (MicroTAS 2003)*, pp. 327-330, 2003.

[10] Q. He, E. Meng, Y.-C. Tai, C. M. Rutherglen, J. Erickson, and J. Pine, "Parylene Neuro-Cages for Live Neural Networks Study," *The 12th International Conference on Solid State Sensors, Actuators and Microsystems (Transducers 03)*, pp. 995-998, 2003.

[11] R. Hagedorn, L. Z. Konstanze, E. Richter, J. Hornung, and A. Voigt, "Characterization of cell movement by impedance measurements on fibroblasts

grown on perforated Si-membranes," *Biochemica et Biophysica Acta - Molecular Cell Research*, vol. 1269, pp. 221-232, 1995.

[12] D. A. Borkholder, I. E. Opris, N. I. Maluf, and G. T. A. Kovacs, "Planar electrode array systems for neural recording and impedance measurements," *International conference of the IEEE Engineering in Medicine and Biology Society*, 1996.

[13] A. Heller, H. Choi, and Lisa Won, ” Volume, Issue, Date, Pages, "Regulation of developing dopaminergic axonal arbor size in three-dimensional reaggregate tissue culture," *The Journal of Comparative Neurology*, vol. 384, pp. 349-358, 1997.

[14] S. Papini, A. Rosellini, D. Campani, A. DeMatteis, C. Selli, and R. P. Revoltella, "Selective growth of epithelial basal cells from human prostate in a three-dimensional organ culture," *The Prostate Early View*, pp. 1-10, 2004.

[15] B. Pardo and P. Honegger, "Differentiation of rat striatal embryonic stem cells in vitro: monolayer culture vs. three-dimensional coculture with differentiated brain cells," *Journal of Neuroscience Research*, vol. 59, pp. 504-512, 2000.

[16] E. Behravesh and Antonios G. Mikos, ” Volume, Issue, Date, Pages., "Three-dimensional culture of differentiating marrow stromal osteoblasts in biomimetic poly(propylene fumarate-co-ethylene glycol)-based macroporous hydrogels," *Journal of Biomedical Materials Research Part A*, vol. 66A, pp. 698-706, 2003.

[17] T. Nyberg, O. Inganäs, and H. Jerregård, "Polymer Hydrogel Microelectrodes for Neural Communication," *Biomedical Microdevices*, 2002.

[18] L. J. Suggs, M. S. Shive, C. A. Garcia, J. M. Anderson, and A. G. Mikos, "In vitro cytotoxicity and in vivo biocompatibility of poly(propylene fumarate-co-ethylene glycol) hydrogels," *Journal of Biomedical Materials Research*, vol. 46, pp. 22-32, 1999.

[19] O. Fromigué, K. Louis, E. Wu, N. Belhacène, A. Loubat, M. Shipp, P. Auberger, and B. Mari, "Active stromelysin-3 (MMP-11) increases MCF-7 survival in three-dimensional Matrigel culture via activation of p42/p44 MAP-kinase," *International Journal of Cancer*, vol. 106, pp. 355-363, 2003.

[20] M. E. Gomes, V. I. Sikavitsas, E. Behravesh, R. L. Reis, and A. G. Mikos, "Effect of flow perfusion on the osteogenic differentiation of bone marrow stromal cells cultured on starch-based three-dimensional scaffolds," *Journal of Biomedical Materials Research Part A*, vol. 67A, pp. 87-95, 2003.

[21] P. K. Campbell, K. E. Jones, R. J. Huber, K. W. Horch, and R. A. Normann, "A silicon-based, three-dimensional neural interface: manufacturing processes for an

intracortical electrode array," *IEEE Transactions on Biomedical Engineering*, vol. 38, 1991.

[22] Q. Bai and K. D. Wise, "Single-unit neural recording with active microelectrode arrays," *IEEE Transactions on Biomedical Engineering*, vol. 48, 2001.

[23] D. T. Kewley, M. D. Hills, D. A. Borkholder, I. E. Opris, N. I. Maluf, C. W. Storment, J. M. Bower, and G. T. A. Kovacs, "Plasma-Etched Neural Probes," *Sensors and Actuators A*, vol. 58, pp. 27 - 35, 1997.

[24] M. O. Heuschkel, M. Fejtl, M. Raggenbass, D. Bertrand, and P. Renaud, "A three-dimensional multi-electrode array for multi-site stimulation and recording in acute brain slices," *Journal of Neuroscience Methods*, vol. 114, pp. 135-148, 2002.

[25] Y. Choi, R. Powers, V. Vernekar, A. B. Frazier, M. LaPlaca, and M. G. Allen, "High Aspect Ratio SU-8 Structures for 3-D Culturing of Neurons," *ASME International Mechanical Engineering Congress and Exposition*, 2003.

[26] M. Li, J. D. Glawe, H. Green, D. K. Mills, M. J. McShane, and B. K. Gale, "Effect of High-Aspect-Ratio Microstructures on Cell Growth and Attachment," *1st Annual International IEEE-EMBS Special Topic Conference on Microtechnologies in Medicine & Biology*, 2000.

[27] V. Seidemann, J. Rabe, M. Feldmann, and S. Büttgenbach, "SU8-micromechanical structures with in situ fabricated movable parts," *Microsystem Technologies*, vol. 8, pp. 348 - 350, 2002.

[28] G. J. Brewer, "Isolation and culture of adult rat hippocampal neurons," *J. Neurosci. Methods*, vol. 71, pp. 145-58, 1997.

[29] L. Griscom, P. Degenaar, M. Denoual, and F. Morin, "Culturing of Neurons in Microfluidic Arrays," *2nd Annual International IEEE-EMBS Special Topic Conference on Microtechnologies in Medicine & Biology*, 2002.

[30] W. L. C. Rutten and J. v. Pelt, "Activity patterns of cultured neural networks on micro electrode arrays," *The 23rd Annual International Conference of the IEEE Engineering in Medicine and Biology Society*, pp. 737-740, 2001.

[31] C. S. Chen, "Microengineered systems to directly manipulate and probe living cells," *Micro Total Analysis System 2003*, pp. 433- 436, 2003.

[32] G. J. Brewer, J. R. Torricelli, E. K. Evege, and P. J. Price, "Optimized survival of hippocampal neurons in B27-supplemented Neurobasal, a new serum-free medium combination," *Journal of Neuroscience Research*, vol. 35, pp. 567-576, 1993.

[33] A. Folch, S. Mezzour, M. During, O. Hurtado, M. Toner, and R. Muller, "Stacks of Microfabricated Structures as Scaffolds for Cell Culture and Tissue Engineering," *Biomedical Microdevices*, vol. 2, pp. 207-214, 2000.

[34] E. Leclerc, Y. Sakai, and T. Fujii, "Cell Culture in 3-Dimensional Microfluidic Structure of PDMS (polydimethylsiloxane)," *Biomedical Microdevices*, 2003.

[35] P. X. Ma and R. Zhang, "Microtubular architecture of biodegradable polymer scaffolds," *Journal of Biomedical Materials Research Part A*, vol. 56, pp. 469-477, 2001.

[36] J. Zimmermann, K. Bittner, B. Stark, and R. Mulhaupt, "Novel hydrogels as supports for in vitro cell growth: poly (ethylene glycol)- and gelatine-based (meth) acrylamidopeptide macromonomers," *Biomaterials*, vol. 23, pp. 2127-2134, 2002.

[37] Y. Choi, S. Choi, R. Powers, Y. Nam, A. Marr, G. J. Brewer, B. C. Weeler, and M. G. Allen, "Three-Dimensional Tower Structures with Integrated Cross-Connects for 3-D Culturing of Neurons," *Digest of Solid-State Sensor, Actuator, and Microsystems Workshop (Hilton Head 2004)*, 2004.

[38] Y. Grisel, L. Saavedra, M. A. Mateescu, D. A. Averill-Bates, and F. Denizeau, "Polyvinylalcohol three-dimensional matrices for improved long-term dynamic culture of hepatocytes," *Journal of Biomedical Materials Research Part A*, vol. 66A, pp. 562-570, 2003.

[39] A. Daridon, V. Fascio, J. Lichtenberg, R. Wütrich, H. Langen, E. Verpoorte, and N. F. d. Rooij, "Multi-layer microfluidic glass chips for microanalytical applications," *Fresenius' Journal of Analytical Chemistry*, vol. 371, pp. 261 - 269, 2001.

[40] W. J. Li, J. D. Mai, and C.-M. Ho, "A MEMS Fabrication Technique for Non-Planar Substrates," *IEEE MEMS'1998*, pp. 268-273, 1998.

[41] A. Welle and E. Gottwald, "UV-Based Patterning of Polymeric Substrates for Cell Culture Applications," *Biomedical Microdevices*, 2002.

[42] Y.-J. Chuang and W.-K. Lin, "A novel fabrication method of embedded micro-channels by using SU-8 thick-film photoresists," *Sensors and Actuators A*, vol. 103, pp. 64-69, 2003.

[43] G. Liu, Y. Tian, and X. Zhang, "Fabrication of microchannels in negative resist," *Microsystem Technologies*, vol. 9, pp. 461–464, 2003.

[44] Y. Yamaguchi and S. Morooka, "3-D Simulation and Visualization of Laminar Flow in a Microchannel with Hair-Pin Curves," *American Institute of Chemical Engineers (AIChE) Journal*, vol. 50, 2004.

[45] J. Brazzle, I. Papautsky, and A. B. Frazier, "Micromachined needle arrays for drug delivery or fluid extraction," *IEEE Engineering in Medicine and Biology Magazine*, vol. 18, 1999.

[46] I.-M. Hsing, R. Srinivasan, M. P. Harold, K. F. Jensen, and M. A. Schmidt, "Finite element simulation strategies for microfluidic devices with chemical reactions," *International Conference on Solid State Sensors and Actuators, TRANSDUCERS '97*, pp. 1015-1018, 1997.

[47] K. Yamasaki, S. Juodkazis, S. Matsuo, and H. Misawa, "Three-dimensional micro-channels in polymers: one-step fabrication," *Applied Physics A Materials Science & Processing*, vol. 77, pp. 371-373, 2003.

[48] G.-H. Feng and E. S. Kim, "Universal concept for fabricating micron to millimeter sized 3-D parylene structures on rigid and flexible substrates," *IEEE The Sixteenth Annual International Conference on Micro Electro Mechanical Systems, MEMS-03*, pp. 594- 597, 2003.

[49] L. A. Tse, P. J. Hesketh, D. W. Rosen, and J. L. Gole, "Stereolithography on silicon for microfluidics and microsensor packaging," *Microsystem Technologies*, vol. 9, pp. 319 - 323, 2003.

[50] K. Ikuta, K. Hirowatari, and T. Ogata, "Three dimensional micro integrated fluid systems (MIFS) fabricatedby stereo lithography," *IEEE Workshop on Micro Electro Mechanical Systems, MEMS '94*, pp. 1-6, 1994.

[51] W. Michaeli and C. Ziegmann, "Micro assembly injection moulding for the generation of hybrid microstructures," *Microsystem Technologies*, vol. 9, pp. 427 - 430, 2003.

[52] B.-H. Jo, L. M. V. Lerberghe, K. M. Motsegood, and D. J. Beebe, "Three-dimensional micro-channel fabrication in polydimethylsiloxane (PDMS) elastomer," *Journal of Microelectromechanical Systems*, vol. 9, 2000.

[53] K. Williams, J. Maxwell, K. Larsson, and M. Boman, "Freeform fabrication of functional microsolenoids, electromagnetsand helical springs using high-pressure laser chemical vapor deposition," *Twelfth IEEE International Conference on Micro Electro Mechanical Systems, MEMS '99*, pp. 232-237, 1999.

[54] F. Wagner and P. Hoffmann, "Structure formation in excimer laser ablation of stretched poly(ethylene therephthalate) (PET): the influence of scanning

ablation," *Applied Physics A: Materials Science & Processing*, vol. 69, pp. S841 - S844, 1999.

[55] M. Han, W. Lee, S. Lee, and L. S, "Microfabrication of 3D Oblique Structures by Inclined UV Lithography," *Micro Total Analysis Systems 2002*, vol. 1, pp. 106-108, 2002.

[56] R. A. Lawes, A. S. Holmes, and F. N. Goodall, "The formation of moulds for 3D microstructures using excimer laser ablation," *Microsystem Technologies*, vol. 3, pp. 17 - 19, 1996.

[57] B. Keiper, H. Exner, U. Löschner, and T. Kuntze, "Drilling of Glass by Excimer Laser Mask Projection Technique," *Proc ICALEO Laser Microfabrication Conference*, 1999.

[58] D. T. Eddington, W. C. Crone, and D. J. Beebb, "Development of Process Protocols to Fine Tune Polydimethylsiloxane Material Properties," *7th lnternational Conference on Miniaturized Chemical and Biochemical Analysts Systems (MicroTAS 2003)*, pp. 1089-1092, 2003.

[59] J. Vukasinovic and A. Glezer, "Countercurrent Flow of an Impinging Round Synthetic Jet," *Bulletin of the American Physical Society-Division of Fluid Dynamics*, vol. 46, pp. 196, 2001.

[60] J. Vukasinovic and A. Glezer, "Supercritical Helical Vortex Flow," *Bulletin of the American Physical Society-Division of Fluid Dynamics*, vol. 45, pp. 37, 2000.

[61] A. S. Widge, "Conductive Polymer “Molecular Wires” for Chronic Neuro-Robotic Interfaces," Ph.D. Proposal, Carnegie Mellon University, 2004.

[62] N. Li, A. Tourovskaia, and A. Folch, "Biology on a Chip: Microfabrication for Studying the Behavior of Cultured Cells," *Critical Reviews™ in Biomedical Engineering*, vol. 31, 2003.

[63] M. Bove, M. Grattarola, S. Martinoia, and G. Verreschi, "Interfacing cultured neurons to planar substrate microelectrodes: characterization of the neuron-to-microelectrode junction," *Bioelectrochemistry and Bioenergetics*, vol. 38, pp. 229-445, 1995.

[64] P. G. Molchanov, A. A. Denisov, G. G. Martinovich, and S. N. Cherenkevich, "Neuroelectronic Systems: Binding Neurons to Electric Circuits," *International Conference on Neural Networks and Artificial (ICNNAI'99)*, 1999.

[65] C.-H. Chang, J.-D. Liao, J.-J. J. Chen, M.-S. Ju, and C.-C. K. Lin, "Alkanethiolate Self-Assembled Monolayers as Functional Spacers to Resist Protein Adsorption

upon Au-Coated Nerve Microelectrode," *Langmuir*, vol. 20, pp. 11656-11663, 2004.

[66] Y. Choi, S. Choi, R. H. Shafer, and M. G. Allen, "Highly Inclined Electrodeposited Metal Lines Using an Excimer Laser Patterning Technique," *Digest of the 13th International Conference on Solid-State and Actuators, Transducers05*, 2005.

[67] S. Maeda, K. Minami, and M. Esashi, "KrF excimer laser induced selective non-planar metallization," *MEMS '94*, 1994.

[68] K. I. Jolic, M. K. Ghantasala, and E. C. Harvey, "Excimer laser machining of corner cube structures," *J. Micromechanics and Microengineering*, vol. 14, pp. 388, 2004.

[69] C. Yang, Y. Hsieh, G. Hwang, and Y. Lee, "Photoablation characteristics of novel polyimides synthesized for high-aspect-ratio excimer laser LIGA process," *J. Micromechanics and Microengineering*, vol. 14, pp. 480, 2004.

[70] J. Pine, "Recording action potentials from cultured neurons with extracellular microcircuit electrodes," *J. Neurosci. Meth.*, vol. 2, pp. 19–31, 1980.

[71] R. R. Harrison and C. Charles, "A low-power, low-noise CMOS amplifier for neural recording applications," *IEEE J. Solid-State Circuits*, vol. 38, 2003.

[72] R. A. Blum, J. D. Ross, E. A. Brown, and S. P. DeWeerth, "An Analog VLSI Stimulation and Recording System for Extracelluar Interfacing," *The 2nd International IEEE EMBS Conference on Neural Engineering*, 2005.

[73] R. A. Blum, J. D. Ross, S. K. Das, E. A. Brown, and S. P. DeWeerth, "Models of Stimulation Artifacts Applied to Integrated Circuit Design," *Proceedings of the IEEE Engineering in Medicine and Biology Society*, 2004.

[74] I. Obeid, M. A. L. Nicolelis, and P. D. Wolf, "A low power multichannel analog front end for portable neural signal recordings," *Journal of Neuroscience Methods*, vol. 133, pp. 27-32, 2004.

[75] D. A. Wagenaar, J. Pine, and S. M. Potter, "Effective parameters for stimulation of dissociated cultures using multi-electrode arrays," *J. Neurosci. Meth.*, vol. 138, pp. 27-37, 2004.

[76] J. D. Ross, S. M. O'Connor, R. A. Blum, E. A. Brown, and S. P. DeWeerth, "Multielectrode Impedance Tuning: Reducing Noise and Improving Stimulation Efficacy," *Proceedings of the IEEE Engineering in Medicine and Biology Society*, 2004.

[77] S. M. Potter, "Distributed processing in cultured neuronal networks.," *Progress In Brain Research*, vol. 130, pp. 49-62, 2001.

[78] S. E. Fraser, J. Pine, and S. M. Potter, "2-Photon time-lapse imaging of transplant integration in cultured rat hippocampal slices," *Soc. Neurosci. Abstr.*, vol. 23, 1997.

[79] S. M. Potter, "3D Time-lapse imaging of hippocampal slices," *Applications of Multiple-Photon Excitation Imaging (Satellite symposium for Microscopy and Microanalysis '97)*, 1997.

[80] A. M. Benediktsson, S. J. Schachtele, S. H. Green, and M. E. Dailey, "Ballistic Labeling and Dynamic Imaging of Astrocytes in Organotypic Hippocampal Slice Cultures," *Journal of Neuroscience Methods*, vol. 141, pp. 41-53, 2005.

[81] D. Kurpius and M. E. Dailey, "A practical guide to imaging microglia in live brain slices and slice cultures," *A Laboratory Manual in Imaging in Neuroscience and Development*, pp. 425-429, 2005.

[82] S.-J. Moon and S. S. Lee, "Fabrication of microneedle array using inclined LIGA process," *12th Innational Conference on Solid-State Sensors, Actuators and Microsystems, TRANSDUCERS2003*, vol. 2, pp. 8-12, 2003.

[83] P. Aggarwal, K. V. I. S. Kaler, and W. Badawy, "Design and implementation of MEMS based microneedles for biomedical applications," *IEEE CCECE 2003. Canadian Conference on Electrical and Computer Engineering*, vol. 3, pp. 1505 - 1508, 2003.

[84] S. Chandrasekaran and A. B. Frazier, "Characterization of surface micromachined metallic microneedles," *Journal of Microelectromechanical Systems*, vol. 12, pp. 289 - 295, 2003.

[85] S. Chandrasekaran, J. D. Brazzle, and A. B. Frazier, "Surface micromachined metallic microneedles," *Journal of Microelectromechanical Systems*, vol. 12, 2003.

[86] S.-J. Paik, u.-M. Lim, I. Jung, Y. Park, S. Byun, S. Chung, K. Chun, J. Chang, and D. D. Cho, "A novel microneedle array integrated with a PDMS biochip for microfluid systems," *12th Innational Conference on Solid-State Sensors, Actuators and Microsystems, TRANSDUCERS*, vol. 2, pp. 1446 - 1449, 2003.

[87] D. V. McAllister, S. Kaushik, P. N. Patel, J. L. Mayberry, M. G. Allen, and M. R. Prausnitz, "Microneedles for transdermal delivery of macromolecules," *Proceedings of the First Joint BMES/EMBS Conference*, vol. 2, pp. 836, 1999.

[88] J.-H. Park, S. Davis, Y.-K. Yoon, M. R. Prausnitz, and M. G. Allen, "Micromachined biodegradable microstructures," *IEEE The Sixteenth Annual International Conference on Micro Electro Mechanical Systems*, pp. 371 - 374, 2003.

[89] K. Kim, D. S. Park, H. M. Lu, W. Che, K. Kim, J.-B. Lee, and C. H. Ahn, "A tapered hollow metallic microneedle array using backside exposure of SU-8," *J. Micromech. Microeng.*, vol. 14, pp. 597–603, 2004.

[90] B. Stoeber and D. Liepmann, "Fluid injection through out-of-plane microneedles," *1st Annual International, Conference On Microtechnologies in Medicine and Biology*, pp. 224 - 228, 2000.

[91] P. Griss and G. Stemme, "Side-opened out-of-plane microneedles for microfluidic transdermal liquid transfer," *Journal of Microelectromechanical Systems*, vol. 12, pp. 296 - 301, 2003.

[92] J. D. Zahn, A. A. Deshmukh, A. P. Pisano, and D. Liepmann, "Continuous on-chip micropumping through a microneedle," *The 14th IEEE International Conference on Micro Electro Mechanical Systems, MEMS 2001.*, pp. 503 - 506, 2001.

[93] S. P. Davis, M. R. Prausnitz, and M. G. Allen, "Fabrication and characterization of laser micromachined hollow microneedles," *12th Innational Conference on Solid-State Sensors, Actuators and Microsystems, TRANSDUCERS*, vol. 2, pp. 1435 - 1438, 2003.

[94] B. H. Gähwiler, M. Capogna, D. Debanne, R. A. McKinney, and S. M. Thompson, "Organotypic slice cultures: a technique has come of age," vol. 20, pp. 471-7, 1997.

[95] H. Jahnsen, B. Kristensen, P. Thiebaud, J. Noraberg, B. Jakobsen, M. Bove, S. Martinoia, M. Koudelka-Hep, M. Grattarola, and J. Zimmer, "Coupling of Organotypic Brain Slice Cultures to Silicon-Based Arrays of Electrodes," *METHODS: A Companion to Methods in Enzymology*, vol. 18, pp. 160-172, 1999.